New Views of Lunar Seismicity Brought by Analysis of Newly Discovered Moonquakes in Apollo Short-Period Seismic Data

Keisuke Onodera[1,2]

[1]Earthquake Research Institute, The University of Tokyo, Yayoi, Tokyo, Japan.
[2]Institut de Physique du Globe de Paris, Université Paris Cité, CNRS, Paris, France

Key Points:

- I found more than 22,000 uncataloged moonquakes in Apollo short-period seismic data.
- Newly discovered 46 shallow moonquakes indicate a two times higher lunar seismicity rate than considered before.
- My results indicate that lunar seismicity has regionality and a higher seismic activity is observed in the northern hemisphere.

Corresponding author: Keisuke Onodera, onodera@eri.u-tokyo.ac.jp

Abstract

In the 1970s, two types of seismometers were installed on the nearside of the Moon. One type is called the Long-Period (LP) seismometer, which is sensitive below 1.5 Hz. The other is called the Short-Period (SP) seismometer, whose sensitivity is high around 2 – 10 Hz. So far, more than 13,000 seismic events have been identified through LP data analyses, which allowed us to investigate lunar seismicity and the internal structure. On the other hand, most of the SP data have remained unanalyzed because they include numerous unnatural signals and/or instrumental noises. This fact leads to the hypotheses that (i) we have missed lots of high-frequency seismic events and (ii) lunar seismicity could be underestimated. To verify these ideas, this study conducted an analysis of the SP data. In the analysis, I denoised the original SP data and performed the event detections by comparing the spectral features between the cataloged high-frequency events (such as shallow moonquakes) and the continuous SP data. Eventually, I discovered 22,000 new seismic events, including thermal moonquakes, impact-induced events, and shallow moonquakes. Among these, I focused on analyzing shallow moonquakes — tectonic-related quakes. Consequently, it turned out that there are nearly three times more tectonic events than considered before. Furthermore, additional detections of shallow moonquakes enabled me to see the regionality in seismicity. Comparing three landing sites (Apollo 14, 15, and 16), I found that the Apollo 15 site is more seismically active than others. These findings can change the conventional views of lunar seismicity.

Plain Language Summary

The seismic observation on the Moon from 1969 through 1977 opened a way to investigate lunar seismicity and the interior structure. There were two types of seismometers called the Long-Period (LP) and Short-Period (SP) seismometers. One has sensitivity below 1.5 Hz and the other is sensitive above 2 Hz. In past studies, only moonquakes detected in the LP data were used. On the contrary, most SP data remained unexplored because of numerous unnatural signals, which raises questions about whether (i) we have missed high-frequency moonquakes and (ii) lunar seismic activity level is underestimated. To answer these questions, I investigated all SP data available today and tried to find undetected moonquakes. As a result, I discovered 22,000 new seismic events, which included thermally driven quakes, meteoroid impact events, and tectonic quakes. Focusing on the tectonic-type events, I re-evaluated lunar seismicity. It turned out there were about three times more tectonic quakes than considered before, changing the conventional views of lunar seismicity. My results also indicate that the northern hemisphere is more seismically active. These findings would contribute to not only the promotion of lunar seismology but also the hazard assessment on the Moon.

1 Introduction

1.1 Apollo lunar seismic observation

The dawn of seismic observations on extraterrestrial bodies goes back to the Apollo missions, in which two types of seismometers were deployed on the nearside of the Moon (Figures 1a-b; Latham et al., 1969). One is called a Long-Period (LP) seismometer with tri-axial components. The LP sensors were operated in two modes: peaked and flat modes, whose sensitivity curves are shown in Figure 1c. Because of the unstable behavior of the flat mode, the LP seismometer was mainly operated in the peaked mode (e.g., Nunn et al., 2020). The other type is called a Short-Period (SP) seismometer with one vertical component, which has a higher sensitivity above 1.5 Hz than the LP sensor (Figure 1c). Quasi-continuous operations of these sensors from 1969 through 1977 brought us about

(a)

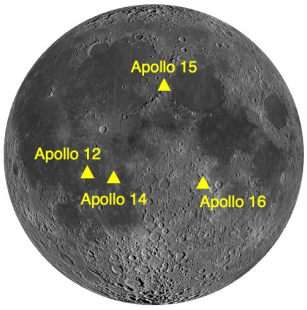

(b)

PSE station	Lat. (°N)	Lon. (°E)
Apollo 12	-3.0099	336.5752
Apollo 14	-3.64408	342.52233
Apollo 15	26.13174	3.63803
Apollo 16	-8.9759	15.4986

(c)

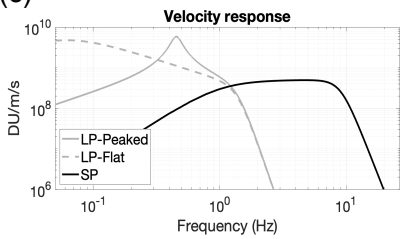

Figure 1. (a) Locations of Apollo 12, 14, 15, 16 seismic stations. The base image was taken by the Wide Angle Camera of the Lunar Reconnaissance Orbiter (Robinson et al., 2010) (the courtesy of NASA and Arizona State University). (b) The coordinates of each Passive Seismic Experiment (PSE) station. The values are referred from Wagner et al. (2017). (c) Response curve of the Apollo lunar seismometers for velocity. The horizontal axis shows frequency and the vertical shows sensitivity in DU/m/s. The gray solid line corresponds to the peaked mode of the LP sensor, the dashed gray line represents the flat mode of the LP sensor, and the black solid curve is for the SP sensor.

13,000 seismic events (Nakamura et al., 1981). The detected signals were categorized into five classes depending on the waveform and spectral features: deep moonquakes (∼7,500 events), shallow moonquakes (28 events), meteoroid or artificial impacts (∼1,700 events), thermal moonquakes (> 555 events), and unclassified events (∼3,300 events) (Nakamura et al., 1981; Nunn et al., 2020). While deep and shallow moonquakes are considered to

be internal origin triggered by tidal stress and/or near-surface fault activities (e.g., Nakamura, 2005; Weber et al., 2009; Kawamura et al., 2017; Goins et al., 1981; Watters et al., 2019), impacts and thermal moonquakes are strongly related to the lunar environment such as lack of thick atmosphere and large temperature variations (e.g., Latham, Ewing, et al., 1970; Duennebier & Sutton, 1974a, 1974b). Over the past 50 years, the studies of the seismicity and internal structure of the Moon have built on the analyses of these moonquakes. The latest review is given by Garcia et al. (2019) and Nunn et al. (2020).

1.2 Potential seismic events in Apollo short-period seismic data

The existing moonquake catalog by Nakamura et al. (1981) includes about 13,000 events. It is worth noting that these events were detected using only LP data. In fact, compared to LP data, SP data have been investigated less so far because of numerous artifacts (Section 3.2) and larger amounts of data due to an 8 times higher sampling rate than that of LP. Even though the initial description of high-frequency events recorded in the SP data was provided by Duennebier and Sutton (1974a) and Duennebier and Sutton (1974b), their analyses were limited to the first one-year of operation at Apollo 14, 15, and 16 stations (Feb. 1971 – Jan. 1972). Lately, Knapmeyer-Endrun and Hammer (2015) analyzed both LP and SP data covering a longer observation period (Apr. 1972 – Jun. 1975) to find new seismic events; yet they only used Apollo 16 data. Therefore, a large portion of the SP data remained unanalyzed until today, which in turn raises the fact that high-frequency events (> 2 Hz) are less cataloged or even undiscovered (Frohlich & Nakamura, 2006).

Then, what kind of events have we missed in the past half-century? There are three possibilities. First, looking at the Apollo data, I often encounter the period when the LP sensor did not function properly while the SP sensor recorded the data appropriately (Figure 2a). In such a case, the event signals can be only recorded by the SP sensor and one could miss them as long as checking only LP data. The second candidate is small shallow moonquakes. It is known that shallow moonquakes excite more energy at high frequencies (> 2 Hz) (e.g., Nakamura et al., 1979; Goins et al., 1981; Binder & Oberst, 1985). Comparing the Root Mean Squared (RMS) envelope of a shallow moonquake (Figure 2b), it is clear that the SP data have a larger amplitude than the LP by a factor of 7 or so. Thus, the SP data are more suitable for detecting small and/or distant shallow moonquakes. The last candidate is thermal moonquakes. This is simply because they typically excite the energy above 2 Hz where the SP sensor has higher sensitivity (Duennebier & Sutton, 1974b). Therefore, it is expected that a thorough search of the SP data would bring us lunar seismic events only recorded in the SP data.

1.3 Objectives of this study

The objectives of this study are (a) to search for undetected moonquakes and (b) to describe the newly discovered events. Among the categorized events, shallow moonquakes, thermal moonquakes, and local meteoroid impacts could be candidates to discover in the SP seismic data because of their high-frequency energy excitation. In particular, shallow moonquakes are the most energetic seismic events (e.g., Goins et al., 1981) and are usually used to evaluate the lunar seismicity (e.g., Lammlein et al., 1974; Banerdt et al., 2020). Even though shallow moonquakes are regarded as one of the primary topics in lunar seismology, their source distributions and focal mechanisms remain uncertain because of their smaller population (Section 1.1). Therefore, discovering new shallow moonquakes is of great importance to refine our understanding of their nature (e.g., spatial distribution, relation to the topographic structures, periodicity, and focal mechanisms) and also leads to the assessment of lunar seismicity.

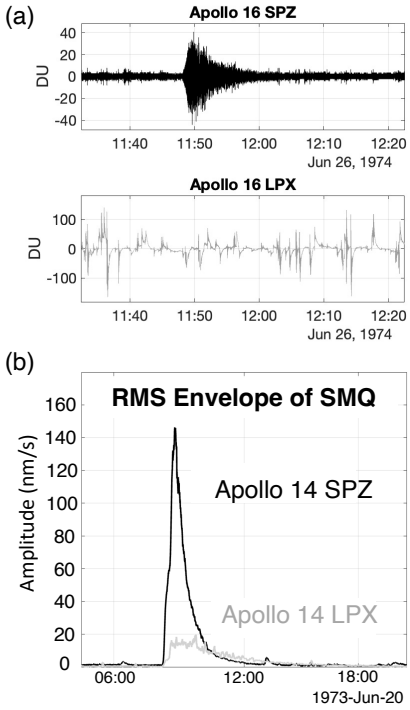

Figure 2. (a) An example of seismic events only detected by SP sensor (Apollo 16, 1974-Jun-28). The top panel shows the waveform recorded by the SP sensor and the bottom panel shows that recorded by the LP sensor. The vertical axis is expressed in Digital Unit (DU). (b) Comparison of Root Mean Squared (RMS) envelope of a shallow moonquake between SP and LP recordings.

This paper is composed of three parts. The first part is dedicated to the detection of new moonquakes and the description of the discovered events (Section 3 – Section 4). In the second part, I will evaluate lunar seismicity, focusing on newly discovered shallow moonquakes (Section 5). In the end, I will provide some implications for future seismic explorations on the Moon based on the updated lunar seismicity (Section 6).

2 High-Frequency Lunar Seismic Events

Among the cataloged seismic events, there are three types of events having energy over 2 Hz where the SP sensor is more sensitive: (i) meteoroid impacts, (ii) shallow moonquakes, and (iii) thermal moonquakes (e.g., McGarr et al., 1969; P. J. Oberst & Nakamura, 1987; Duennebier & Sutton, 1974a, 1974b; Nakamura et al., 1979; Nakamura, 1980). Hereafter, I summarize their characteristics, which would be helpful for interpreting the newly detected events.

2.1 Meteoroid impacts

Identification of the impact-induced events was achieved owing to the artificial impact experiments, where some Saturn rocket boosters (S-IVB) and Lunar Modules (LM) were intentionally dropped on the lunar surface (e.g., Latham, Ewing, et al., 1970; Latham, McDonald, & Moore, 1970). Because of the well-determined source locations, origin times, and impact parameters (e.g., angle, speed, and mass), these have been commonly used

as references for both data analyses and numerical simulations (e.g., Gudkova et al., 2011; Onodera et al., 2021, 2022; Rajšić et al., 2021).

Based on the characteristics of the waveform and spectral contents for the artificial impacts, previous studies were able to identify 1743 meteoroid impacts in the LP recordings (e.g., Nakamura et al., 1981, 1982). Duennebier and Sutton (1974a) reported that the meteoroid impacts were also recorded by the SP sensor and described the characteristics at higher frequency part (> 2 Hz). Figures 3a-b compare the waveforms and spectrograms of the artificial impacts and some of the largest meteoroid impacts selected by Oberst and Nakamura (1989). Due to the intense scattering within the regolith or megaregolith layer (e.g., Blanchette-Guertin et al., 2012; Gillet et al., 2017; Onodera et al., 2022), the waveform shows a spindle shape and lasts for 20 min or longer. Looking at the spectrograms, the main energy is excited up to $8 - 12$ Hz and monotonically decreases toward lower frequencies, which differs from what is observed for other moonquakes, such as shallow moonquakes (Figure 3c).

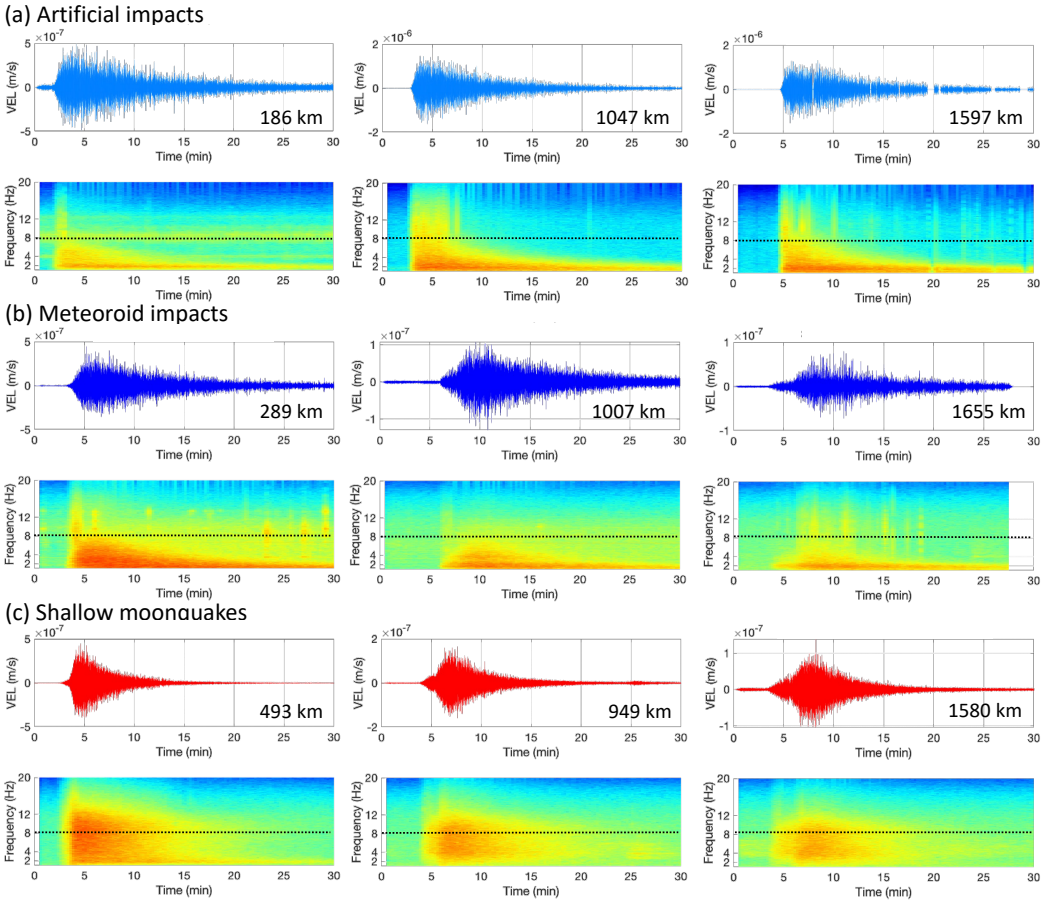

Figure 3. Waveforms of SP data and spectrograms for (a) artificial impacts, (b) meteoroid impacts, and (c) shallow moonquakes located at various epicentral distances.

Similar features have been confirmed for the Martian impacts, which were detected by the seismometer installed by NASA's InSight (Interior Exploration using Seismic Investigations, Geodesy and Heat Transport) (Garcia et al., 2022; Posiolova et al., 2022) (Figures A1a-b in Appendix A). Because the scattering is weaker on Mars than on the Moon (Onodera et al., 2023; Menina et al., 2023) and the epicentral distances are smaller

than the identified lunar impacts, the event duration is shorter, but a similar tendency — the energy decays from 8 Hz toward 2 Hz — can be confirmed. Therefore, the monotonical energy decrease from a high frequency toward 2 Hz can be a solid criterion to identify the impact-generated events.

2.2 Shallow moonquakes

Shallow moonquakes or high-frequency teleseismic (HFT) events are one of the most energetic events (e.g., Nakamura et al., 1979; Goins et al., 1981). According to the estimates by Goins et al. (1981), they radiate 10^4 times larger energy than that of deep moonquakes, mainly controlling the lunar seismic moment release rate. As their name suggests, they are considered to occur in shallow depth. The estimates in focal depth vary from 0 to 250 km depending on studies (e.g., Nakamura et al., 1979; Gillet et al., 2017; Watters et al., 2019). So far, 28 shallow moonquakes have been discovered (e.g., Nakamura et al., 1979), and most of them were located in the mare region or near the boundary between the mare and highland regions (Figure 4). Their source mechanisms have not been fully understood yet. However, because some shallow quake sources fall in the vicinity of lobate scarps (tectonic-related morphology), it is considered that young fault activities may cause shallow moonquakes (Watters et al., 2019).

The prominent differences from other types of moonquakes are their waveform and spectral features. As shown in the middle and right panel in Figure 3c, almost all shallow moonquakes show two energy packets corresponding to the scattered P- and S-waves, respectively. In addition, the energy decays differently from that of impact-related events. In the case of shallow moonquakes, the energy decay shows less frequency dependence compared to that of the impacts, making high-frequency energy ($>$ 8 Hz) travel at a longer distance (Figure 3c).

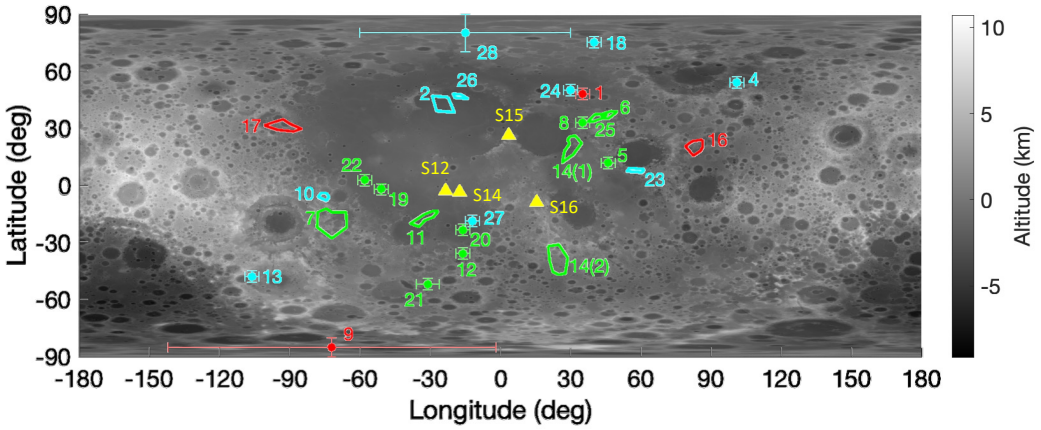

Figure 4. Possible source locations of cataloged shallow moonquakes estimated by Nakamura et al. (1979) and Watters et al. (2019). Each number is linked with the event ID in Table 1. The color of plots shows magnitude M defined by Nakamura et al. (1979) (green: $M < 1.5$, cyan: $1.5 \leq M < 2.5$, red: $2.5 \leq$ M). Yellow triangles correspond to the Apollo seismic stations. The background image is the digital elevation model by Araki et al. (2009).

2.3 Thermal moonquakes

Most seismic signals included in the Apollo SP data are thermal moonquakes, which show impulsive and short-duration ($<$ 5 min) signals (Duennebier & Sutton, 1974b). These

events are known to be repeatable quakes with a period of 29.5 days (i.e., one lunation). Depending on the characteristics of their waveforms and spectra, thermal moonquakes are roughly divided into two types: (a) Lunar Module (LM) events and (b) natural events.

LM events show the impulsive signal with a duration of less than 5 min. They normally have distinct resonances in 4 and/or 8 Hz or higher (Figure 5a). Because these signals show similar amplitude, waveform, and duration, they are thought to share the same source. Considering the fact that the number of events abruptly increases just after sunset and/or sunrise (i.e., rapid response to thermal change), Duennebier and Sutton (1974b) concluded that these events stem from the thermal contraction or expansion of the LM structure or freezing of trapped volatiles within the module. Differences in the spectral contents or timing of occurrence might reflect the responses of different parts of the LM structure to the external temperature changes (Duennebier & Sutton, 1974b).

Natural thermal moonquakes have a relatively longer duration ($>$ 5 min) without strong resonances (Figure 5b). Long duration implies that the wave traveled longer distances. As LM events, the event number increases with the period of one lunation. Yet, the main difference is their delayed response. While the LM events typically start to occur about 2 days after sunrise or sunset, the natural ones take 7 days to respond to the external temperature changes. With these characteristics, Duennebier and Sutton (1974b) speculated that they are driven by the thermal contraction or expansion of surface rocks or boulders. Since thermal fatigue is an important factor in the surface degradation process, understanding the mechanism of thermal moonquakes can give us some insights into the surface evolution of the Moon.

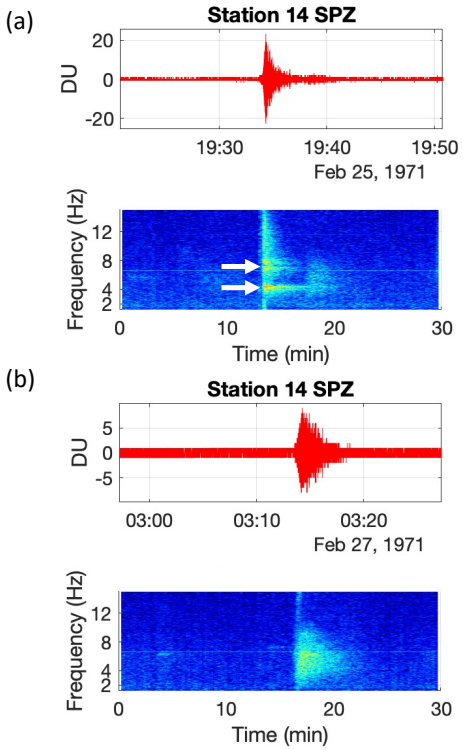

Figure 5. (a) An example of the waveform and spectrogram of a thermal moonquake (LM event). (b) An example of the waveform and spectrogram of a thermal moonquake (Natural event).

3 Method

3.1 Dataset and preprocessing

I utilized the newly archived Apollo lunar seismic data by Nunn et al. (2022), which is available via the Incorporated Research Institutions for Seismology Data Management Center (IRIS/DMC). Their thorough corrections of errors — such as variable sampling rate with temperature, data gaps, and incorrect timestamps — made it much easier to process the Apollo seismic data. In the following analysis, the SP seismic recordings at the Apollo 14, 15, and 16 stations were used.

For preprocessing, I corrected the sampling rate of the original Apollo data and filled the data gaps with linear interpolation. These processes can be performed with some programs provided by Nunn et al. (2022). After that, I performed detrending to the signal with a simple linear function. In the following, I call this data "preprocessed data".

3.2 Data cleaning

I performed a denoising to reduce the contamination of artifacts and/or instrumental noises from the Apolo SP data. In this study, I employed one of the classical methods to remove noises, where the noise is detected based on the residual between the moving average value and the recorded signals. First, I computed the exponentially weighted moving average (S_{ema}) of the absolute values of the preprocessed SP data and its standard deviation (S_{ems}). The time window was empirically determined as 20 s. For noise detection, I considered the following criteria:

$$||S_{\mathrm{sp}}(t)| - S_{\mathrm{ema}}(t)| = \begin{cases} \geq N_{\mathrm{ths}} \times S_{\mathrm{ems}}(t) & \text{for noise signal} \\ < N_{\mathrm{ths}} \times S_{\mathrm{ems}}(t) & \text{for natural signal} \end{cases} \tag{1}$$

where S_{sp} is the preprocessed SP time trace and N_{ths} is the threshold empirically set to 5. When the left-hand term in Equation 1 exceeds $N_{\mathrm{ths}} \times S_{\mathrm{ems}}(t)$, the value is replaced with $S_{\mathrm{ema}}(t)$. Repeating this procedure several times gives me a cleaned SP time series (Figure 6). For the SP data, I found that three times repeating was sufficient to reduce the unnatural signals, such as around 0 – 3 hr in the top panel in Figure 6.

It is worth noting that my denoising process does not work perfectly at any time. Sometimes, mechanical noises cannot be removed completely, leading to false detections. It might be possible to remove these noises by giving more strict conditions to the denoising algorithm. However, this is likely to affect natural signals (i.e., event signals). To avoid varying the event-related signals significantly, I employed relatively gentle conditions.

3.3 Event detection through coherence analysis

For detecting high-frequency events in the Apollo SP data, I focused on the spectral features of the already cataloged moonquakes that excite energy at higher frequencies ($>$ 2 Hz). In this study, I used shallow moonquakes as references and then computed coherence between the continuous SP data and the references. As reference events for the coherence analysis, I selected shallow moonquakes with (i) a high signal-to-noise ratio (SNR), (ii) no data gap within the event time window, and (iii) no simultaneous encounter with other seismic events were selected. The selected events at each seismic station are displayed in Table 1, and some examples of selected and unselected events are shown in Figures A2a-d in Appendix A.

Coherence between a reference event and continuous SP data trimmed with the length of reference event duration (nominally 20 – 30 min) was computed for a given time window. For i-th time window, coherence $H_{coh,i}$ is defined as follows:

$$H_{coh,i}(\omega) = \frac{|P_{rc,i}(\omega)|^2}{P_{rr}(\omega)P_{cc,i}(\omega)}, \tag{2}$$

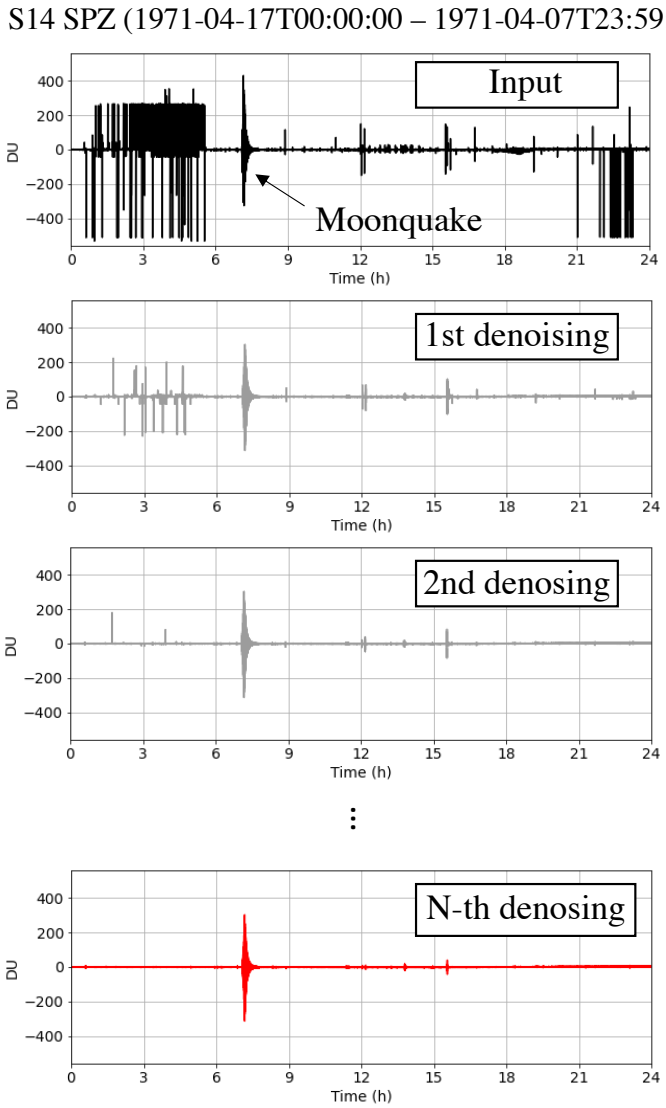

Figure 6. The denoising process applied to the Apollo seismic time trace recorded on April 17-1971 with Apollo 14 short-period seismometer. The top panel represents the input time series (i.e., the preprocessed SP data). From the second raw to the bottom, the comparison of the denoised seismic signals at different repeating rounds is made.

where ω is the angular frequency, $P_{rc,i}$ is the cross-spectrum of a reference event and continuous signal within i-th time window, P_{rr} is the power spectrum of a reference event, and $P_{cc,i}$ is the power spectrum of the continuous signal within i-th time window. For the actual detection, the median value of coherence over 1 – 20 Hz ($\langle H \rangle_i$) was used, which corresponds to making the detection criterion less strict. The spirit of my detection procedure is to find the high-frequency events (not a particular type of events). Therefore, although shallow moonquakes are referenced (i.e., more weight is put on them), any type of signal could be detected as long as it has energy at high frequencies. The (i+1)-th median coherence is computed by sliding the time window with a 25% overlap. Running this procedure all the way through the Apollo observation period gave me the time evolution of the median coherence. Figures 7a-c shows an example of the Apollo 14 data

Table 1. Reference event list. DOY means "Day of Year". Start time was referred from Nakamura et al. (1981). In the 8th - 10th column, the availability and quality of seismic data are displayed. ◯ represents the signal-to-noise ratio (SNR) is high enough for the analysis, △ means the SNR is not high enough as a reference or the data include mechanical noise, data gap, and/or simultaneous encounter of other seismic events, and × represents the data are not available. The minimum body wave magnitude in the 7-th column was re-assessed with the same condition described in Section 5.

Event ID	Year	DOY	Month	Day	Start time (UTC)	Min. m_b	S14	S15	S16
N-SMQ-1	1971	107	4	17	07:04	> 6.3	◯	×	×
N-SMQ-2	1971	140	5	20	19:05	> 5.6	△	×	×
N-SMQ-3	1971	192	7	11	14:15	> 5.5	◯	×	×
N-SMQ-4	1972	002	1	2	22:32	> 5.6	◯	△	×
N-SMQ-5	1972	261	9	17	14:38	> 4.8	◯	△	△
N-SMQ-6	1972	341	12	6	23:10	> 5.2	◯	◯	◯
N-SMQ-7	1972	344	12	9	03:52	–	△	△	△
N-SMQ-8	1973	039	2	8	22:53	> 4.7	◯	◯	◯
N-SMQ-9	1973	072	3	13	08:01	> 6.5	◯	△	◯
N-SMQ-10	1973	171	6	20	20:25	> 5.8	△	◯	◯
N-SMQ-11	1973	274	10	1	04:00	> 5.1	△	△	△
N-SMQ-12	1974	054	2	23	21:17	> 4.9	△	◯	△
N-SMQ-13	1974	086	3	27	09:11	> 5.2	◯	△	◯
N-SMQ-14	1974	109	4	19	13:39	> 4.5	△	◯	◯
N-SMQ-15	1974	149	5	29	20:45	> 4.1	◯	△	△
N-SMQ-16	1974	192	7	11	00:52	> 6.1	◯	◯	◯
N-SMQ-17	1975	003	1	3	01:47	> 6.3	◯	◯	◯
N-SMQ-18	1975	012	1	12	03:17	> 5.4	△	◯	◯
N-SMQ-19	1975	013	1	13	00:28	> 5.0	◯	◯	◯
N-SMQ-20	1975	044	2	13	22:05	> 5.2	◯	◯	◯
N-SMQ-21	1975	127	5	7	06:40	> 5.0	△	△	◯
N-SMQ-22	1975	147	5	27	23:32	> 5.3	◯	◯	◯
N-SMQ-23	1975	314	11	10	07:56	> 5.5	△	◯	◯
N-SMQ-24	1976	004	1	4	11:20	> 5.5	△	◯	△
N-SMQ-25	1976	012	1	12	08:22	> 5.4	△	◯	◯
N-SMQ-26	1976	066	3	6	10:16	> 5.9	◯	◯	◯
N-SMQ-27	1976	068	3	8	14:44	> 5.6	◯	◯	◯
N-SMQ-28	1976	137	5	16	12:36	> 5.7	△	◯	△

recorded on July 19, 1975. Comparing the SP spectrogram and the time evolution of the median coherence, it can be seen that $\langle H \rangle$ gets higher when strong energy is excited in the high frequencies (e.g., 2 – 12 Hz around 3 hr in Figure 7b-c). If $\langle H \rangle$ exceeds the empirical threshold 0.6 and the timing does not coincide with the cataloged events, the corresponding signal is regarded as a "candidate" of a new moonquake. It is worth noting that the threshold value was determined based on the test runs to see whether all the cataloged shallow moonquakes can be detected with this method. It turned out that 0.6 worked for the successful detection.

Because the detected candidates include both natural seismic events and unnatural signals that could not be removed in the denoising process, the down-selection of the candidates needs to be performed. To reduce false detections, I quantitatively evaluated the envelope shape by taking the median value of the normalized RMS envelope, which enabled me to rule out the spiky noises or step-like signals (see Section Appendix B for the details). Eventually, the detection process brought me 8,000 – 10,000 candidates at each station.

4 Newly Detected High-Frequency Events

4.1 Event classification

Looking through all the candidate events, I found that they can be roughly divided into 9 types based on waveforms and spectral contents (Figure 8). Among these, Type-

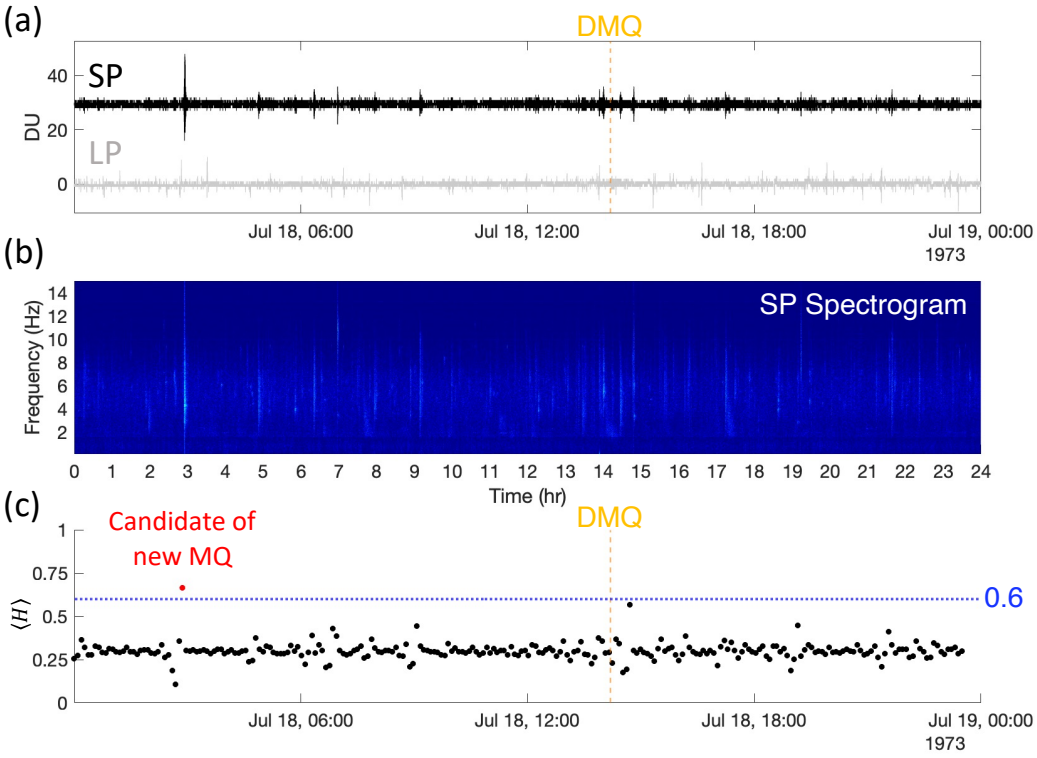

Figure 7. (a) Waveforms of LP (gray) and SP (black) seismic data recorded at Apollo 14 station on July 19, 1975. 30 DU offset is added to the SP data. The vertical orange line indicates the occurrence timing of a cataloged deep moonquake. (b) Spectrogram of the SP data. (c) Time evolution of the median coherence. The red plot means the signal has coherence higher than 0.6 and is regarded as a candidate for a new moonquake.

0 is regarded as a non-seismic event. Based on the waveforms, spectral features, and temporal distribution of occurrence, I interpret Type-1 through Type-5 as thermal moonquakes, Type-6 as meteoroid impacts, and Type-7 as shallow moonquakes. Type-8 events are considered to be natural origins. Yet, they are mixed within the same time window, and I was not confident enough to put them in the right type. Therefore, I categorized them as "unclassified events". Table 2 shows the event numbers of each type at the respective seismic stations. It is worth noting that I found some additional Type-7 events over the manual check and added them to the event list (numbers in parentheses in Table 2). The relevant information on the classified seismic events is available on Onodera (2023) or in Table A1 in Appendix A.

It should be noted that when there are several events included in a time window, I performed the classification based on the largest amplitude signal (Figure A3a in Appendix A). This usually happens to thermal moonquakes (Type-1 through Type-5). Because my detection algorithm is targeted for quakes that typically continue 10 – 15 min long and is not optimized for short-duration events such as thermal moonquakes, the algorithm detected those successive events as one event (Figure A3a in Appendix A). Thus, I stress that the numbers presented in Table 2 for Type-1 through 5 are the minimum values. As an exceptional case, I picked up Type-6 or Type-7 over other large amplitude signals for the classification if they were separable from others (Figure A3b in Appendix A).

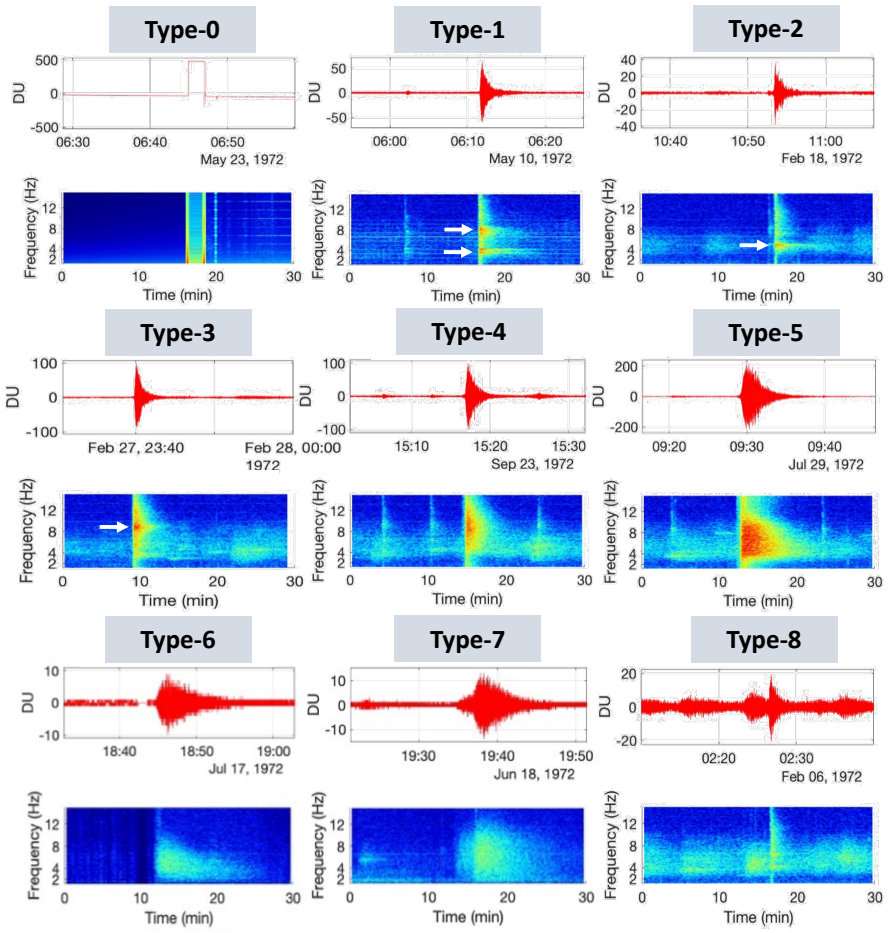

Figure 8. Classification of signal types. For each type, the SPZ time series in DU and spectrogram are presented. Type-0 includes mechanical noises, Type-1 has a clear resonance in 4 and 8 Hz, Type-2 has a resonance in 4 Hz, Type-3 has an 8 Hz resonance, Type-4 does not have resonance and the event lasts less than 5 min, Type-5 has a coda longer than 5 min with strong energy above 4 Hz, Type-6 shows a linear decay of energy from the high frequency toward 2 Hz with a long coda, Type-7 has two energy packets (e.g., P and S coda) with high energy contents, and Type-8 includes various signals mixed within the time window or unclassified signals.

In the following sections, I will explain the characteristics of the respective types. I would especially spare more space for the descriptions of shallow moonquakes since the highest priority is put on them in the discussion section (Section 5).

4.2 Thermal moonquakes (Type-1 – Type-5)

The most characteristic features of Type-1 through Type-5 are their periodic occurrence and a high correlation with surface temperature changes. This is a representative feature of thermal moonquakes (Duennebier & Sutton, 1974b). Figure 9a represents the temporal distribution of event occurrence of Type-1 through 4 (red) and Type-5 (green), respectively. Interestingly, the event number of these types spikes every two weeks (0.5 lunations) with 7 days (0.25 lunations) offset between Type-1 through 4 and Type-5. Correlation with the temperature variations can be seen in Figures 9b-f, where

Table 2. The population of the candidate events for each type. The number in the parenthesis indicates the number of additional detections through a manual check.

Type	Event Class	S14	S15	S16
Type-0	Not Event	4,761	965	684
Type-1	LM Thermal Moonquake	1,932	2,047	1,568
Type-2	LM Thermal Moonquake	706	2,175	1,254
Type-3	LM Thermal Moonquake	1,656	2,145	3,763
Type-4	LM Thermal Moonquake	256	210	671
Type-5	Thermal Moonquake	698	715	50
Type-6	Meteoroid Impact	112	39	26
Type-7	Shallow Moonquake	5 (+1)	19 (+25)	0 (+2)
Type-8	Unclassified	687	1,760	63
	Total Number	10,822 (+1)	10,075 (+25)	8,079 (+2)

the histogram of each type is shown with the horizontal axis of days from sunrise at Station 14. Type-1 and Type-3 (Figures 9b,d) have two distinct peaks after sunrise (< 3 days) and after sunset (around 14 – 20 days). The event number of Type-2 increases after sunset (Figure 9c), and that of Type-4 shows the opposite trend (Figure 9e). Type-5 events occur 7 days or later after sunset (Figure 9f), which is a different tendency from others.

As seen in Figure 8, Type-1, 2, 3, and 4 events show high similarity in their waveforms such as sharp energy arrival with rapid attenuation ($\sim$ 5 min duration), which indicates that these events propagated a similar distance. Compared to them, Type-5 events show longer duration ($\sim$ 10 min), which implies a longer travel distance. Building on the interpretation by Duennebier and Sutton (1974b), Type-1 through 4 are considered to be LM thermal moonquakes, and Type-5 is natural thermal moonquakes.

Putting together my results and the past interpretation, both thermal expansion and contraction of LM structure generate Type-1 and 4, and either of them generates Type-2 or Type-4 events. The different resonance patterns might imply that the different parts of the LM structure respond to the thermal changes. For Type-5 both thermal expansion and contraction of surface rocks or regolith could drive the events. The 7 days (0.25 lunations) offset of the event occurrence between Type-1 through 4 and Type-5 seems to result from the difference in the thermal conductivity of source materials (roughly metal vs. rocks or soils).

In this study, I divided the detected thermal moonquakes into 5 types. Yet, as discussed by Duennebier and Sutton (1974b), thermal moonquakes could be further classified into 48 types at Station 14 and 245 types at Station 15 based on waveform similarities (e.g., amplitude and cross-correlation coefficient) and the occurrence periodicity. In spite of their large population, thermal moonquakes have not been used for the investigation of the subsurface structure due to the large uncertainties in source locations and origin times (especially for natural ones). In addition, the source mechanism — an important factor for the topography degradation process — is not fully understood yet. Thus, investigation of thermal moonquakes using the detected events in this study would improve our knowledge of the above points. Because thermal moonquakes are not the main focus of the following discussions, I would limit myself to providing the event information (Onodera, 2023) and pass down this topic to future studies.

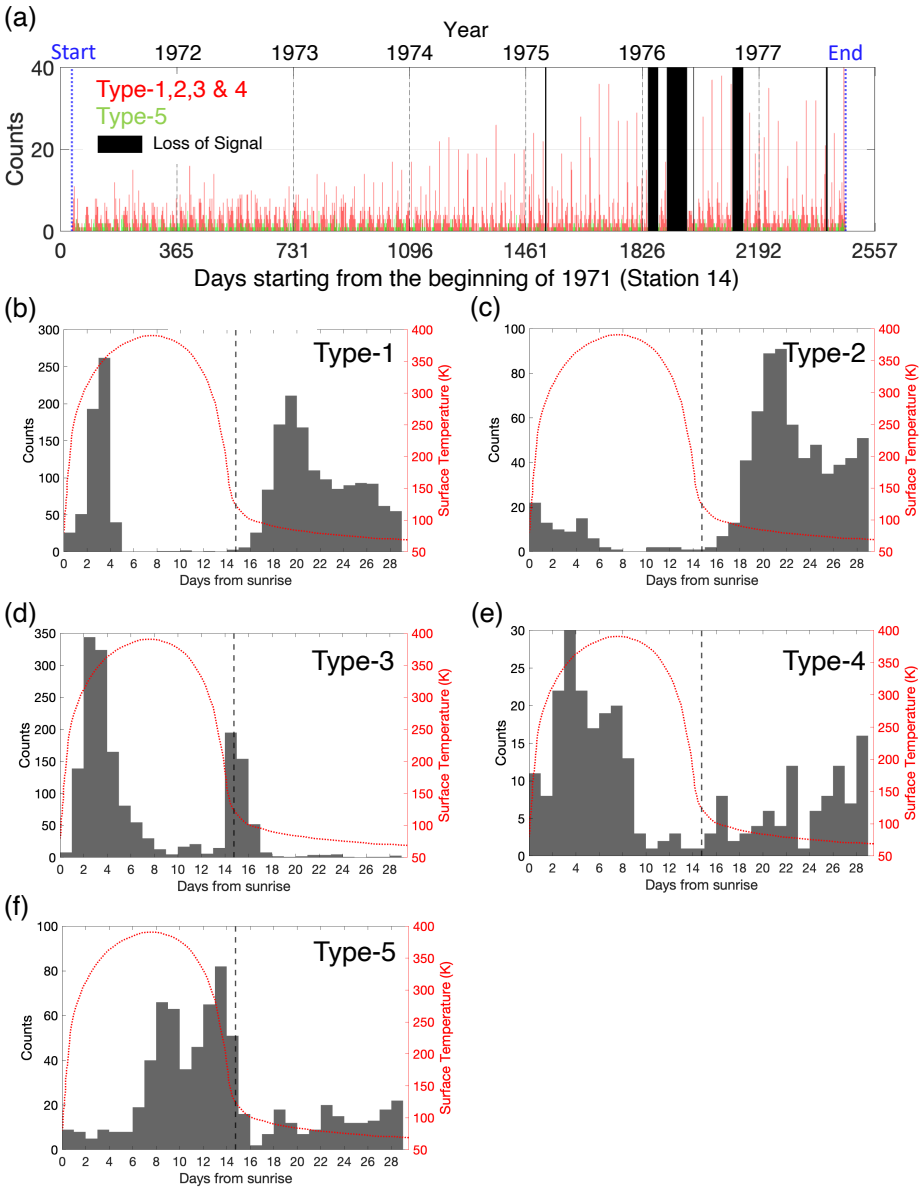

Figure 9. (a) Histogram of Type-1, 2, 3, and 4 (red) and Type-5 (green) events for Station 14 SPZ. The lower horizontal axis shows the lapse day starting from 1971 and the upper horizontal axis shows the year. The vertical axis shows the event number. (b-f) The temporal distribution of event occurrence of Type-1 through Type-5. The horizontal axis shows the days from sunrise and the vertical dotted line corresponds to sunset. The red profile indicates the evolution of surface temperature.

4.3 Meteoroid impacts (Type-6)

The characteristics of Type-6 events are their longer duration (> 10 - 15 min) with monotonic energy decay from high frequency toward low frequency, which is in accordance with the impact-induced seismic events (Section 2.1). Over the course of the classification process, I identified 112, 39, and 26 new impacts at Stations 14, 15, and 16, respectively (Figures 10a-c). Since most of them were recorded at only a single station,

these impacts are considered to be local events at each site. This leads to the idea that there is asymmetricity in the spatial distribution of meteoroid impacts on the Moon.

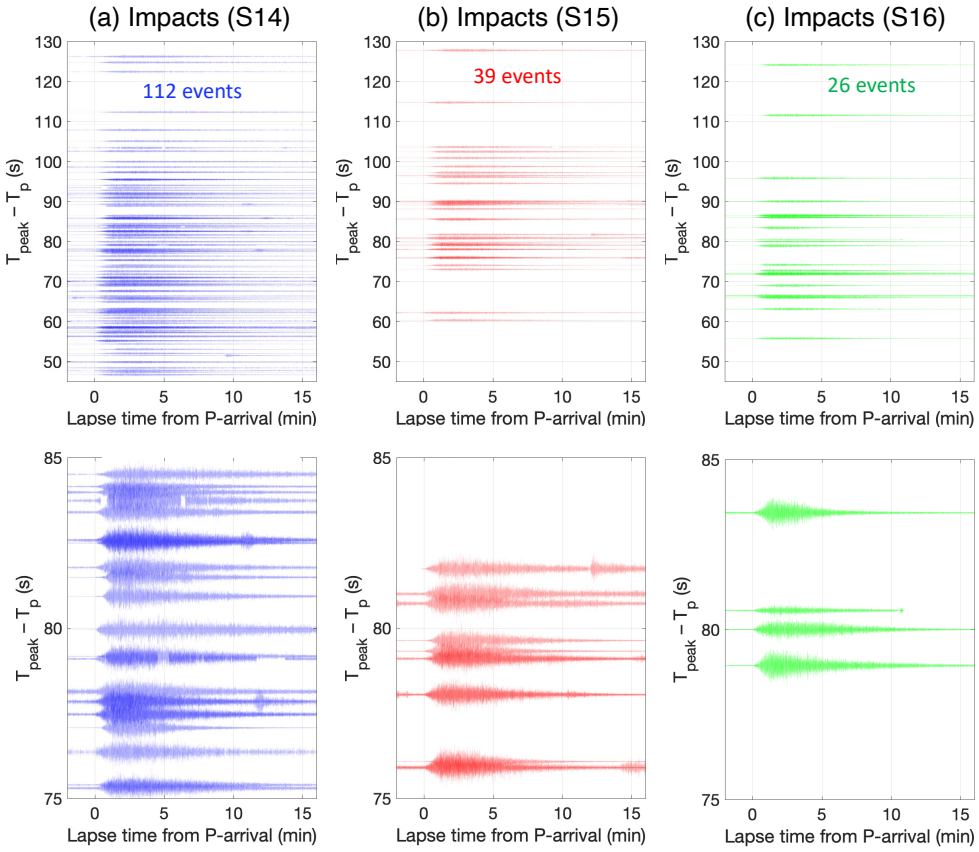

Figure 10. Arbitrary scaled waveforms of newly discovered impact-type events at (a) Station 14, (b) Station 15, and (c) Station 16. The waveforms are aligned based on the peak arrival subtracted by P-wave arrival. The top panel covers 45 s $\leq T_{peak} - T_p \leq$ 130 s and the bottom panel zooms in 75 s $\leq T_{peak} - T_p \leq$ 85 s.

In fact, the asymmetricity of the lunar impact flux has been indicated by past studies. For example, Kawamura et al. (2011) found that the source locations of large meteoroid impacts detected by Apollo seismic stations are situated more on the western side than the eastern side by 1.4 – 1.9 times. Also, the lunar impact flash observations from the ground (e.g., J. Oberst et al., 2012) and theoretical models (e.g., Le Feuvre & Wieczorek, 2008) support this idea. Furthermore, Speyerer et al. (2016) investigated the spatial distribution of new craters generated in the 2010s using the Lunar Reconnaissance Orbiter Camera (LROC) image data. Looking at their results, the newly formed craters appear situated more on the western side. Therefore, four individual approaches (seismic, lunar impact flash, remote sensing observations, and theoretical modeling) indicate that the asymmetricity in the impact flux does exist.

Based on the previous studies, these asymmetric features are explained by the fact that the western side corresponds to the leading side (i.e., the Moon moves toward that direction). This allows the lunar western side to obtain a higher relative velocity for a given impactor, resulting in a higher energy flux on the leading side than the trailing side.

Although I would not go into further details in this report, combining the newly discovered impacts with the already cataloged events would allow us to evaluate the asymmetric impact flux more precisely. Since this topic is important for both future lunar seismic explorations and human activities on the lunar surface, I would encourage that kind of study using my event catalog (Onodera, 2023).

4.4 Shallow moonquakes (Type-7)

4.4.1 General characteristics

The characteristic features of Type-7 events are two energy packets with energy excitation from 2 Hz to 8 Hz or higher (Figures 11c-d). As these characteristics match those of the cataloged shallow moonquakes (Figures 11a-b), I interpret Type-7 events as shallow moonquakes. In the following sentences, I call them "new shallow moonquakes" in order to distinguish them from the already cataloged shallow moonquakes. The relevant information on new shallow moonquakes is summarized in Table A1 in Appendix A. While most of them were detected at a single station, I found that several events were visible at multiple stations. In particular, I could confirm both P and S arrivals of the O-SMQ-6 event at Stations 14, 15, and 16, respectively (Figures 12d-f and Figure A4 in Appendix A), which allowed me to determine the source location (Section 4.4.3).

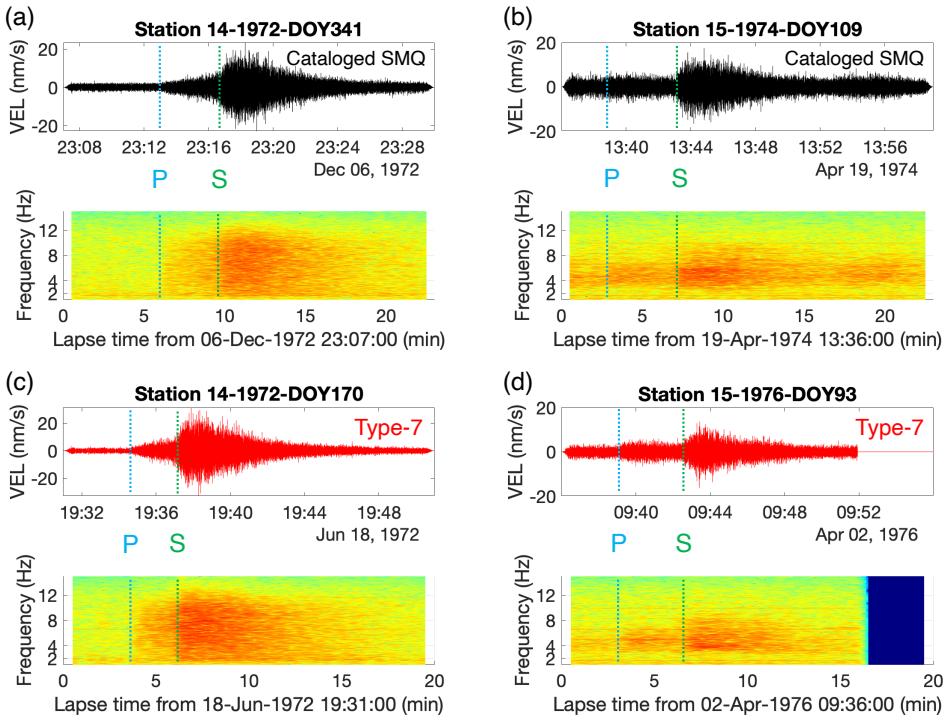

Figure 11. Waveforms and spectrograms for the cataloged shallow moonquakes (a-b) and the Type-7 events (c-d). The vertical lines indicate the P and S arrivals.

I display the waveforms of the cataloged and new shallow moonquakes in Figures 12a-f. The waveforms are aligned with the S – P arrival times. The remarkable point is that Station 15 has larger numbers of events compared to other stations, implying that the seismically active regions lie in the vicinity of the Apollo 15 landing site or the northern latitude from that site ($> 30°$N). Further discussion of the spatial variations in seismic activity can be found in Section 5.2.

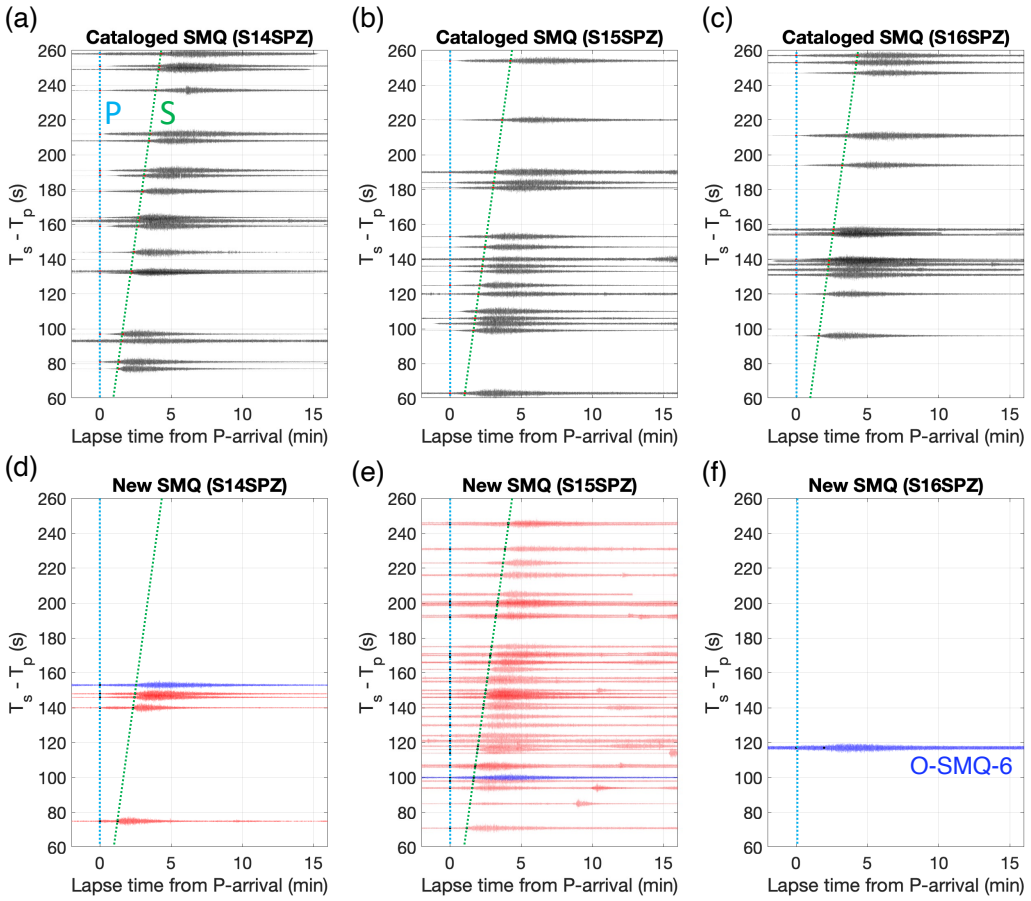

Figure 12. Waveforms of cataloged shallow moonquakes recorded in (a) Apollo 14 SPZ data, (b) Apollo 15 SPZ data, and (c) Apollo 16 SPZ data, and those of new shallow moonquakes detected in (d) Apollo 14 SPZ data, (e) Apollo 15 SPZ data, and (f) Apollo 16 SPZ data. In each panel, the horizontal axis shows the lapse time from the P arrival and the vertical axis shows the S − P arrival time. Two dotted lines indicate the P arrival (cyan) and the S arrival (green) for respective events. The blue waveform indicates the O-SMQ-6 event in Table A1 in Appendix A, which was detected at all stations with clear P and S arrivals.

4.4.2 Focal distance

The focal distance of new shallow moonquakes was computed using "get_tavel_times"" function in the Obspy module (Beyreuther et al., 2010). For the internal structure models, I assumed three models proposed by Garcia et al. (2019) (Figure 13a). I also took into account the uncertainty in the focal depth of shallow moonquakes (0 – 250 km: Nakamura et al., 1979; Gillet et al., 2017; Watters et al., 2019). The computed travel times for the P and S phases for different structure models and two focal depth cases are presented in Figure 13b. Note that the p and s phases were also considered for a deeper source (250 km). Possible ranges of focal distance for new shallow moonquakes were assessed by comparing the observed S – P times and those for the computed ones (Figure 13c). As a result, I found that the new shallow moonquakes ranged between 500 and 3500 km, which is similar to those of cataloged events (e.g., Nakamura et al., 1979; Oberst, 1987).

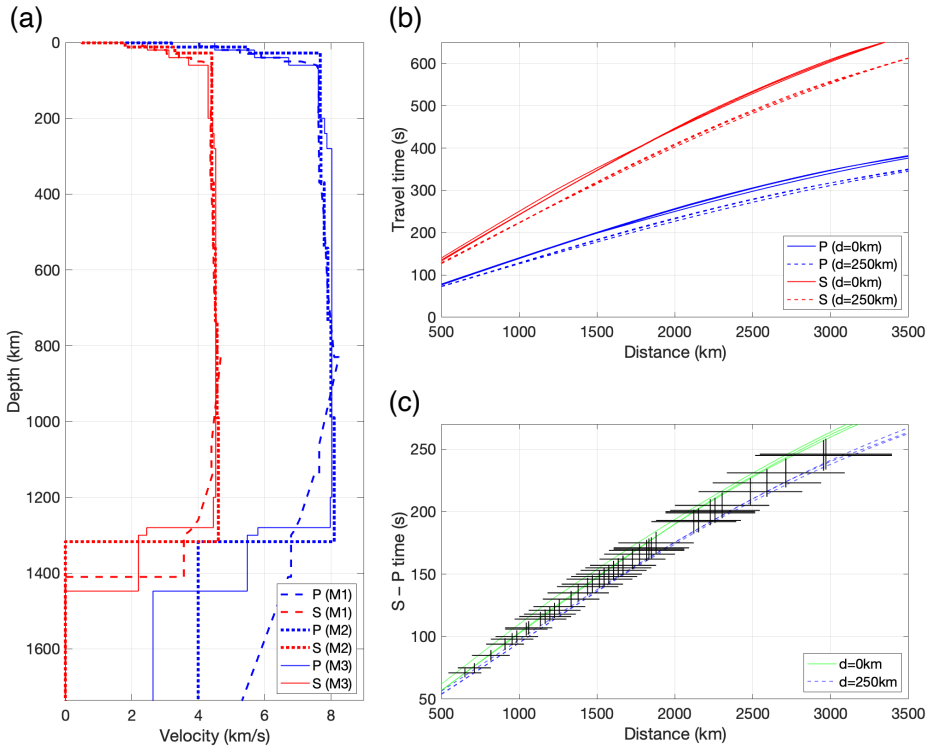

Figure 13. (a) Three lunar internal structure models (M1, M2, and M3) proposed by Garcia et al. (2019). (b) Travel time curves of P and S phases for three structure models in (a). The solid lines are for the case with a source depth of 0 km, and the dashed lines are for the case with a source depth of 250 km. (c) Expected distances for new shallow moonquakes. The green lines show S – P times for the case of 0 km source depth, and the blue lines show S – P times for the case of 250 km source depth. The cross plots represent the uncertainty of travel times and estimated distances for each shallow moonquake.

4.4.3 Source location of O-SMQ-6 event

As both P- and S-wave arrivals were identified at Station 14, 15, and 16 for the O-SMQ-6 event (Figure A4b in Appendix A), I estimated the epicentral distances from each station and located the source. Regarding O-SMQ-4 (another event detected at three stations), it was hard to determine the source location because of the low signal-to-noise ratio (Figure A4 in Appendix A). Figure 14a represents the estimated source location of O-SMQ-6. The colored arcs indicate the focal distances of O-SMQ-6 from each station (the color links to each station). The region within the yellow plots is the area where three arcs overlap (i.e., the possible epicenteral location of O-SMQ-6).

Figure 14b displays the close-up of the O-SMQ-6 source location. I found that several sources of the cataloged events were also situated in the same region. Among them, the O-SMQ-6 source overlaps one of the possible source locations of N-SMQ-14, implying the possibility of a "repeatable" shallow moonquake. The discussion about repeaters will be focused on in a future publication. At least, as far as I checked the similarity of the observed waveforms of O-SMQ-6 and N-SMQ-14, it does not seem that they share the same source.

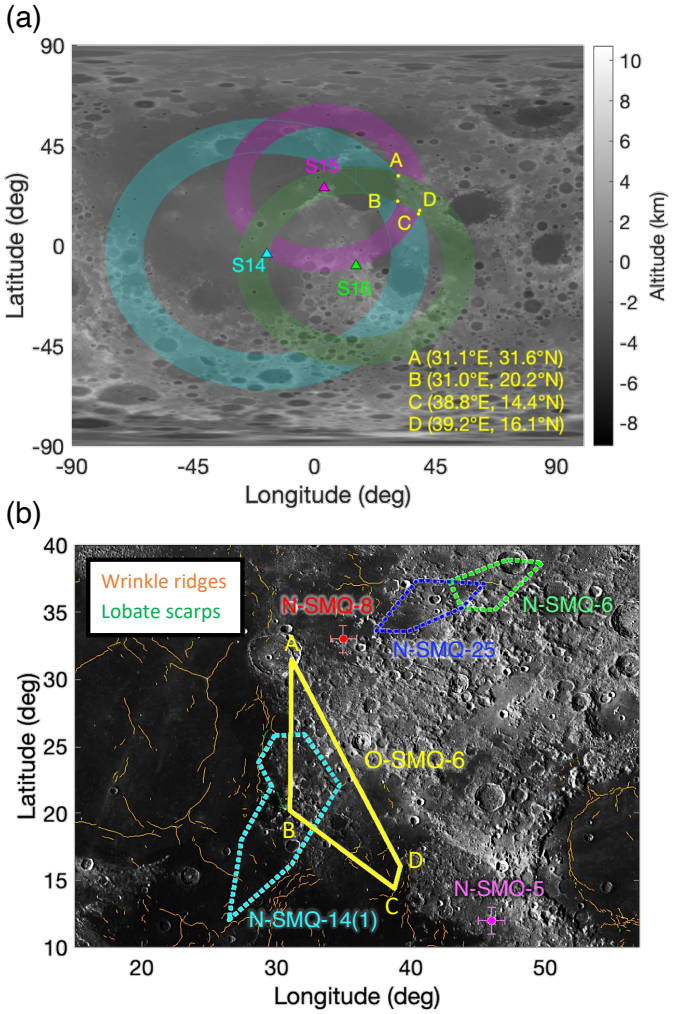

Figure 14. (a) Estimated source location of the O-SMQ-6 event. Each triangle shows the Apollo seismic station (cyan: S14, magenta: S15, and green: S16). See the text for more explanation. (b) Close-up around the O-SMQ-6 source location. The base image is taken by the Wide Angle Camera (WAC) of the Lunar Reconnaissance Orbiter Camera (Robinson et al., 2010). The orange and green lines show the wrinkle ridges and lobate scarps. The yellow area indicates the estimated source location of the O-SMQ-6. Each character (A - D) corresponds to the coordinates shown in panel (a). The other colored dotted areas and circles with error bars represent the source locations estimated by Nakamura et al. (1979) and Watters et al. (2019). Since N-SMQ-14 carries 180° ambiguity in latitude, one of two possible source sites is shown here (N-SMQ-14(1)).

Another notable point is that the shallow moonquake sources do not necessarily fall on the tectonic-related structures on the surface such as wrinkle ridges and lobate scarps (Figure 14b). This indicates that potential geological structures are required to account for these seismic events. Further discussion about the source mechanism is provided in Section 5.2 by referring to the gravity data.

4.4.4 Source parameters

Since shallow moonquakes show the highest similarity to earthquakes of all types of moonquakes, it is reasonable to assume that the same physical properties and dynamics as earthquakes are applicable to shallow moonquakes (e.g., Oberst, 1987). Here, following the approach applied to the cataloged shallow moonquakes by Goins et al. (1981) and Oberst (1987), I investigate the source parameters of new shallow moonquakes such as the energy release (E_{rel}), seismic moment (M_0), and stress drop ($\Delta\sigma$). According to Goins et al. (1981), each parameter can be written as:

$$E_{rel} = 4\pi R_{ray}^2 \rho v \frac{1}{2\pi} \frac{(4\pi)^3}{3} \Omega_0^2 f_c^3, \tag{3}$$

$$M_0 = 4\pi R_{ray} \rho v^3 \Omega_0, \tag{4}$$

$$\Delta\sigma = 12 M_0 f_c^3 / v^3, \tag{5}$$

where R_{ray} is focal distance, ρ is the density of a near-surface medium, v is wave propagation speed near the focal region of shallow moonquakes, Ω_0 is the amplitude of the source spectrum below the corner frequency f_c. When considering only the S-wave part in the analysis, by multiplying 3/4, Equations 3 and 4 becomes

$$E_{rel} = 32\pi^3 R_{ray}^2 \rho v \Omega_0^2 f_c^3, \tag{6}$$

$$M_0 = 3\pi R_{ray} \rho v^3 \Omega_0, \tag{7}$$

respectively (Oberst, 1987).

To obtain the key parameters such as Ω_0 and f_c, the displacement spectrum during a seismic event is usually used (e.g., Aki, 1967). Because of the uncertainties in several factors (e.g., source location, radiation pattern), some corrections need to be applied to the observed moonquakes' displacement spectrum. Combining the correction factors proposed by Oberst (1987) and general source terms, we can model the observed displacement spectrum of the entire event signal $A(\omega)$ as follows:

$$A(\omega) = I_{sp} \times I_{cor} \times I_{site} \times A^S(\omega) = \left(\frac{v}{v^*}\right)^{1/2} \times \Omega(\omega) \times e^{-\omega T_{tr}/2Q}, \tag{8}$$

where ω is the angular frequency, $A^S(\omega)$ is the displacement spectrum around the peak S-wave energy, $\Omega(\omega)$ is the source spectrum, v^* is the wave propagation speed below the scattering layer, T_{tr} is the travel time of S-wave, Q is the intrinsic quality factor near the seismic source. It is worth noting that we usually use the spectrum of the S-wave peak energy $A^S(\omega)$ instead of $A(\omega)$ because the P-wave energy level is often comparable with the noise level. I_{sp} (=2.1 for Apollo 14 and 2.3 for Apollo 15 and 16) is the empirical correction factor, which is defined as the ratio of the energy density of the entire event signal over the short-term energy density around the peak S-wave energy (Oberst, 1987). I_{cor} (=1.37) is the correction factor of the radiation pattern and the interaction of body waves with a free surface (see Goins et al. (1981) and Oberst (1987) for the details). I_{site} is the mean amplitude correction at the respective Apollo seismic stations. I_{site}=0.6, 1.3, and 1.1 for Apollo 14, 15, and 16, respectively (e.g., Oberst, 1987).

Solving Equation 8 for $\Omega(\omega)$ gives us

$$\Omega(\omega) = I_{sp} \times I_{cor} \times I_{site} \times \left(\frac{v}{v^*}\right)^{-1/2} \times A^S(\omega) \times e^{\omega T_{tr}/2Q}. \tag{9}$$

For the analysis, I trimmed a 54 s-long window near the peak S-wave energy as shown in the top panels in Figures 15a-b and computed the displacement spectrum $A^S(\omega)$. Assuming v=4.4 km/s, v^*=3.2 km/s (Garcia et al., 2019), ρ = 3000 kg/m^3 (Oberst, 1987), and Q = 15000 (Nakamura & Koyama, 1982) together with the corrections factors mentioned above (I_{sp}, I_{cor}, and I_{site}), I corrected $A^S(\omega)$ and obtained $\Omega(\omega)$ (the bottom panels in Figures 15a-b). The determination of Ω_0 is performed by averaging the amplitude

below a corner frequency f_c (Figure 15a). Note that the spectrum increases above 10 – 12 Hz, which is due to the correction of instrumental response. In other words, the signal above 10 Hz reaches the detection limit of the sensor. Some shallow moonquakes show a roll-off below 10 Hz in their displacement spectra (Figure 15a) and others stay flat until 10 Hz (Figure 15b). In the latter case, I preliminary assigned $f_c = 10$ Hz following the previous works (e.g., Goins et al., 1981; Nakamura et al., 1979; Oberst, 1987). Therefore, I stress that the source parameters (E_{ref}, M_0, $\Delta\sigma$) for some events are underestimated.

Combining the assumed parameters and the obtained Ω_0 and f_c with Equations 6, 7, and 5 brought me E_{ref}, M_0, and $\Delta\sigma$ (Table A1 in Appendix A). The relation between the released seismic energy (E_{rel}) and the body wave magnitude (m_b) is given by Richter (1958) as

$$\log_{10}(E_{rel} \times 10^7) = 5.8 + 2.4m_b. \tag{10}$$

Since it is uncertain whether Equation 10 is directly applicable to the Moon, I use it for the purpose of relative comparison in the following discussion. The computed m_b is listed in Table A1 in Appendix A.

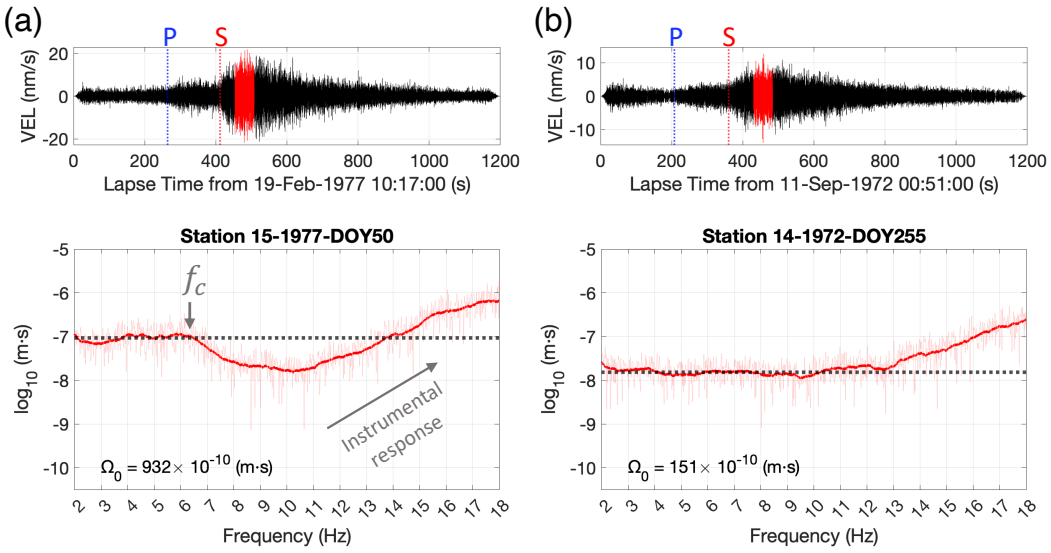

Figure 15. Examples of displacement spectra corrected for the instrumental response and anelastic attenuation effect. The top panels show the waveform of shallow moonquakes with the P and S arrivals. For the analyses, the S-wave energy part in red was used. The displacement spectrum of the S-wave energy part is presented in the bottom panels. The transparent red curves show the original spectrum and the solid red curves are the smoothed spectrum.

5 Updated Lunar Seismicity and Implications for Source Mechanism

5.1 Assessment of b-value of the Moon

On Earth, it is known that earthquakes obey the Gutenberg-Richter (G-L) law, where the number of quakes greater than magnitude m can be fitted with the following equation:

$$\log_{10}(N_m) = a - bm, \tag{11}$$

where N_m is the cumulative number of events whose magnitude is greater than m, a and b are constants. The constant b is called "b-value", and it takes almost 1 for earthquakes,

meaning that the occurrence rate of magnitude m events is 10 times higher than that of magnitude (m+1) events. Recently, Knapmeyer et al. (2023) showed that marsquakes also follow the G-R law (b=1.06).

In the case of the Moon, shallow moonquakes are often used to assess lunar seismicity because of the highest energy release and their similarity to the tectonic quakes on Earth (e.g., Banerdt et al., 2020). In previous works (e.g., Nakamura et al., 1979), the lunar b-value was estimated to be 0.5 – 0.6, which means that the small shallow quakes occur on the Moon less than predicted by the G-R law. However, by adding the newly discovered shallow moonquakes to the statistics, I found that they actually obey the G-R law (b=0.91, Figure 16). Although the large events ($m_b \geq 5.5$) stay at the same level as predicted before, the seismicity rate of the smaller ones ($m_b \leq 5$) is at least two times higher than considered before. It is worth mentioning that Figure 16 reflects the seismicity around the Apollo 15 sites rather than the global seismicity.

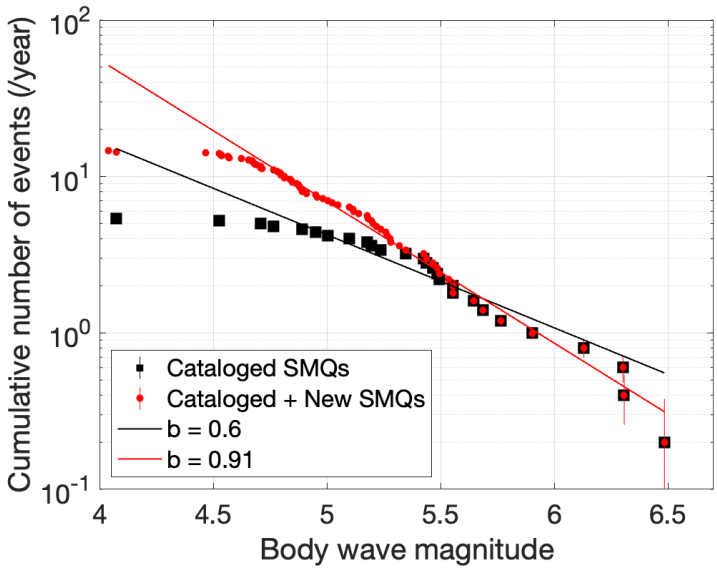

Figure 16. Cumulative number of shallow moonquakes per year against the minimum body wave magnitude (m_b). Note that m_b carries uncertainty in the absolute value and the relative value is more reliable. The black plots include only cataloged events, and the red plots include both cataloged and new shallow moonquakes. The fitting of the b-value was performed using the data between 4.7 and 6 in body wave magnitude.

5.2 Temporal and spatial distribution of shallow moonquakes

5.2.1 Relation with Earth-Moon distance

Lately, Watters et al. (2019) demonstrated that some of the re-located shallow moonquakes fall near young thrust faults — one of the evidence of recent tectonic activity. Additionally, they investigated the correlation between the time of shallow-moonquake occurrences and the Earth-Moon distance and found that the majority of them occur at the near-apogee distance ($\sim 4.0\times10^5$ km). Together with the fact that the surface degradation rate near the fault scarps is higher than in other regions, they concluded that the young thrust faults could be the prime source of shallow moonquakes.

By adding the new shallow moonquakes, I investigated whether the same conclusion as that of Watters et al. (2019) would be derived or not. Figure 17a represents the time evolution of the Earth-Moon (E-M) distance (d_{EM}) with the occurrence time of shallow moonquakes and the corresponding E-M distance plotted (red and green circles). Figure 17b represents the histogram of the shallow moonquakes occurring at the respective E-M distances. Here, I focus on the events whose E-M distances are larger than 4.0×10^5 km or smaller than 3.7×10^5 km (cyan and magenta area in Figure 17b) and computed the probability of shallow moonquake's occurrences at each range.

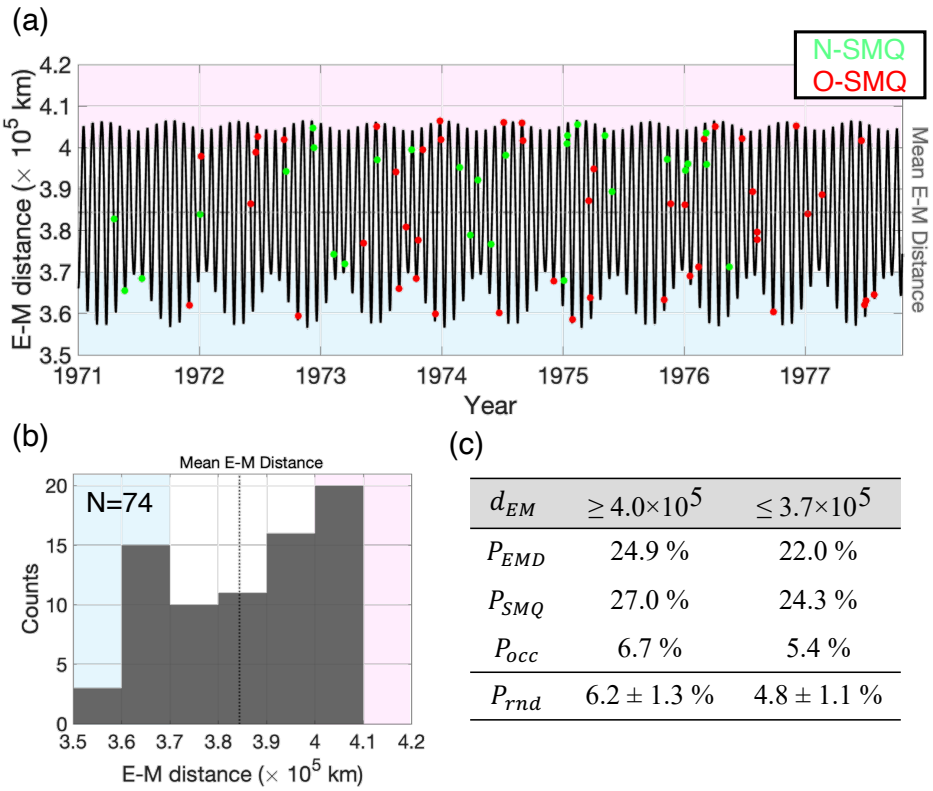

d_{EM}	$\geq 4.0\times10^5$	$\leq 3.7\times10^5$
P_{EMD}	24.9 %	22.0 %
P_{SMQ}	27.0 %	24.3 %
P_{occ}	6.7 %	5.4 %
P_{rnd}	6.2 ± 1.3 %	4.8 ± 1.1 %

Figure 17. (a) Time evolution of Earth-Moon distance computed with SPICE "mice_spkpos" function (C. H. Acton, 1996; C. Acton et al., 2018).The green and red plots correspond to the event times of the cataloged shallow moonquakes and those of the new shallow moonquakes, respectively. See the text about P_{EMD}. (b) Histogram of the Earth-Moon distance at the time of shallow moonquake's occurrences. N denotes the total number of the detected shallow moonquakes. (c) The parameter list of probabilities for the respective E-M distance cases. See the main text for the details of each parameter.

The occurrence probability (P_{occ}) can be assessed by multiplying the time dominant ratio for a given E-M distance range (P_{EMD}) and the ratio of the event number at the corresponding distance range over all the detected events (P_{SMQ}). For the case of $d_{EM} \geq 4.0 \times 10^5$ km, $P_{EMD} = 24.9\%$ and $P_{SMQ} = 27.0\%$, giving us $P_{occ} = 6.7\%$. In the same way, P_{occ} becomes 5.4% for $d_{EM} \leq 3.7 \times 10^5$ km (Figure 17c). To evaluate whether these estimates are statistically significant, I considered randomly occurring events. For computing the probability of random occurrences (P_{rnd}), I can approximate $P_{SMQ} = P_{EMD}$; therefore $P_{rnd}=(P_{EMD})^2$, resulting in 6.2% and 4.8% for the cases of $d_{EM} \geq 4.0\times10^5$ km and $d_{EM} \leq 3.7\times10^5$ km, respectively. After several numerical

tests of the random occurrences, I found an error range of about 1% (Figure 17c). The comparison of the obtained P_{occ} and P_{rnd} indicates that the shallow moonquakes occur "randomly" rather than correlating with the E-M distance (in other words, tidal stress). Thus, my results claim that shallow moonquakes occur randomly and the tidal stress does not play a significant role in driving them, which differs from the interpretation by Watters et al. (2019) and supports the conventional ideas (e.g., Nakamura, 1980).

5.2.2 Relation with tropical month

Frohlich and Nakamura (2006) investigated the relationship between the times for shallow moonquake occurrence and the sidereal or tropical month (both can be approximated as equal in several years periods). They found that the majority of shallow moonquakes occur during the tropical phase between $-90°$ and $+90°$ (see Figure 18a and green plots in Figure 18b), meaning that shallow moonquakes occur when a part of the lunar nearside faces a specific direction on the celestial sphere (between Leo and Virgo in this case). As a possible interpretation of this, Frohlich and Nakamura (2006) proposed collision of high energy particles from the extra-solar system, called nuclearite or strange quark matter (e.g., De Rújula & Glashow, 1984), as a seismic source.

Adding the new events on Figure 18b revealed that the majority of events occur between $-90°$ and $+180°$, indicating that shallow moonquakes do not necessarily occur at the time of the Moon facing in the direction of Leo and Virgo. Because the nuclearites do not have to come from the direction between Leo and Virgo solely, my results do not exclude their hypothesis. On the other hand, it has not been understood yet how the nuclearites produce the intra-earthquake-like waveforms of shallow moonquakes. Therefore, it is difficult to provide a solid conclusion on whether the nuclearite could be a source of shallow moonquakes at this moment.

Another notable point is that the number of shallow moonquakes is small between $-90°$ and $-180°$ in the tropical phase (yellow area in Figures 18a-b). Since the source locations of almost all new events have not been determined, it is hard to interpret this in detail (e.g., the relation between the tropical month phase, tidal stress state, and seismic source locations). Yet, there might be a particular phase in which shallow moonquakes are unlikely to be generated.

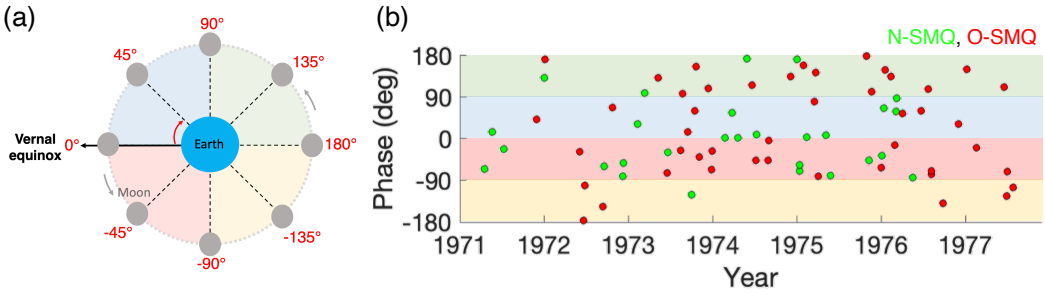

Figure 18. (a) Definition of tropical month phase. (b) Tropical month phase vs. Year for all detected shallow moonquakes. The green and red plots correspond to the cataloged and new events, respectively. The background color is linked with the quadrant in (a).

5.2.3 Regionality of seismicity and relation with geological features

The interpretation of the fact that more shallow moonquakes are detected at Station 15 than at other sites (Figure 12e) is that seismically active regions are possibly lo-

cated (a) in the vicinity of Station 15 and/or (b) in the higher latitude than 26°N. In fact, a similar discussion was given by Nakamura et al. (1979). They speculated that the source locations of shallow moonquakes were not randomly distributed but concentrated around the Apollo 12-14 and/or Apollo 15 sites (Figure 4). At that time, it was hard to claim which site was more seismically active. However, my results clearly suggest that the Apollo 15 site is more active than other Apollo landing sites and also raise the possibility that lunar seismicity largely varies from place to place.

To observe whether the regionality of seismicity correlates with geological features on the surface, I looked into the distribution of wrinkle ridges and lobate scarps — the morphology related to tectonic activities. According to Watters et al. (2019), shallow moonquakes are considered to be caused by these structures. Looking at Figure 19a, I found more numbers of ridges or scarps at Apollo 12 and 14 sites. If shallow moonquakes were related to these structures, they should be detected more at Station 12 or 14 than at other stations, which is inconsistent with our results (Figure 12). Furthermore, it seems strange that the source of the highest magnitude event (N-SMQ-1 in Figure 19a) does not coincide with particular geological structures seen on the surface.

While Watters et al. (2019) proposes a very shallow source (< 1 km), some studies indicate the possibility of a deeper source (50 – 250 km: Nakamura et al., 1979; Gillet et al., 2017). Seeking the likelihood of a deeper source, I checked gravity data and investigated underlying structures (e.g., dikes, intrusions). With the Gravity Recovery and Interior Laboratory (GRAIL) data, the Bouger gravitational gradient — the second derivative of the Buguer potential — was computed to clarify the spatial distribution of igneous intrusions.

Figure 19b shows the 2-D map of the gravitational gradients measured in Eötvös Unit ($= 10^{-9}$ s^{-2}), where the negative gradients (blue areas) correspond to the positive density anomalies. Especially, the linear negative gradient patterns are interpreted as dikes or vertical tabular intrusions (Andrews-Hanna et al., 2013). The largest igneous intrusion system is observed in the Procellarum KREEP Terrance (PKT) region, where heat-producing elements are highly concentrated (e.g., Andrews-Hanna et al., 2014). In particular, the thick intrusion areas near the border of the PKT region (white plots in Figure 19b) are considered to be the frozen remnants of lave-filled rifts formed by the extensions due to thermal stresses at the time of cooling in the PKT region (Andrews-Hanna et al., 2014). As observed on Earth, fault systems could develop, accompanied by igneous intrusions, becoming seismic sources. Since the thickest intrusion is found in the northeast part of the PKT region, it could be possible that a larger number of fault branches were developed within the crust in that area, generating more seismic events. Interestingly, the source of N-SMQ-1 (one of the largest quakes) falls near the thickest intrusion part. Given the presented evidence, it appears reasonable to think the large igneous intrusions or the fault system developed from them cause shallow moonquakes although this is still a qualitative hypothesis. I leave further discussions to future works (e.g., assessment of expected stress drops, sophisticated gravity data analysis).

6 Proposals for Future Seismic Observations on the Moon

Investigation of the Apollo SP data brought more than 22,000 new seismic events. Among them, shallow moonquakes are important events in terms of both science and human explorations. On the scientific side, because of their highest similarity to terrestrial tectonic quakes, they are the key to our understanding of the current lunar tectonism, which also contributes to better illustrating the history of thermal stresses and volcanisms (e.g., Andrews-Hanna et al., 2013, 2014). In addition, as shallow moonquakes are the most energetic events (10^4 times larger energy release than deep moonquakes; Goins et al., 1981), lunar seismicity is controlled by them. Thus, for the precise assessment of the global seismicity and the comparison with other planetary bodies, it is necessary to

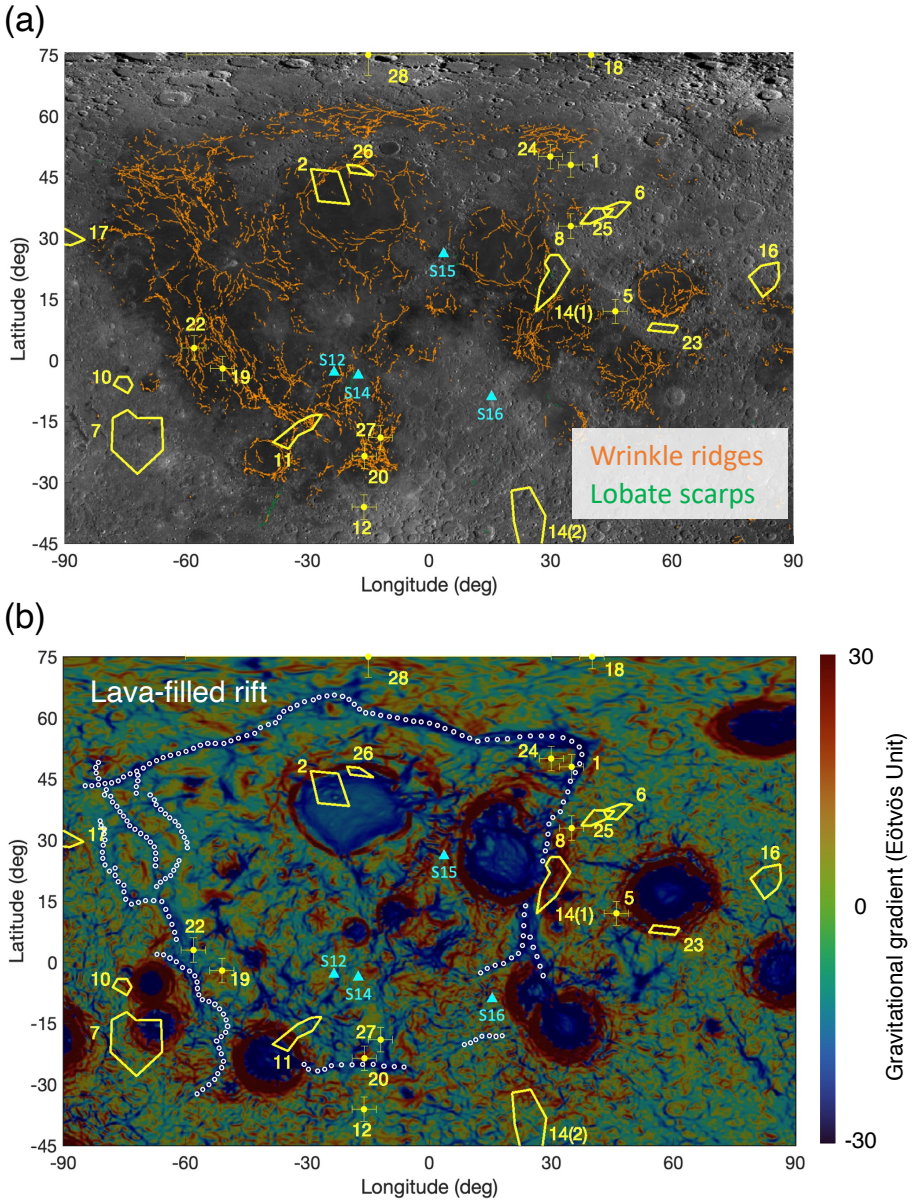

Figure 19. (a) Distribution of wrinkle ridges and lobate scarps on the nearside of the Moon. The original map was produced in LROC: QuickMap. The yellow areas and plots with error bars represent the locations of the cataloged shallow moonquake sources (Table 1). The cyan triangles are the positions of Apollo seismometers. (b) 2-D map of Bouger gravity gradients. The original data were retrieved from LROC: QuickMap. The white circles trace possible lava-filled rifts indicated by Andrews-Hanna et al. (2014).

investigate shallow moonquakes further. In fact, this point is important for future human exploration as well. For safe activities on the lunar surface, we need to assess and/or forecast the current geological activities on the Moon. The discussions in this study (e.g., Section 5.2) suggest that the activity level of moonquakes largely varies from place to place. In other words, once the hazard map is produced, it would be a strong support

for the site selections. For these reasons, I suppose shallow moonquakes would be one of the prime targets in future lunar seismic explorations.

Here, I would like to propose a possible strategy for efficient construction of the seismic network for the investigation of shallow moonquakes. The top panels in Figures 20a-b compare the cataloged and new shallow moonquakes' spectra. These panels indicate that the majority of the new shallow moonquakes show a smaller amplitude (10^{-7}–10^{-8} m/s/Hz$^{0.5}$), which leads to the low Signal-to-Noise (S/N) ratio when observed with the Apollo SP sensor in time series (the bottom panel in Figure 20b). This is the main reason that small shallow moonquakes were hard to detect.

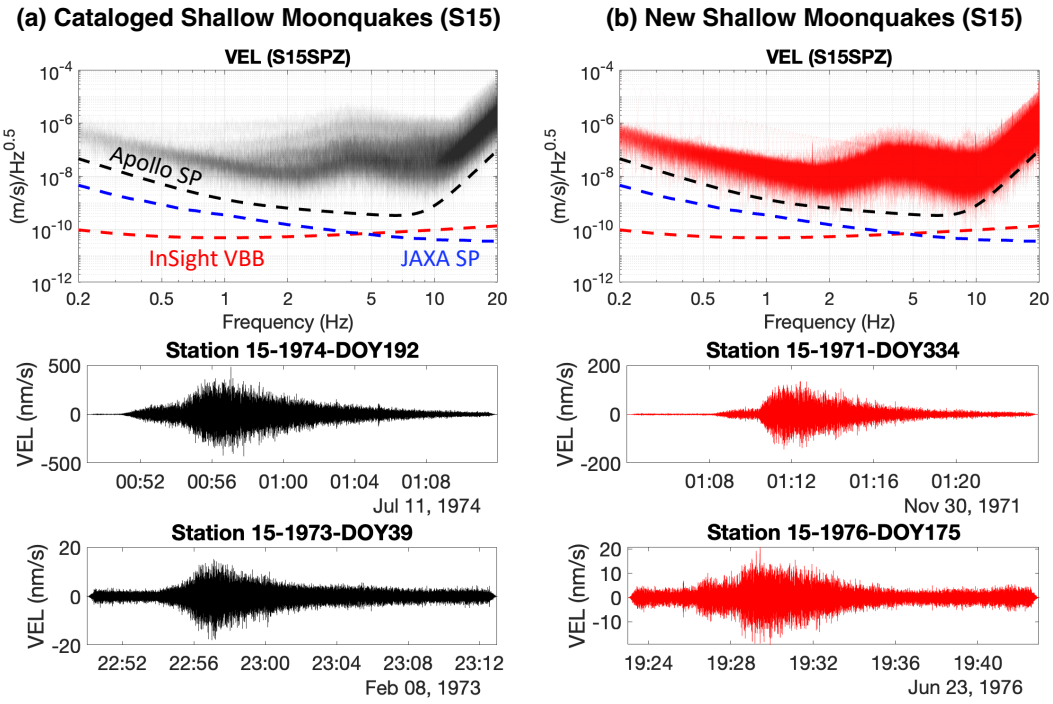

Figure 20. Comparison of the observed shallow moonquakes' amplitude spectral density (ASD) and the sensitivity curve of seismometers developed in planetary seismology (top), and two examples of the detected events (second and third rows). The left column is for the cataloged shallow moonquakes and the right is for the newly discovered shallow moonquakes in this study. In the top panel, the black and red solid lines show the amplitude spectral densities for the cataloged and newly discovered shallow moonquakes, and the black, blue, and red broken lines show the sensitivity curves of the Apollo Short-Period sensor (Latham et al., 1969), JAXA's Short-Period sensor (Yamada et al., 2013), and InSight's Very-Broad-Band sensor (Lognonné et al., 2019).

Better observations are expected by utilizing the present generation seismometers such as (a) Very Broad Band seismometer (VBB) — used in NASA's InSight mission (Lognonné et al., 2019) and under preparation for Farside Seismic Suite (FSS; Panning et al., 2022) and (b) JAXA's Short-Period (SP) seismometer – originally developed for the Japanese LUNAR-A mission (e.g., Mizutani et al., 2003) and now under preparation for NASA's Dragonfly mission to Titan (e.g., Lorenz et al., 2019). For the purpose of shallow moonquake detections, both seismometers have already achieved a high enough sensitivity (top panels in Figure 20). For the research on source mechanisms, with its

broadband sensitivity, the VBB sensor has the advantage of suppressing the intense scattering effect that is the main cause preventing us from obtaining information about polarization and seismic phases. On the other hand, although we need to embrace the scattering effect for JAXA's SP sensor, it gives us an option of multiple deployments with penetrators — hard-landing system developed for the LUNAR-A mission (e.g., Mizutani et al., 2003), resulting in by far an efficient construction of the seismic network. Fortunately, shallow moonquakes show relatively clear P- and S-wave arrivals in spite of their strongly scattered waves (e.g., Figures 11 and 20). Therefore, the network of JAXA's SP sensors (even with one vertical component) is good enough for locating their sources, which contributes to the seismicity assessment at different regions.

Ideally, the global network with broadband seismometers is preferable, yet it is not realistic on the Moon due to some unavoidable restrictions (e.g., weight, cost). A more realistic way is to construct a hybrid network using both VBB and JAXA's SP seismometers. Although the VBB seismometer requires careful treatment in the installation and is deployable only at one site per launch, an ideal observation would be realized once it is operated. Since a single station has difficulties in locating the seismic source, additional 3 – 4 JAXA's SP seismometers packaged in penetrators would function as supporting stations.

7 Concluding Remarks

In this study, I analyzed all available Apollo short-period seismic data to detect uncataloged moonquakes. Even though numerous spike noises contaminated the original SP data, a simple denoising process and a classical coherence analysis allowed me to detect more than 22,000 new lunar seismic events. It turned out that most of the newly discovered events shared the same characteristics as those of the cataloged moonquakes, such as thermal moonquakes, impact-induced events, and shallow moonquakes.

Focusing on shallow moonquakes — the most energetic and most similar events to terrestrial quakes, I re-evaluated lunar seismicity. While only 28 shallow moonquakes were discovered before this study, I found 46 new events whose body wave magnitude is smaller than those of the cataloged ones ($m_b \leq 5$). Increasing the event number in a smaller magnitude resulted in a higher b-value (0.91), demonstrating that the Gutenberg-Richter law is also applicable to the Moon besides the Earth and Mars. This suggests that there are more tectonic-related quakes, and the Moon is more geologically active than considered before.

Furthermore, the spatial distribution of shallow moonquakes gave me new insight that seismic activity level strongly differs from place to place. My results indicate that the northern hemisphere, where the thickest igneous intrusions exist, is more seismically active than other regions of the Moon. A statistical evaluation demonstrated that shallow moonquakes occur randomly and are not correlated with the E-M distance (i.e., tidal stress). These results imply that the surface fault activities triggered by tidal stresses are not the representative source mechanism for shallow moonquakes. Further quantitative source modeling and detailed investigation of gravity data may consolidate my hypothesis that the subsurface fault activities near igneous intrusions drive shallow moonquakes.

Because of their large energy release and shallow focal depth, it is considered that shallow moonquakes should affect human activities on the Moon. Thus, it is important to know their activity levels, focal mechanisms, and source locations. To improve our knowledge of shallow moonquakes, I proposed a hybrid seismic network combining both broadband and high shock-resistivity short-period seismometers, which gives us the option to construct the lunar seismic network efficiently.

8 Open Research

All the Apollo seismic data were retrieved from the International Federation of Digital Seismograph Networks (Nunn, 1969). Every tool used in the preprocessing is provided by Nunn et al. (2022). The SEIS data from the InSight mission used in this study can be retrieved through InSight Mars SEIS Data Service (2019) and InSight Marsquake Service (2022). The event catalog of new moonquakes is available at Onodera (2023).

Acknowledgments

This work was supported by JSPS KAKENHI Grant Number 23K13157. I would like to show my gratitude to Dr. Yosio Nakamura of University of Texas at Austin for discussing the results and checking the paper draft, which helped me enrich the discussion part. I acknowledge NASA, CNES, their partner agencies and Institutions (UKSA, SSO, DLR, JPL, IPGP-CNRS, ETHZ, IC, and MPS- MPG), and the flight operations team at JPL, SISMOC, MSDS, IRIS-DMC, and PDS for acquiring and providing InSight data, including SEED SEIS data.

Appendix A Supplementary Figures and Tables

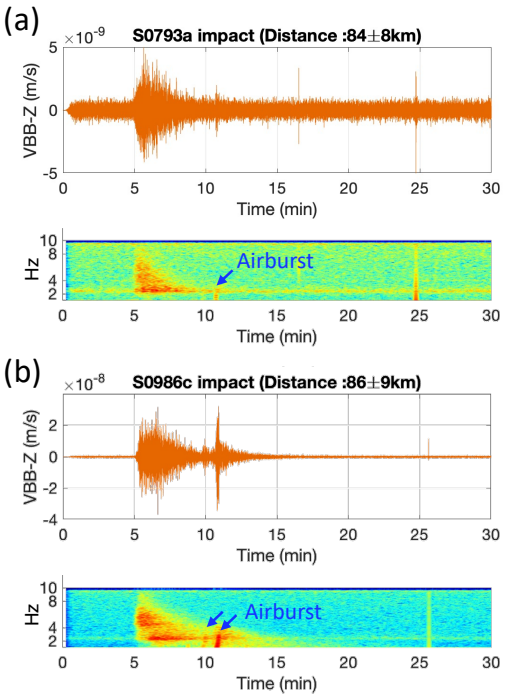

Figure A1. Waveforms and spectrograms for impact-induced seismic waves on Mars detected by the vertical component of InSight Very-Broad Band seismometer (VBB; Lognonné et al., 2019) on (a) Sol 793 and (b) Sol 986 (Sol means Martian day). The blue arrows indicate the acoustic signals generated by airbursts (see Garcia et al. (2022) for the details).

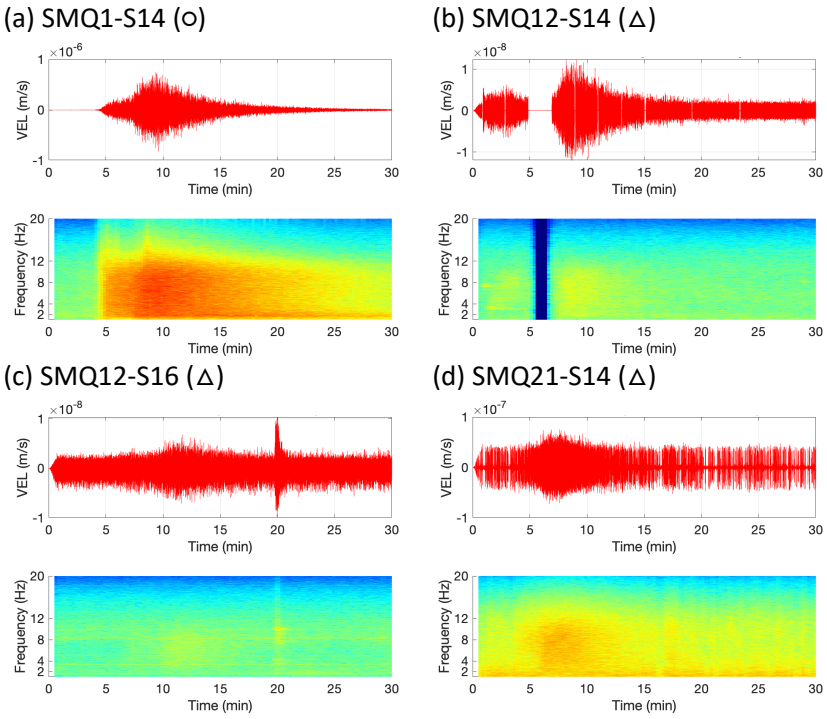

Figure A2. Example of velocity waveforms and spectrograms of shallow moonquakes listed in Table 1. (a) SMQ1 observed at Station 14, (b) SMQ12 observed at Station 14, (c) SMQ12 observed at Station 16, and (d) SMQ21 observed at Station 14. See Table 1 for the description of each symbol (◯ and △).

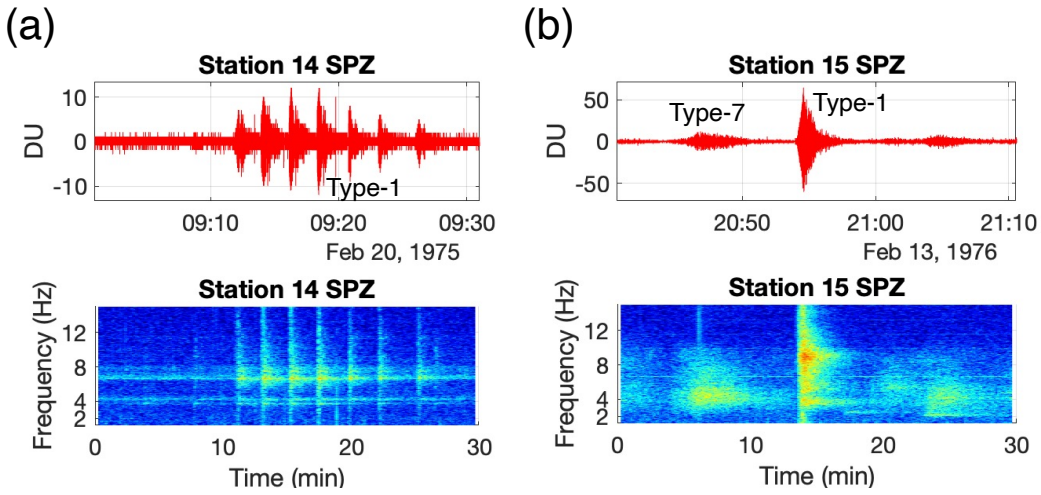

Figure A3. Examples of multiple event detections within a time window: (a) several successive Type-1 events and (b) simultaneous detection of Type-7 and Type-1 events.

Table A1. List of new shallow moonquakes

Event ID	Year	DOY	Start time (UTC)	T_s–T_p (s)	Focal distance (km)	Min. f_c (Hz)	Min. E_{rel} (J)	Min. M_0(Nm)	Min. $\Delta\sigma$ (MPa)	Min. m_b	Station
O-SMQ-1	1971	334	01:07:57	148±7.4	1545 ± 212	> 5.0	$> 1.2 \times 10^{12}$	$> 2.1 \times 10^{15}$	> 36.6	> 5.5	S15
O-SMQ-2	1972	005	22:42:33	148±7.4	1545 ± 212	> 10.0	$> 1.1 \times 10^{10}$	$> 7.0 \times 10^{13}$	> 9.8	> 4.7	S14 (+S15)
O-SMQ-3	1972	154	16:49:07	162±8.1	1727 ± 212	> 5.5	$> 2.7 \times 10^{11}$	$> 8.5 \times 10^{14}$	> 20.0	> 5.3	S15 (+S14)
O-SMQ-4	1972	170	19:34:31	146±7.3	1515 ± 212	> 10.0	$> 2.7 \times 10^{10}$	$> 1.1 \times 10^{14}$	> 15.4	> 4.8	S14 (+S15, S16)
O-SMQ-5	1972	176	12:27:49	243±12.2	2591 ± 348	> 4.0	$> 3.0 \times 10^{11}$	$> 1.4 \times 10^{15}$	> 13.0	> 5.3	S15
O-SMQ-6	1972	255	00:54:27	153±7.7	1606 ± 212	> 10.0	$> 5.9 \times 10^{9}$	$> 5.1 \times 10^{13}$	> 7.2	> 4.6	S14 (+S15, S16)
O-SMQ-7	1972	298	14:25:25	140±7.0	1439 ± 197	> 4.5	$> 4.9 \times 10^{9}$	$> 1.5 \times 10^{14}$	> 2.0	> 4.5	S14
O-SMQ-8	1973	129	11:02:13	200±10.0	2227 ± 288	> 5.5	$> 2.6 \times 10^{10}$	$> 2.6 \times 10^{14}$	> 6.2	> 4.8	S15
O-SMQ-9	1973	168	12:59:43	94±4.7	909 ± 121	> 5.0	$> 1.3 \times 10^{10}$	$> 2.2 \times 10^{14}$	> 6.2	> 4.8	S15
O-SMQ-10	1973	226	19:10:25	135±6.8	1379 ± 197	> 5.5	$> 2.1 \times 10^{10}$	$> 2.4 \times 10^{14}$	> 5.5	> 4.8	S15
O-SMQ-11	1973	236	04:07:35	85±4.3	818 ± 121	> 7.0	$> 2.2 \times 10^{10}$	$> 1.7 \times 10^{14}$	> 8.2	> 4.8	S15
O-SMQ-12	1973	257	04:31:37	71±3.6	651 ± 106	> 5.0	$> 1.1 \times 10^{10}$	$> 1.9 \times 10^{14}$	> 3.4	> 4.7	S15
O-SMQ-13	1973	287	23:07:04	201±10.1	2257 ± 288	> 7.0	$> 3.7 \times 10^{11}$	$> 6.9 \times 10^{14}$	> 33.4	> 5.3	S15
O-SMQ-14	1973	294	20:23:02	150±7.5	1576 ± 212	> 4.0	$> 3.5 \times 10^{10}$	$> 4.9 \times 10^{14}$	> 4.4	> 4.9	S15
O-SMQ-15	1973	307	17:37:13	231±11.6	2712 ± 379	> 5.0	$> 1.9 \times 10^{10}$	$> 2.6 \times 10^{14}$	> 4.5	> 4.8	S15
O-SMQ-16	1973	346	08:39:31	246±12.3	2969 ± 424	> 7.0	$> 2.7 \times 10^{11}$	$> 5.9 \times 10^{14}$	> 28.3	> 5.3	S15
O-SMQ-17	1973	360	07:37:04	114±5.7	1136 ± 167	> 4.5	$> 4.9 \times 10^{9}$	$> 1.5 \times 10^{14}$	> 2.0	> 4.5	S15
O-SMQ-18	1973	363	08:50:41	169±8.5	1818 ± 242	> 4.0	$> 8.2 \times 10^{10}$	$> 7.5 \times 10^{14}$	> 6.8	> 5.0	S15
O-SMQ-19	1974	172	19:17:30	98±4.9	954 ± 136	> 5.0	$> 5.7 \times 10^{9}$	$> 1.4 \times 10^{14}$	> 2.5	> 4.6	S15
O-SMQ-20	1974	187	18:44:53	75±3.8	712 ± 106	> 4.5	$> 3.1 \times 10^{8}$	$> 3.9 \times 10^{13}$	> 0.5	> 4.0	S14
O-SMQ-21	1974	242	10:47:49	107±5.4	1061 ± 152	> 6.0	$> 1.0 \times 10^{10}$	$> 1.5 \times 10^{14}$	> 4.4	> 4.7	S15
O-SMQ-22	1974	245	17:59:37	155±7.8	1636 ± 212	> 6.0	$> 3.9 \times 10^{10}$	$> 2.8 \times 10^{14}$	> 8.5	> 4.9	S15
O-SMQ-23	1974	338	03:43:17	157±7.9	1667 ± 212	> 4.0	$> 3.0 \times 10^{10}$	$> 4.6 \times 10^{14}$	> 4.1	> 4.9	S15
O-SMQ-24	1975	029	09:57:38	193±9.7	2151 ± 273	> 4.5	$> 3.2 \times 10^{10}$	$> 4.0 \times 10^{14}$	> 5.1	> 4.9	S15
O-SMQ-25	1975	078	03:05:53	142±7.1	1470 ± 197	> 4.5	$> 2.1 \times 10^{11}$	$> 1.1 \times 10^{15}$	> 13	> 5.2	S15
O-SMQ-26	1975	082	21:10:13	185±9.3	1879 ± 242	> 5.0	$> 1.9 \times 10^{11}$	$> 8.3 \times 10^{14}$	> 14.5	> 5.2	S15
O-SMQ-27	1975	093	05:21:57	166±8.3	1773 ± 227	> 7.0	$> 1.7 \times 10^{11}$	$> 4.7 \times 10^{14}$	> 22.8	> 5.2	S15
O-SMQ-28	1975	304	04:03:28	245±12.3	2954 ± 439	> 4.5	$> 7.1 \times 10^{10}$	$> 5.9 \times 10^{14}$	> 7.6	> 5.0	S15
O-SMQ-29	1975	325	16:10:49	170±8.5	1833 ± 227	> 5.0	$> 5.0 \times 10^{10}$	$> 4.2 \times 10^{14}$	> 7.4	> 5.0	S15
O-SMQ-30	1976	002	12:28:19	116±5.8	1167 ± 167	> 7.0	$> 1.4 \times 10^{11}$	$> 4.2 \times 10^{14}$	> 20.2	> 5.1	S15
O-SMQ-31	1976	018	13:20:35	118±5.9	1197 ± 167	> 5.0	$> 1.3 \times 10^{10}$	$> 2.1 \times 10^{14}$	> 3.7	> 4.7	S15
O-SMQ-32	1976	044	20:44:14	94±4.7	909 ± 121	> 5.0	$> 3.2 \times 10^{10}$	$> 3.4 \times 10^{14}$	> 5.9	> 4.9	S15
O-SMQ-33	1976	060	21:09:51	199±10.0	2227 ± 288	> 4.5	$> 1.2 \times 10^{10}$	$> 2.4 \times 10^{14}$	> 3.0	> 4.7	S15
O-SMQ-34	1976	093	09:39:05	215±10.8	2303 ± 303	> 5.5	$> 9.4 \times 10^{9}$	$> 1.6 \times 10^{14}$	> 3.7	> 4.7	S15
O-SMQ-35	1976	175	19:26:18	124±6.2	1257 ± 167	> 6.0	$> 2.1 \times 10^{10}$	$> 2.1 \times 10^{14}$	> 6.2	> 4.8	S15
O-SMQ-36	1976	206	17:24:10	140±7.0	1439 ± 197	> 4.0	$> 2.7 \times 10^{10}$	$> 4.3 \times 10^{14}$	> 3.9	> 4.8	S15
O-SMQ-37	1976	220	0:18:59	121±6.1	1227 ± 167	> 5.0	$> 7.9 \times 10^{9}$	$> 1.7 \times 10^{14}$	> 2.9	> 4.6	S15
O-SMQ-38	1976	220	15:19:07	192±9.6	2121 ± 273	> 5.0	$> 2.2 \times 10^{10}$	$> 2.8 \times 10^{14}$	> 4.9	> 4.8	S15
O-SMQ-39	1976	269	22:22:25	166±8.3	1773 ± 227	> 5.0	$> 3.3 \times 10^{9}$	$> 1.1 \times 10^{14}$	> 1.9	> 4.5	S15
O-SMQ-40	1976	337	12:45:41	146±7.3	1515 ± 212	> 7.5	$> 1.2 \times 10^{11}$	$> 3.6 \times 10^{14}$	> 21.2	> 5.1	S15
O-SMQ-41	1977	008	16:20:31	146±7.3	1515 ± 212	> 10.0	$> 2.9 \times 10^{11}$	$> 3.6 \times 10^{14}$	> 50.6	> 5.3	S15
O-SMQ-42	1977	050	10:21:24	148±7.4	1545 ± 212	> 6.5	$> 5.7 \times 10^{10}$	$> 3.0 \times 10^{14}$	> 11.8	> 5.0	S15
O-SMQ-43	1977	169	15:37:25	106±5.3	1045 ± 136	> 6.0	$> 2.0 \times 10^{10}$	$> 2.0 \times 10^{14}$	> 6.2	> 4.8	S15
O-SMQ-44	1977	179	02:13:40	130±6.5	1333 ± 182	> 5.0	$> 1.1 \times 10^{10}$	$> 1.9 \times 10^{14}$	> 3.4	> 4.7	S15
O-SMQ-45	1977	183	02:01:29	171±8.6	1848 ± 242	> 5.0	$> 1.2 \times 10^{11}$	$> 6.5 \times 10^{14}$	> 11.4	> 5.1	S15
O-SMQ-46	1977	207	18:19:45	216±10.8	2485 ± 333	> 5.5	$> 3.3 \times 10^{10}$	$> 3.0 \times 10^{14}$	> 7.0	> 4.9	S15

manuscript submitted to *JGR: Planets*

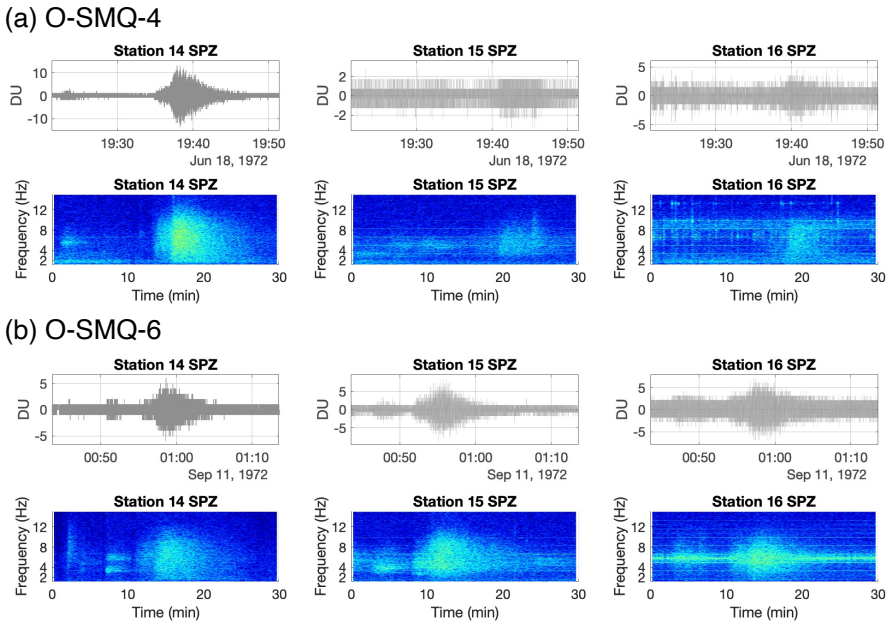

Figure A4. Waveforms and spectrograms for (a) O-SMQ-4 and (b) O-SMQ-6 events.

Appendix B Redundancy of false detections

To quantitatively evaluate the envelope shape, I computed the RMS envelopes of the candidates detected through the coherence analysis in Section 3.3. The moving average was done with a time window of 3.8 s (200 data points), and the RMS amplitude was normalized with the maximum amplitude value. Figures B1a-c show examples of three different types of signal (spike noise, moonquake, and step-like noise). In the case of a spiky signal, the median amplitude value gets small (~ 0.01, Figure B1a). On the other hand, a step-like signal returns a higher median value (~ 1, Figure B1c). Typically, moonquakes take a median value of 0.2 (Figure B1b). In the analysis, I regarded the signals with a median value of the normalized RMS envelope between 0.015 and 0.8 as natural event signals (i.e., candidate signals).

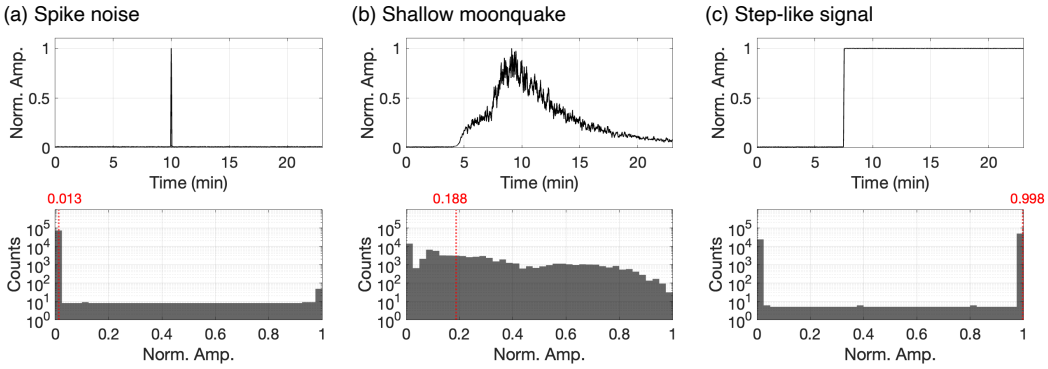

Figure B1. Examples of the normalized RMS envelopes (top) and the amplitude histograms (bottom) for (a) spike noise, (b) shallow moonquake, and (c) step-like signal. The red text and dotted line in the bottom panels show the median value.

References

Acton, C., Bachman, N., Semenov, B., & Wright, E. (2018). A look towards the future in the handling of space science mission geometry. *Planetary and Space Science*, *150*, 9-12. (Enabling Open and Interoperable Access to Planetary Science and Heliophysics Databases and Tools) doi: https://doi.org/10.1016/j.pss.2017.02.013

Acton, C. H. (1996). Ancillary data services of nasa's navigation and ancillary information facility. *Planetary and Space Science*, *44*(1), 65-70. (Planetary data system) doi: https://doi.org/10.1016/0032-0633(95)00107-7

Aki, K. (1967). Scaling law of seismic spectrum. *Journal of Geophysical Research (1896-1977)*, *72*(4), 1217-1231. doi: https://doi.org/10.1029/JZ072i004p01217

Andrews-Hanna, J. C., Asmar, S. W., Head, J. W., Kiefer, W. S., Konopliv, A. S., Lemoine, F. G., ... Zuber, M. T. (2013). Ancient igneous intrusions and early expansion of the moon revealed by grail gravity gradiometry. *Science*, *339*(6120), 675-678. doi: 10.1126/science.1231753

Andrews-Hanna, J. C., Besserer, J., Head III, J. W., Howett, C. J. A., Kiefer, W. S., Lucey, P. J., ... Zuber, M. T. (2014). Structure and evolution of the lunar procellarum region as revealed by grail gravity data. *Nature*, *514*(7520), 68-71. doi: 10.1038/nature13697

Araki, H., Tazawa, S., Noda, H., Ishihara, Y., Goossens, S., Sasaki, S., ... Shum, C. (2009). Lunar global shape and polar topography derived from kaguya-lalt laser altimetry. *Science*, *323*(5916), 897-900. doi: 10.1126/science.1164146

Banerdt, W. B., Smrekar, S. E., Banfield, D., Giardini, D., Golombek, M., Johnson, C. L., ... Wieczorek, M. (2020). Initial results from the insight mission on mars. *Nature Geoscience*, *13*(3), 183-189. Retrieved from `https://doi.org/10.1038/s41561-020-0544-y` doi: 10.1038/s41561-020-0544-y

Beyreuther, M., Barsch, R., Krischer, L., Megies, T., Behr, Y., & Wassermann, J. (2010). ObsPy: A Python Toolbox for Seismology. *Seismological Research Letters*, *81*(3), 530-533. doi: 10.1785/gssrl.81.3.530

Binder, A. B., & Oberst, J. (1985). High stress shallow moonquakes: evidence for an initially totally molten moon. *Earth and Planetary Science Letters*, *74*(2), 149-154. doi: https://doi.org/10.1016/0012-821X(85)90018-4

Blanchette-Guertin, J.-F., Johnson, C. L., & Lawrence, J. F. (2012). Investigation of scattering in lunar seismic coda. *Journal of Geophysical Research: Planets*, *117*(E6). doi: https://doi.org/10.1029/2011JE004042

De Rújula, A., & Glashow, S. L. (1984). Nuclearites—a novel form of cosmic radiation. *Nature*, *312*(5996), 734-737. doi: 10.1038/312734a0

Duennebier, F., & Sutton, G. H. (1974a). Meteoroid impacts recorded by the short-period component of apollo 14 lunar passive seismic station. *Journal of Geophysical Research (1896-1977)*, *79*(29), 4365-4374. doi: https://doi.org/10.1029/JB079i029p04365

Duennebier, F., & Sutton, G. H. (1974b). Thermal moonquakes. *Journal of Geophysical Research (1896-1977)*, *79*(29), 4351-4363. doi: https://doi.org/10.1029/JB079i029p04351

Frohlich, C., & Nakamura, Y. (2006). Possible extra-solar-system cause for certain lunar seismic events. *Icarus*, *185*(1), 21-28. doi: https://doi.org/10.1016/j.icarus.2006.07.002

Garcia, R. F., Daubar, I. J., Beucler, É., Posiolova, L. V., Collins, G. S., Lognonné, P., ... Banerdt, W. B. (2022). Newly formed craters on mars located using seismic and acoustic wave data from insight. *Nature Geoscience*, *15*(10), 774-780. doi: 10.1038/s41561-022-01014-0

Garcia, R. F., Khan, A., Drilleau, M., Margerin, L., Kawamura, T., Sun, D., ... Zhu, P. (2019). Lunar seismology: An update on interior structure models. *Space Science Reviews*, *215*(8), 50. doi: 10.1007/s11214-019-0613-y

Gillet, K., Margerin, L., Calvet, M., & Monnereau, M. (2017). Scattering attenuation profile of the moon: Implications for shallow moonquakes and the structure of the megaregolith. *Physics of the Earth and Planetary Interiors*, *262*, 28-40. doi: https://doi.org/10.1016/j.pepi.2016.11.001

Goins, N. R., Dainty, A. M., & Toksöz, M. N. (1981). Seismic energy release of the moon. *Journal of Geophysical Research: Solid Earth*, *86*(B1), 378-388. doi: https://doi.org/10.1029/JB086iB01p00378

Gudkova, T., Lognonné, P., & Gagnepain-Beyneix, J. (2011). Large impacts detected by the apollo seismometers: Impactor mass and source cutoff frequency estimations. *Icarus*, *211*(2), 1049-1065. doi: https://doi.org/10.1016/j.icarus.2010.10.028

InSight Mars SEIS Data Service. (2019). *SEIS raw data, InSight mission.* IPGP, JPL, CNES, ETHZ, ICL, MPS, ISAE-Supaero, LPG, MFSC. doi: 10.18715/SEIS.INSIGHT.XB_2016

InSight Marsquake Service. (2022). *Mars Seismic Catalogue, InSight Mission; V12 2022-10-01.* ETHZ, IPGP, JPL, ICL, Univ. Bristol. doi: 10.12686/A18

Kawamura, T., Lognonné, P., Nishikawa, Y., & Tanaka, S. (2017). Evaluation of deep moonquake source parameters: Implication for fault characteristics and thermal state. *Journal of Geophysical Research: Planets*, *122*(7), 1487-1504. doi: https://doi.org/10.1002/2016JE005147

Kawamura, T., Morota, T., Kobayashi, N., & Tanaka, S. (2011). Cratering asymmetry on the moon: New insight from the apollo passive seismic experiment. *Geophysical Research Letters*, *38*(15). doi: https://doi.org/10.1029/2011GL048047

Knapmeyer, M., Stähler, S., Plesa, A.-C., Ceylan, S., Charalambous, C., Clinton, J., ... Banerdt, W. B. (2023). The global seismic moment rate of mars after event s1222a. *Geophysical Research Letters*, *50*(7), e2022GL102296. doi: https://doi.org/10.1029/2022GL102296

Knapmeyer-Endrun, B., & Hammer, C. (2015). Identification of new events in apollo 16 lunar seismic data by hidden markov model-based event detection and classification. *Journal of Geophysical Research: Planets*, *120*(10), 1620-1645. doi: https://doi.org/10.1002/2015JE004862

Lammlein, D. R., Latham, G. V., Dorman, J., Nakamura, Y., & Ewing, M. (1974). Lunar seismicity, structure, and tectonics. *Reviews of Geophysics*, *12*(1), 1-21. doi: https://doi.org/10.1029/RG012i001p00001

Latham, G., Ewing, M., Dorman, J., Press, F., Toksoz, N., Sutton, G., ... Yates, M. (1970). Seismic data from man-made impacts on the moon. *Science*, *170*(3958), 620–626.

Latham, G., Ewing, M., Press, F., & Sutton, G. (1969). The apollo passive seismic experiment. *Science*, *165*(3890), 241-250.

Latham, G., McDonald, W. G., & Moore, H. J. (1970). Missile impacts as sources of seismic energy on the moon. *Science*, *168*(3928), 242–245.

Le Feuvre, M., & Wieczorek, M. A. (2008). Nonuniform cratering of the terrestrial planets. *Icarus*, *197*(1), 291-306. doi: https://doi.org/10.1016/j.icarus.2008.04.011

Lognonné, P., Banerdt, W. B., Giardini, D., Pike, W. T., Christensen, U., Laudet, P., ... Wookey, J. (2019). Seis: Insight's seismic experiment for internal structure of mars. *Space Science Reviews*, *215*(1), 12. doi: 10.1007/s11214-018-0574-6

Lorenz, R., Panning, M., Stähler, S., Shiraishi, H., Yamada, R., Turtle, E., et al. (2019). Titan seismology with dragonfly: Probing the internal structure of the most accessible ocean world. In *Lunar and planetary science conference* (Vol. 50, p. 2173).

McGarr, A., Latham, G. V., & Gault, D. E. (1969). Meteoroid impacts as sources of seismicity on the moon. *Journal of Geophysical Research (1896-1977)*, *74*(25),

5981-5994. doi: https://doi.org/10.1029/JB074i025p05981

Menina, S., Margerin, L., Kawamura, T., Heller, G., Drilleau, M., Xu, Z., ... Banerdt, W. B. (2023). Stratification of heterogeneity in the lithosphere of mars from envelope modeling of event s1222a and near impacts: Interpretation and implications for very-high-frequency events. *Geophysical Research Letters*, *50*(7), e2023GL103202. doi: https://doi.org/10.1029/2023GL103202

Mizutani, H., Fujimura, A., Tanaka, S., Shiraishi, H., & Nakajima, T. (2003). Lunar-a mission: Goals and status. *Advances in Space Research*, *31*(11), 2315-2321. doi: https://doi.org/10.1016/S0273-1177(03)00542-8

Nakamura, Y. (1980). Shallow moonquakes: How they compare with earthquakes. In *Proceedings of lunar and planetary science conference* (p. 1847-1853).

Nakamura, Y. (2005). Farside deep moonquakes and deep interior of the moon. *Journal of Geophysical Research: Planets*, *110*(E1). doi: https://doi.org/10.1029/2004JE002332

Nakamura, Y., & Koyama, J. (1982). Seismic q of the lunar upper mantle. *Journal of Geophysical Research: Solid Earth*, *87*(B6), 4855-4861. doi: https://doi.org/10.1029/JB087iB06p04855

Nakamura, Y., Latham, G. V., & Dorman, H. J. (1982). Apollo lunar seismic experiment—final summary. *Journal of Geophysical Research: Solid Earth*, *87*(S01), A117-A123. doi: https://doi.org/10.1029/JB087iS01p0A117

Nakamura, Y., Latham, G. V., Dorman, H. J., & Harris, J. E. (1981). *Passive seismic experiment long period event catalog (ver. 1008c).* UTIG Technical Report, No. 118. Retrieved from `http://www-udc.ig.utexas.edu/external/yosio/PSE/catsrepts/`

Nakamura, Y., Latham, G. V., Dorman, H. J., Ibrahim, A.-B. K., Koyama, J., & Horvath, P. (1979). Shallow moonquakes: Depth, distribution and implications as to the present state of the lunar interior. In *Proceedings of lunar and planetary science conference* (p. 2299-2309).

Nunn, C. (1969). *Apollo passive seismic experiments.* International Federation of Digital Seismograph Networks. Retrieved from `https://www.fdsn.org/networks/detail/XA_1969/` doi: 10.7914/SN/XA_1969

Nunn, C., Garcia, R. F., Nakamura, Y., Marusiak, A. G., Kawamura, T., Sun, D., ... Zhu, P. (2020). Lunar seismology: A data and instrumentation review. *Space Science Reviews*, *216*(5), 89. doi: 10.1007/s11214-020-00709-3

Nunn, C., Nakamura, Y., Kedar, S., & Panning, P. P. (2022). A new archive of apollo's lunar seismic data. *Planet. Sci. J.*, *3*(219), 1-10.

Oberst, J. (1987). Unusually high stress drops associated with shallow moonquakes. *Journal of Geophysical Research: Solid Earth*, *92*(B2), 1397-1405. doi: https://doi.org/10.1029/JB092iB02p01397

Oberst, J., Christou, A., Suggs, R., Moser, D., Daubar, I., McEwen, A., ... Robinson, M. (2012). The present-day flux of large meteoroids on the lunar surface—a synthesis of models and observational techniques. *Planetary and Space Science*, *74*(1), 179-193. (Scientific Preparations For Lunar Exploration) doi: https://doi.org/10.1016/j.pss.2012.10.005

Oberst, J., & Nakamura, Y. (1989). A New Estimate of the Meteoroid Impact Flux on the Moon. In *Lunar and planetary science conference* (Vol. 20, p. 802). Retrieved from `https://ui.adsabs.harvard.edu/abs/1989LPI....20..802O`

Oberst, P. J., & Nakamura, Y. (1987). Distinct meteoroid families identified on the lunar seismograms. *Journal of Geophysical Research: Solid Earth*, *92*(B4), E769-E773. doi: https://doi.org/10.1029/JB092iB04p0E769

Onodera, K. (2023). *High frequency moonquake catalog.* Zenodo. doi: 10.5281/zenodo.8373651

Onodera, K., Kawamura, T., Tanaka, S., Ishihara, Y., & Maeda, T. (2021). Numerical simulation of lunar seismic wave propagation: Investigation of subsurface scattering properties near apollo 12 landing site. *Journal of Geophysical*

Research: Planets, *126*(3), e2020JE006406. doi: https://doi.org/10.1029/2020JE006406

Onodera, K., Kawamura, T., Tanaka, S., Ishihara, Y., & Maeda, T. (2022). Quantitative evaluation of the lunar seismic scattering and comparison between the earth, mars, and the moon. *Journal of Geophysical Research: Planets*, *127*(12), e2022JE007558. doi: https://doi.org/10.1029/2022JE007558

Onodera, K., Maeda, T., Nishida, K., Kawamura, T., Margerin, L., Menina, S., ... Banerdt, W. B. (2023). Seismic scattering and absorption properties of mars estimated through coda analysis on a long-period surface wave of s1222a marsquake. *Geophysical Research Letters*, *50*(13), e2022GL102716. doi: https://doi.org/10.1029/2022GL102716

Panning, M., Kedar, S., Bowles, N., Calcutt, S., Drilleau, M., Garcia, R., ... Wilhelm, A. (2022). Farside Seismic Suite (FSS): First-ever seismology on the farside of the Moon and a model for long-lived lunar science. In *European planetary science congress* (p. EPSC2022-672). doi: 10.5194/epsc2022-672

Posiolova, L. V., Lognonné, P., Banerdt, W. B., Clinton, J., Collins, G. S., Kawamura, T., ... Zenhäusern, G. (2022). Largest recent impact craters on mars: Orbital imaging and surface seismic co-investigation. *Science*, *378*(6618), 412-417. doi: 10.1126/science.abq7704

Rajšić, A., Miljković, K., Wójcicka, N., Collins, G. S., Onodera, K., Kawamura, T., ... Daubar, I. J. (2021). Numerical simulations of the apollo s-ivb artificial impacts on the moon. *Earth and Space Science*, *8*(12), e2021EA001887. doi: https://doi.org/10.1029/2021EA001887

Richter, C. F. (1958). *Elementary seismology.* San Francisco, United States: W. H. Freeman.

Robinson, M. S., Brylow, S. M., Tschimmel, M., Humm, D., Lawrence, S. J., Thomas, P. C., ... Hiesinger, H. (2010). Lunar reconnaissance orbiter camera (lroc) instrument overview. *Space Science Reviews*, *150*(1), 81-124. doi: 10.1007/s11214-010-9634-2

Speyerer, E. J., Povilaitis, R. Z., Robinson, M. S., Thomas, P. C., & Wagner, R. V. (2016). Quantifying crater production and regolith overturn on the moon with temporal imaging. *Nature*, *538*(7624), 215-218. doi: 10.1038/nature19829

Wagner, R., Nelson, D., Plescia, J., Robinson, M., Speyerer, E., & Mazarico, E. (2017). Coordinates of anthropogenic features on the moon. *Icarus*, *283*, 92-103. (Lunar Reconnaissance Orbiter - Part II) doi: https://doi.org/10.1016/j.icarus.2016.05.011

Watters, T. R., Weber, R. C., Collins, G. C., Howley, I. J., Schmerr, N. C., & Johnson, C. L. (2019). Shallow seismic activity and young thrust faults on the moon. *Nature Geoscience*, *12*(6), 411-417. doi: 10.1038/s41561-019-0362-2

Weber, R. C., Bills, B. G., & Johnson, C. L. (2009). Constraints on deep moonquake focal mechanisms through analyses of tidal stress. *Journal of Geophysical Research: Planets*, *114*(E5). doi: https://doi.org/10.1029/2008JE003286

Yamada, R., Garcia, R. F., Lognonné, P., Kobayashi, N., Takeuchi, N., Nébut, T., ... Ganepain-Beyneix, J. (2013). On the possibility of lunar core phase detection using new seismometers for soft-landers in future lunar missions. *Planetary and Space Science*, *81*, 18-31. doi: https://doi.org/10.1016/j.pss.2013.03.009

Figure1.

(a)

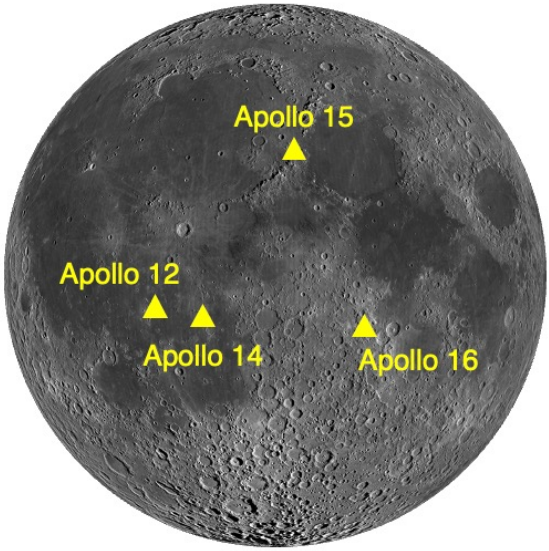

(b)

PSE station	Lat. (°N)	Lon. (°E)
Apollo 12	-3.0099	336.5752
Apollo 14	-3.64408	342.52233
Apollo 15	26.13174	3.63803
Apollo 16	-8.9759	15.4986

(c)

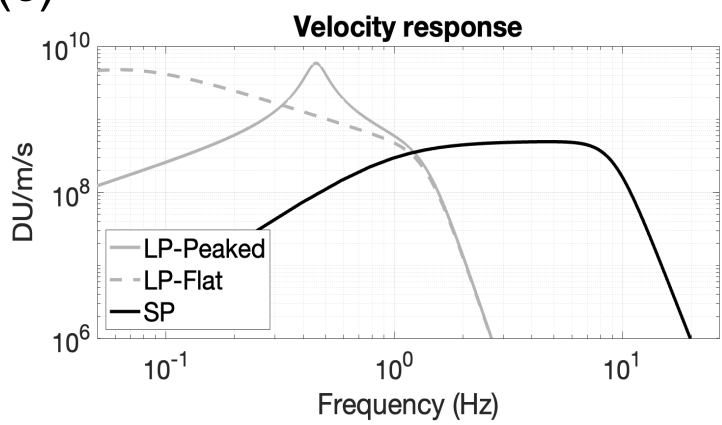

Figure2.

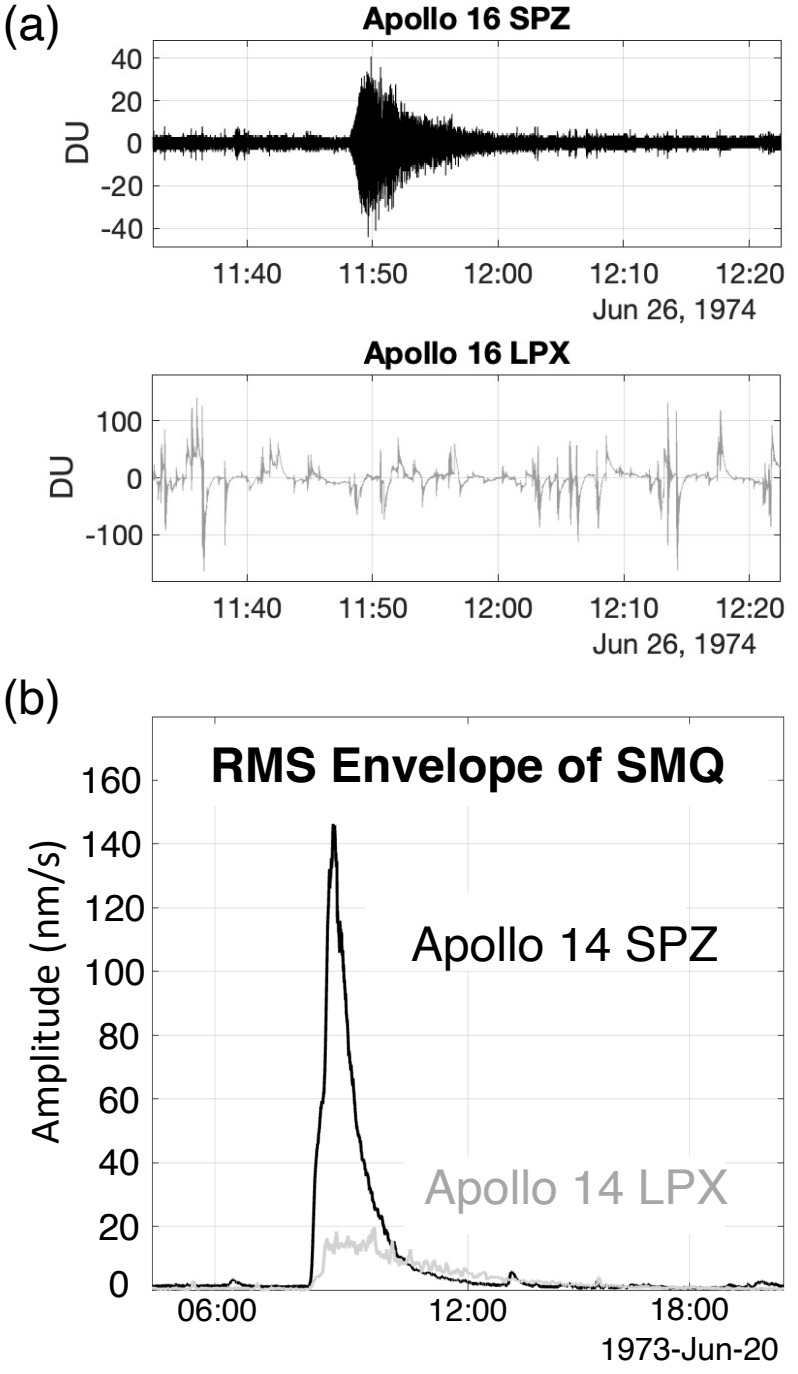
(a)
Apollo 16 SPZ
DU
40
20
0
-20
-40
11:40
11:50
12:00
12:10
12:20
Jun 26, 1974
Apollo 16 LPX
DU
100
0
-100
11:40
11:50
12:00
12:10
12:20
Jun 26, 1974
(b)
RMS Envelope of SMQ
Amplitude (nm/s)
160
140
120
100
80
60
40
20
0
Apollo 14 SPZ
Apollo 14 LPX
06:00
12:00
18:00
1973-Jun-20

Figure3.

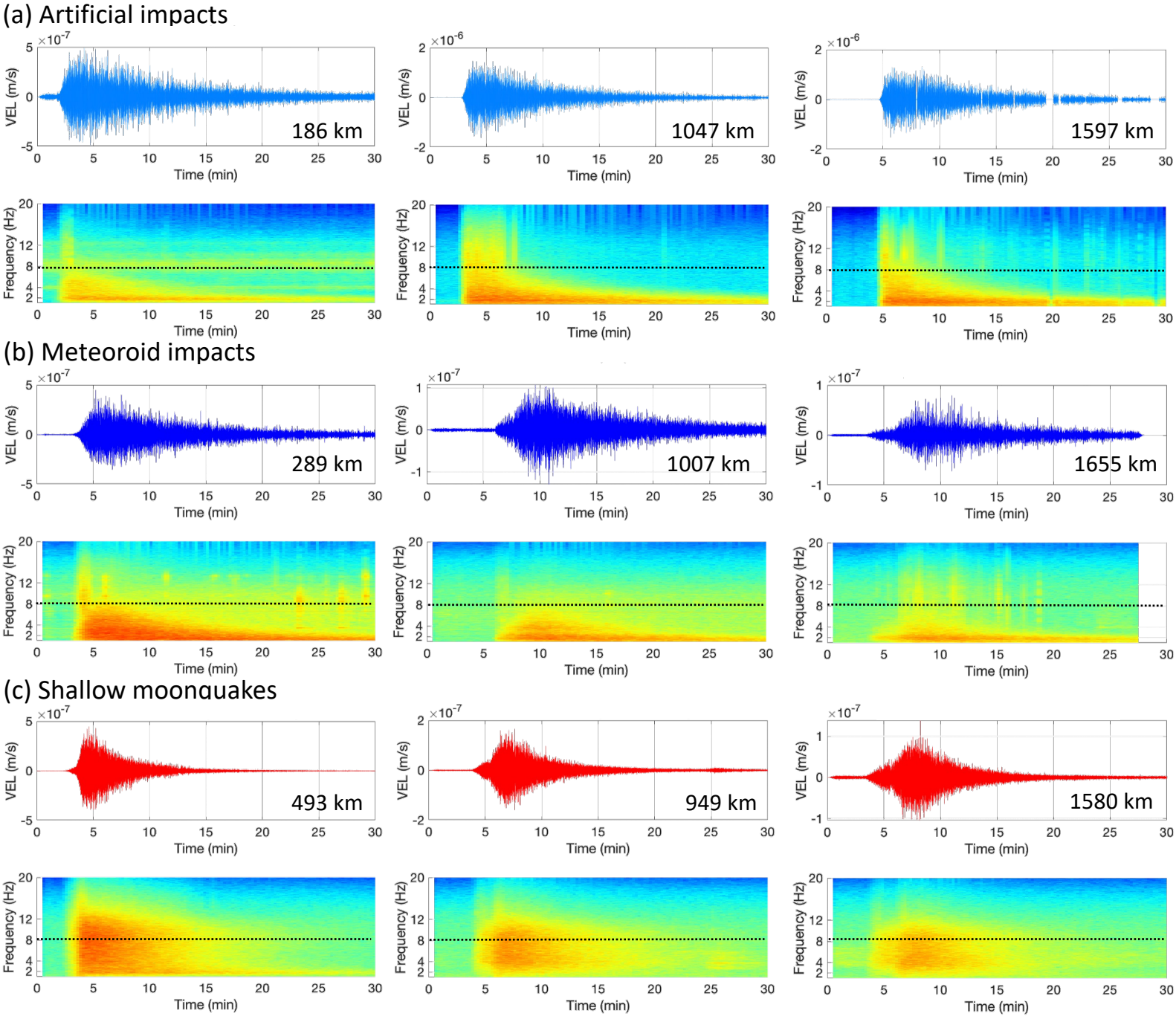
(a) Artificial impacts
186 km
1047 km
1597 km
(b) Meteoroid impacts
289 km
1007 km
1655 km
(c) Shallow moonquakes
493 km
949 km
1580 km
VEL (m/s)
Frequency (Hz)
Time (min)

Figure4.

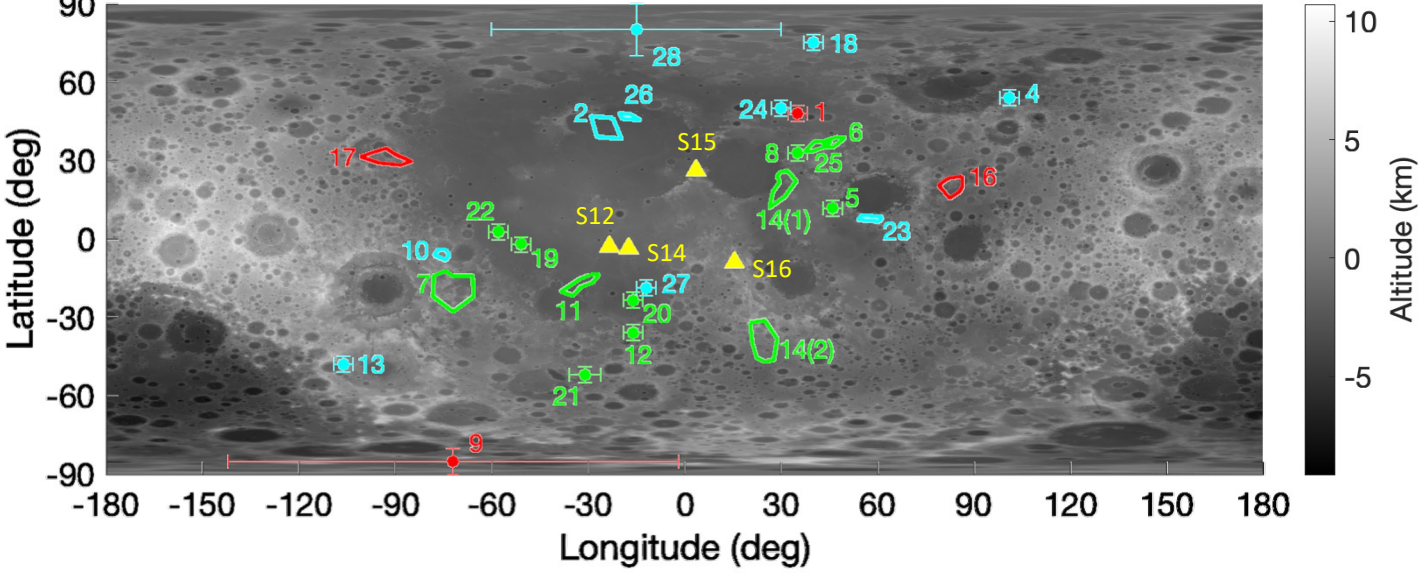
Latitude (deg)
Longitude (deg)
Altitude (km)
90
60
30
0
-30
-60
-90
-180
-150
-120
-90
-60
-30
0
30
60
90
120
150
180
10
5
0
-5
28
18
26
2
24
1
4
S15
6
8
25
17
16
14(1)
5
22
S12
23
10
19
S14
S16
27
11
20
7
12
14(2)
13
21
9

Figure5.

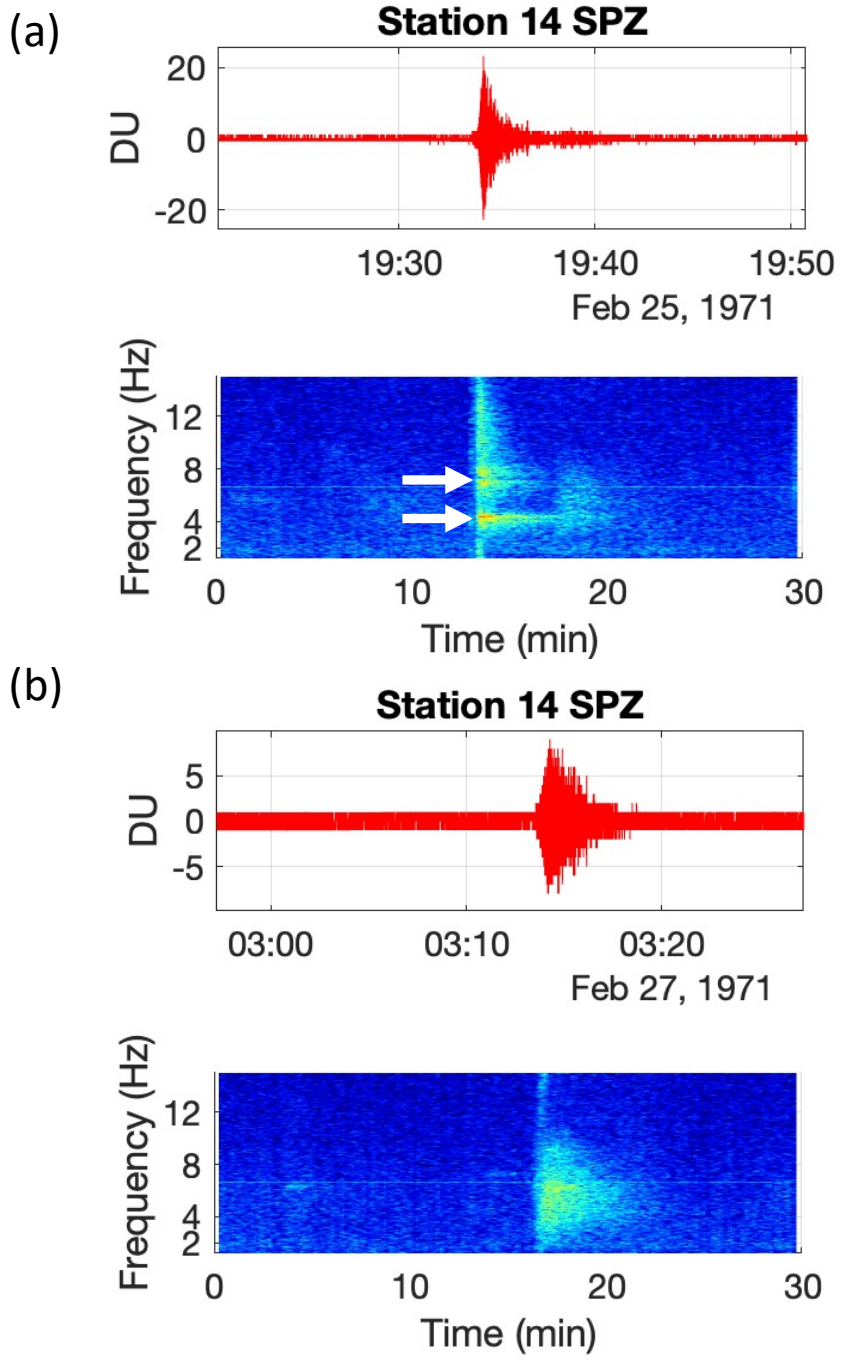
(a)
Station 14 SPZ
DU
20
0
-20
19:30
19:40
19:50
Feb 25, 1971
Frequency (Hz)
12
8
4
2
0
10
20
30
Time (min)
(b)
Station 14 SPZ
DU
5
0
-5
03:00
03:10
03:20
Feb 27, 1971
Frequency (Hz)
12
8
4
2
0
10
20
30
Time (min)

Figure6.

S14 SPZ (1971-04-17T00:00:00 – 1971-04-07T23:59:59)

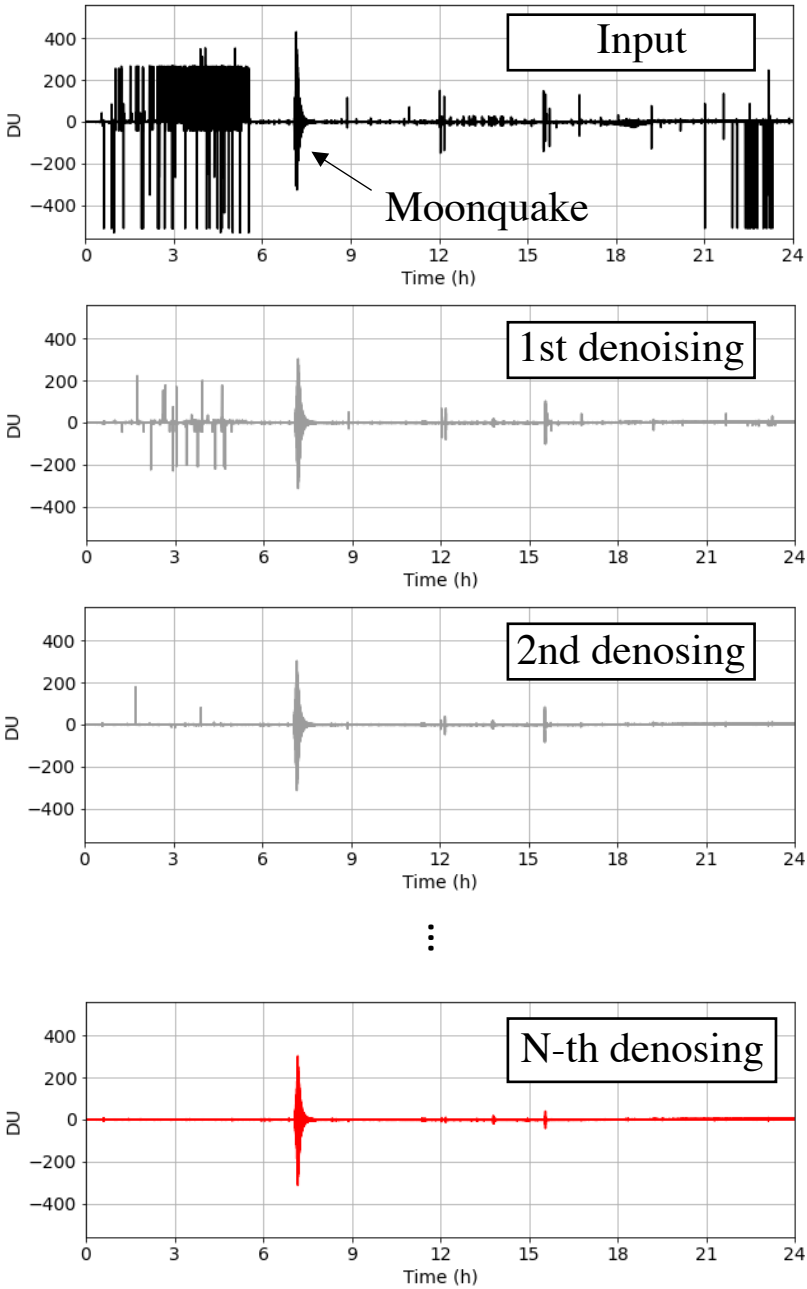

Figure7.

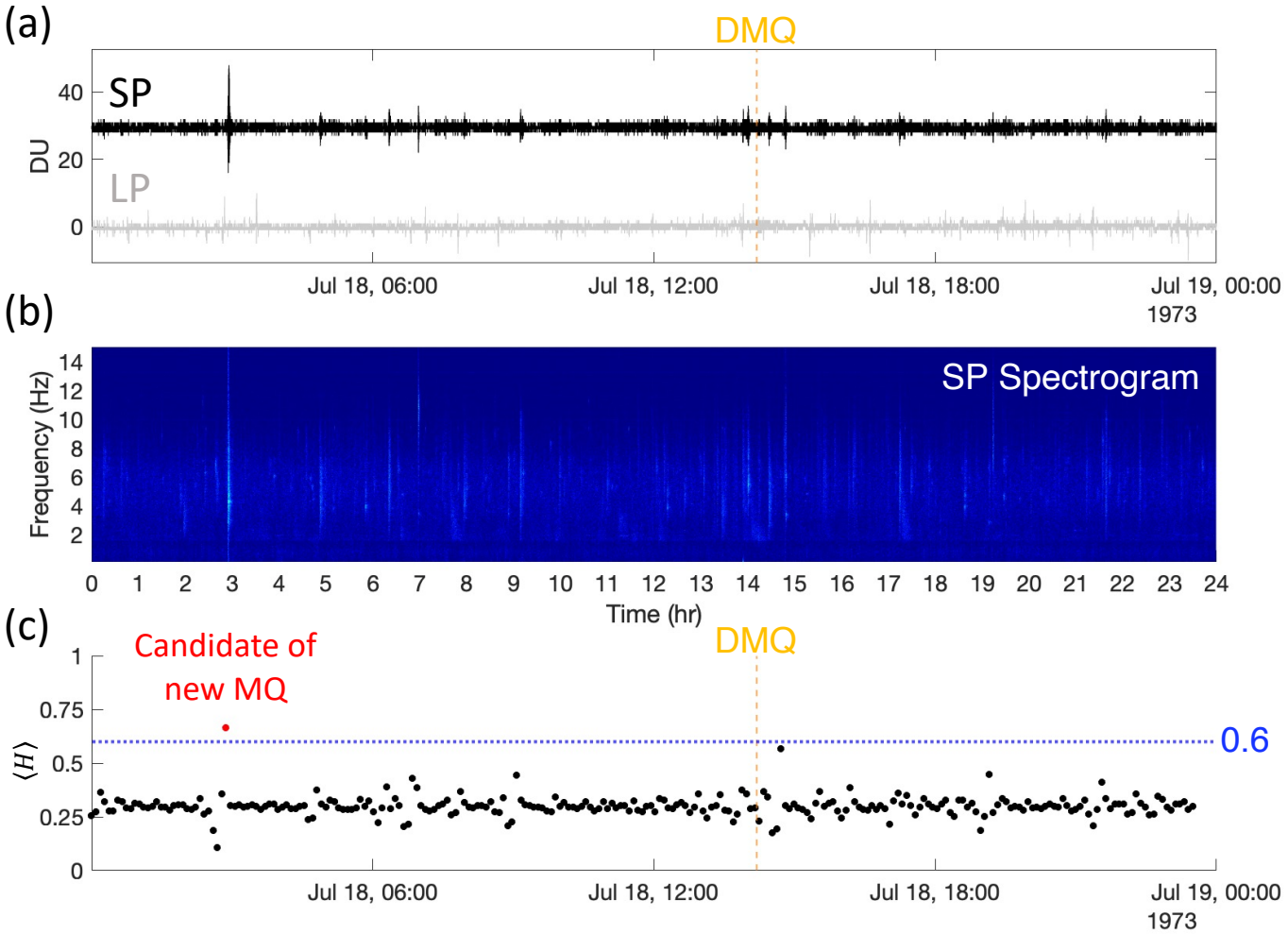
(a)
DMQ
SP
LP
DU
40
20
0
Jul 18, 06:00
Jul 18, 12:00
Jul 18, 18:00
Jul 19, 00:00
1973
(b)
SP Spectrogram
Frequency (Hz)
14
12
10
8
6
4
2
0 1 2 3 4 5 6 7 8 9 10 11 12 13 14 15 16 17 18 19 20 21 22 23 24
Time (hr)
(c)
Candidate of
new MQ
DMQ
0.6
⟨H⟩
1
0.75
0.5
0.25
0
Jul 18, 06:00
Jul 18, 12:00
Jul 18, 18:00
Jul 19, 00:00
1973

Figure8.

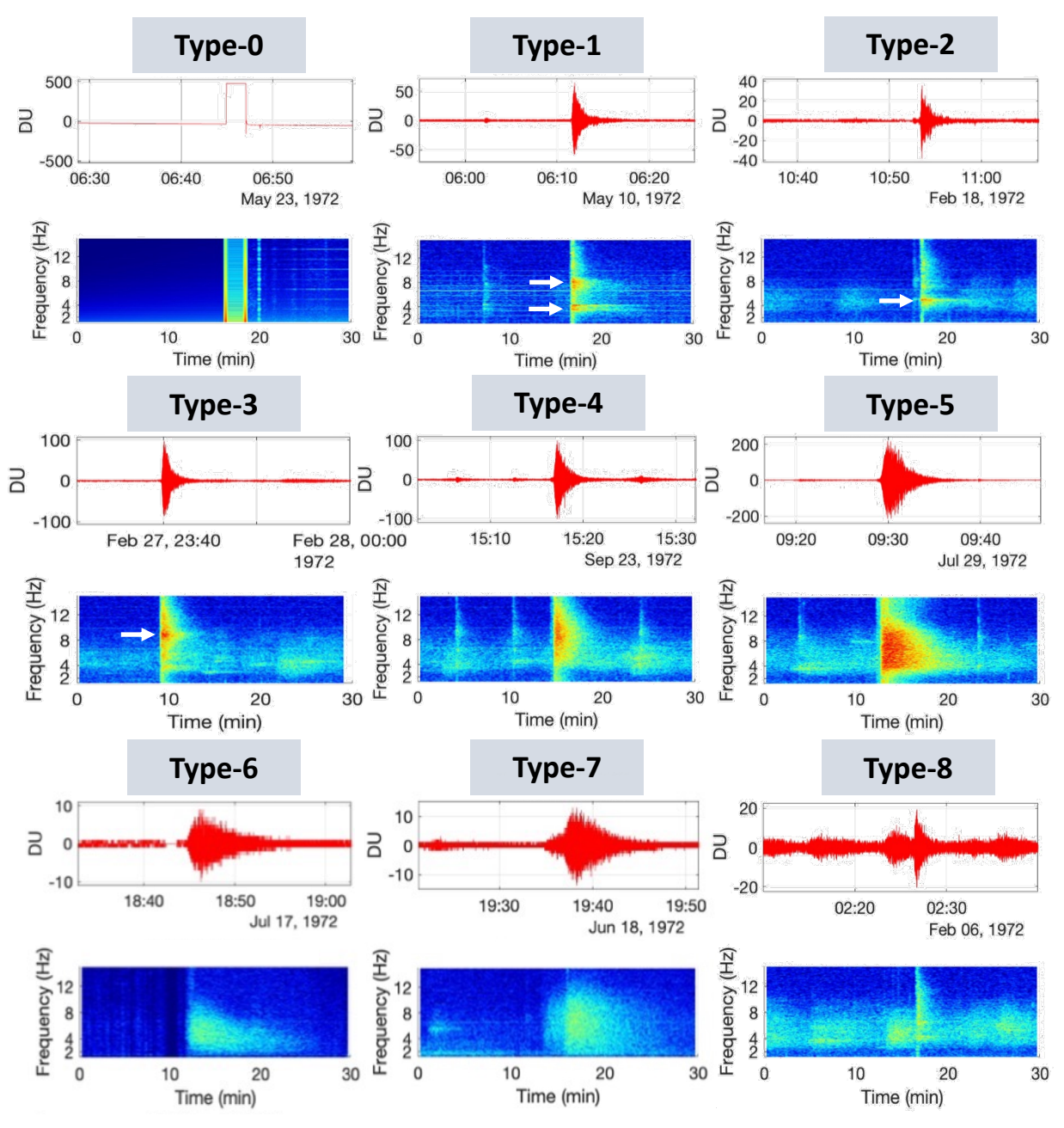
Type-0
Type-1
Type-2
Type-3
Type-4
Type-5
Type-6
Type-7
Type-8
DU
Frequency (Hz)
Time (min)
May 23, 1972
May 10, 1972
Feb 18, 1972
Feb 27, 23:40
Feb 28, 00:00
1972
Sep 23, 1972
Jul 29, 1972
Jul 17, 1972
Jun 18, 1972
Feb 06, 1972

Figure9.

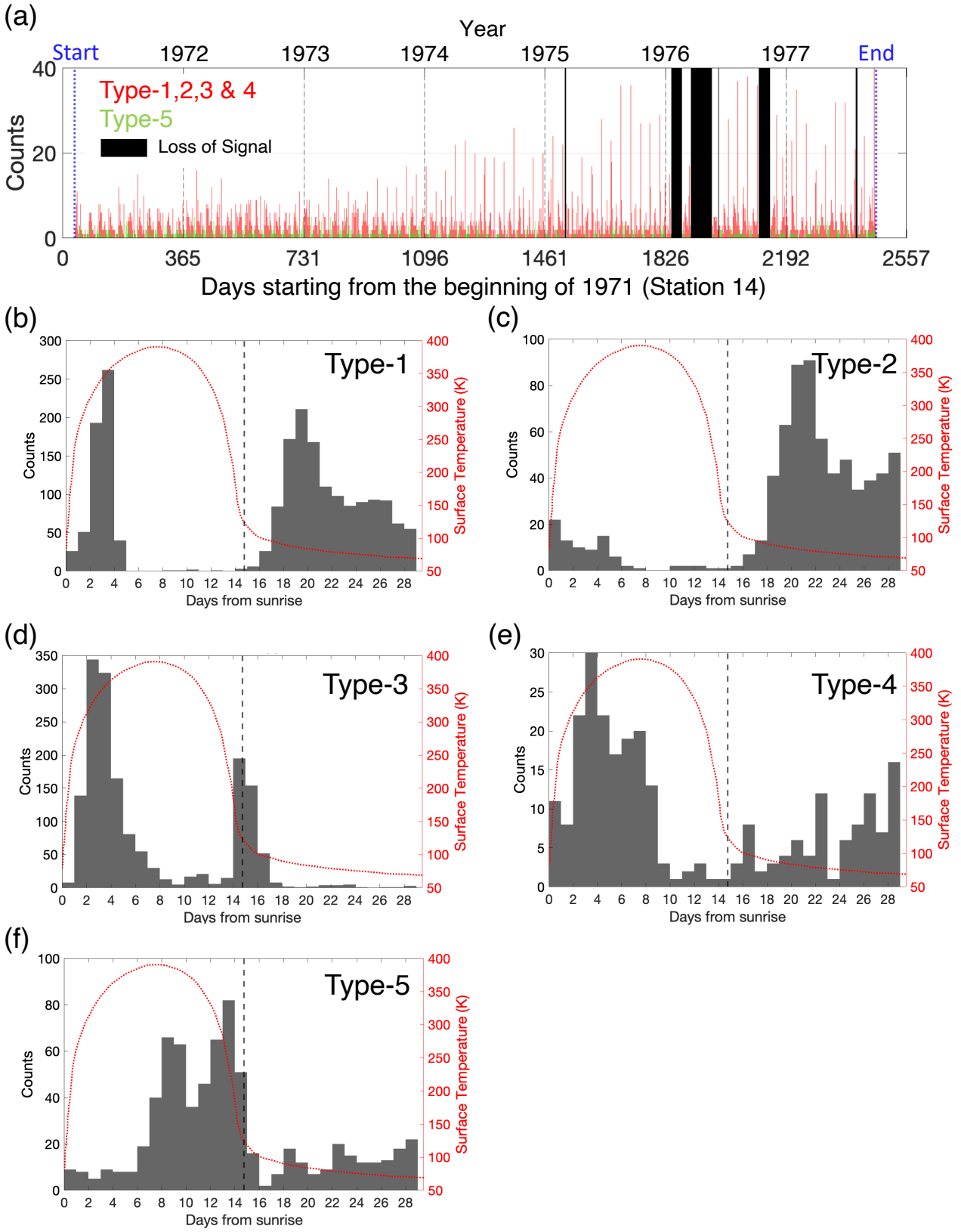
(a)
Year
Start
1972
1973
1974
1975
1976
1977
End
Type-1,2,3 & 4
Type-5
Loss of Signal
Counts
Days starting from the beginning of 1971 (Station 14)
(b)
Type-1
(c)
Type-2
(d)
Type-3
(e)
Type-4
(f)
Type-5
Counts
Surface Temperature (K)
Days from sunrise

Figure10.

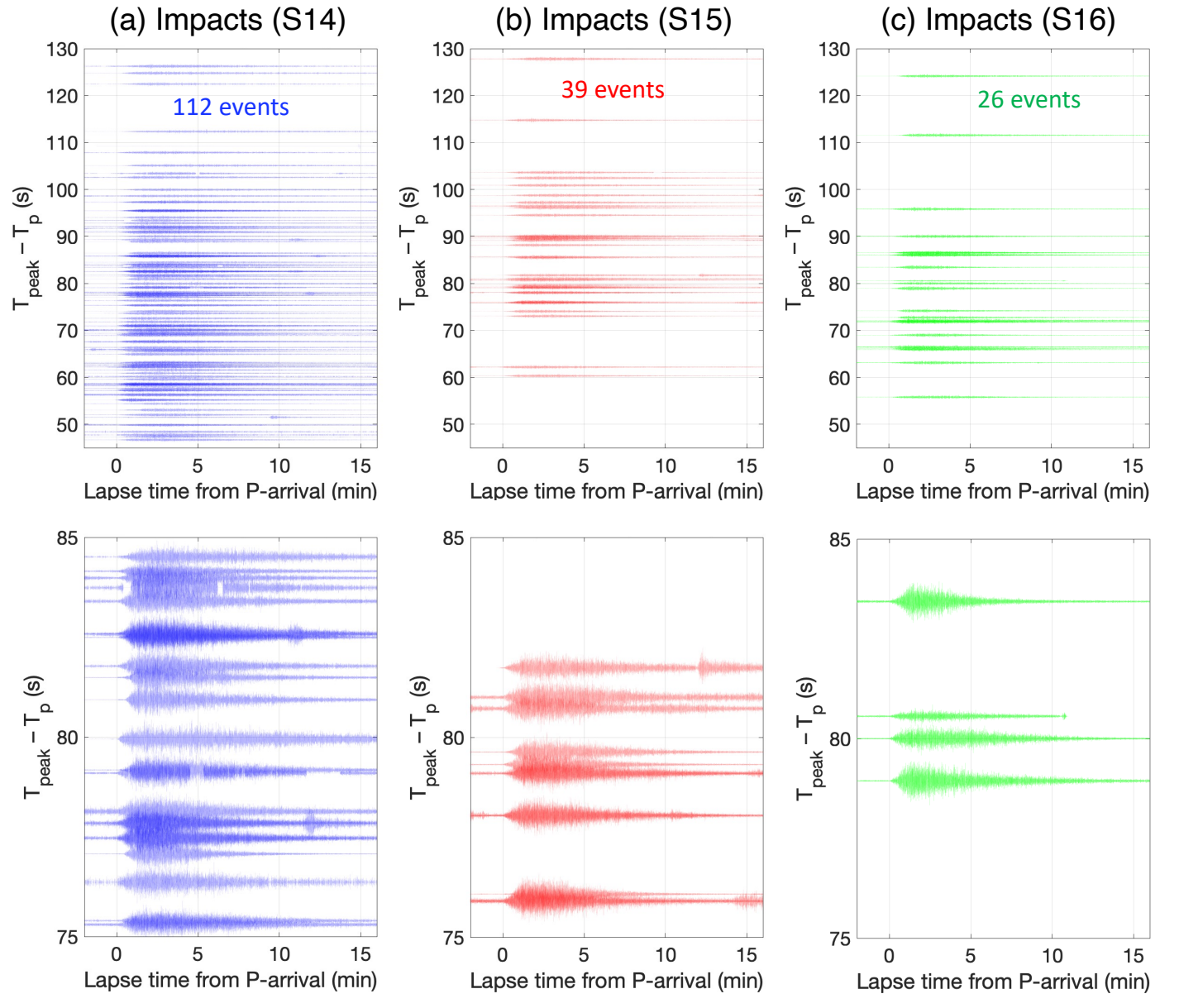
(a) Impacts (S14)
(b) Impacts (S15)
(c) Impacts (S16)
112 events
39 events
26 events
$T_{peak} - T_p$ (s)
Lapse time from P-arrival (min)

Figure11.

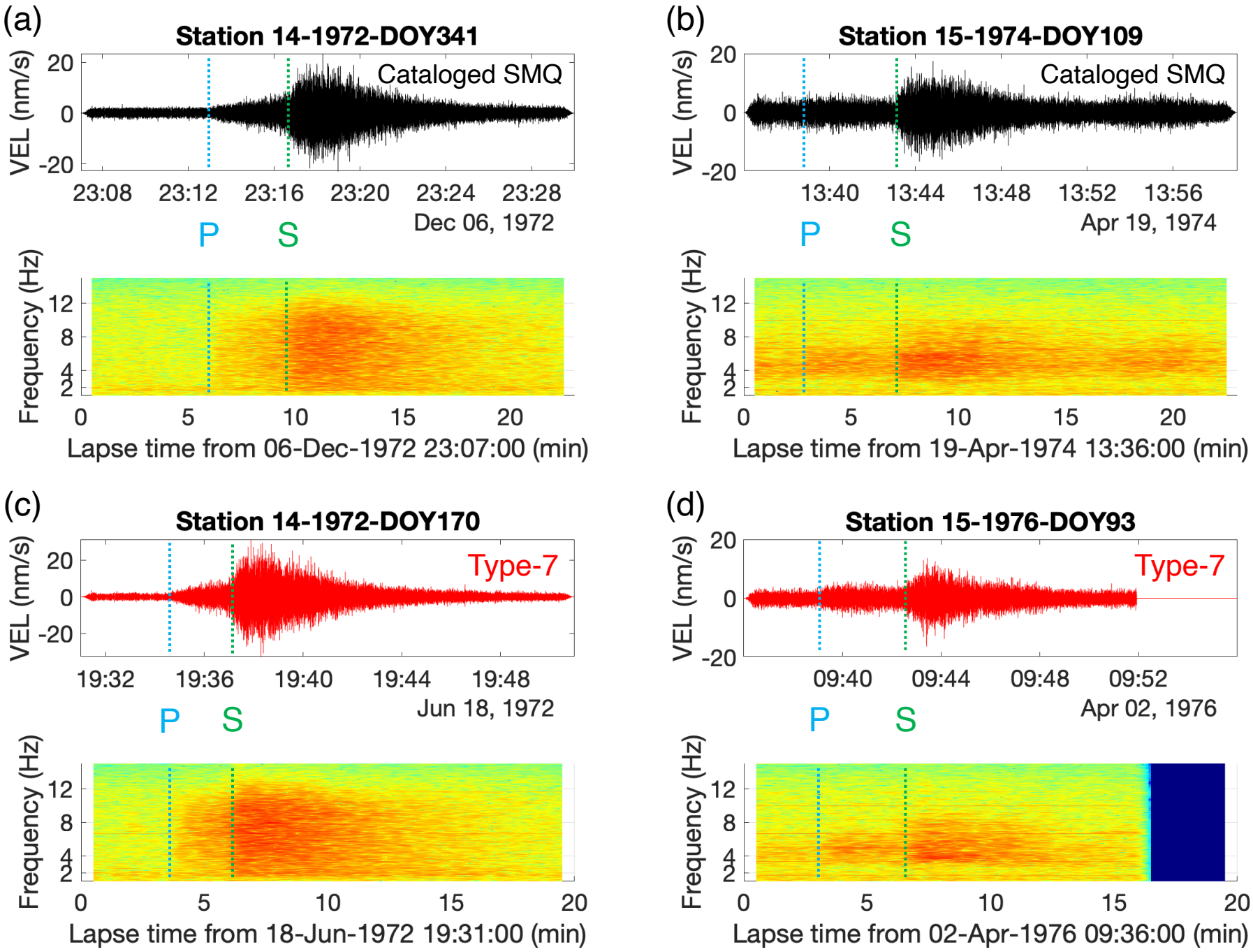
(a)
Station 14-1972-DOY341
Cataloged SMQ
VEL (nm/s)
20
0
-20
23:08
23:12
23:16
23:20
23:24
23:28
Dec 06, 1972
P
S
Frequency (Hz)
12
8
4
2
0
5
10
15
20
Lapse time from 06-Dec-1972 23:07:00 (min)
(b)
Station 15-1974-DOY109
Cataloged SMQ
VEL (nm/s)
20
0
-20
13:40
13:44
13:48
13:52
13:56
Apr 19, 1974
P
S
Frequency (Hz)
12
8
4
2
0
5
10
15
20
Lapse time from 19-Apr-1974 13:36:00 (min)
(c)
Station 14-1972-DOY170
Type-7
VEL (nm/s)
20
0
-20
19:32
19:36
19:40
19:44
19:48
Jun 18, 1972
P
S
Frequency (Hz)
12
8
4
2
0
5
10
15
20
Lapse time from 18-Jun-1972 19:31:00 (min)
(d)
Station 15-1976-DOY93
Type-7
VEL (nm/s)
20
0
-20
09:40
09:44
09:48
09:52
Apr 02, 1976
P
S
Frequency (Hz)
12
8
4
2
0
5
10
15
20
Lapse time from 02-Apr-1976 09:36:00 (min)

Figure12.

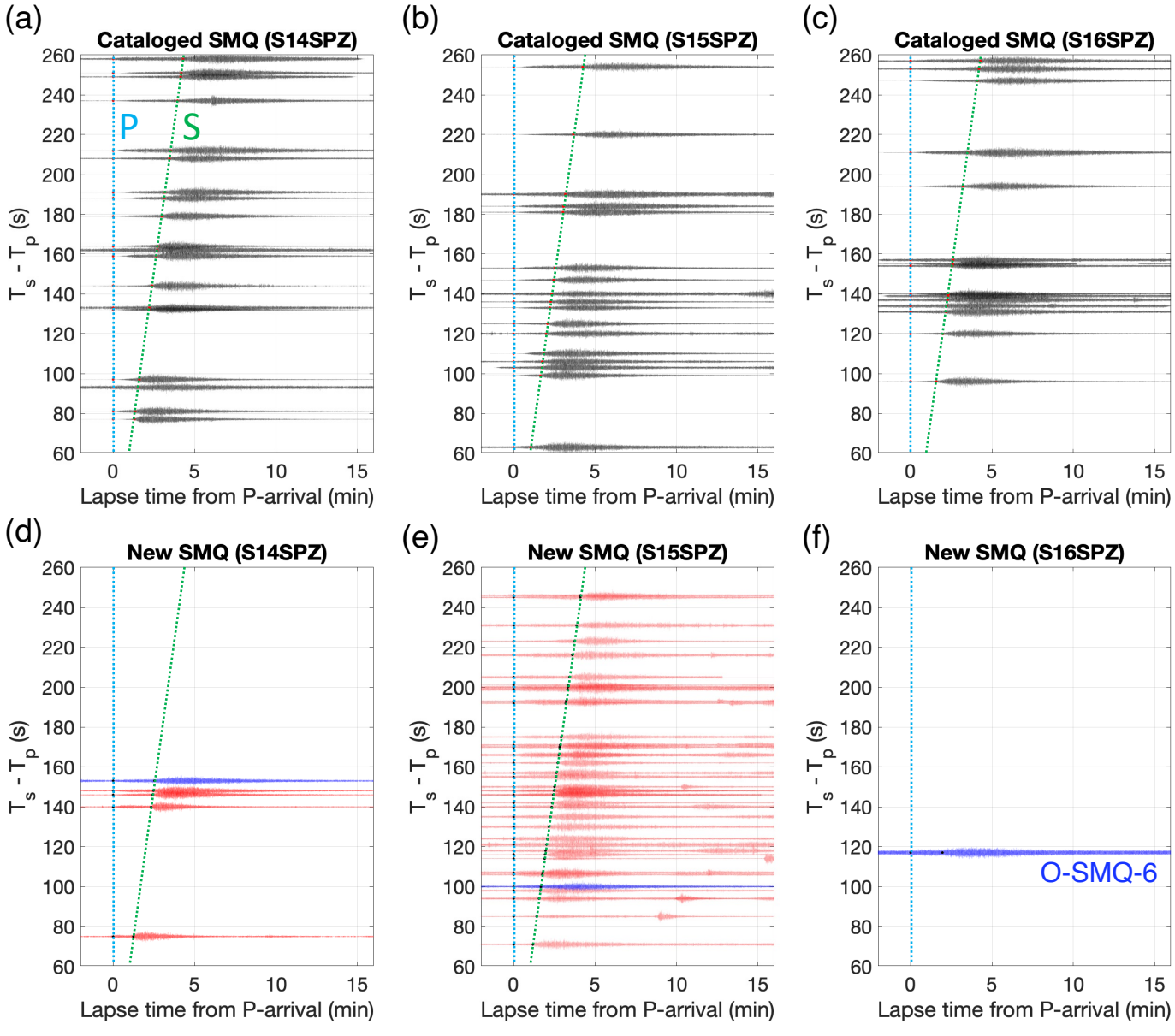
(a)
Cataloged SMQ (S14SPZ)
P
S
(b)
Cataloged SMQ (S15SPZ)
(c)
Cataloged SMQ (S16SPZ)
(d)
New SMQ (S14SPZ)
(e)
New SMQ (S15SPZ)
(f)
New SMQ (S16SPZ)
O-SMQ-6
$T_s - T_p$ (s)
Lapse time from P-arrival (min)

Figure13.

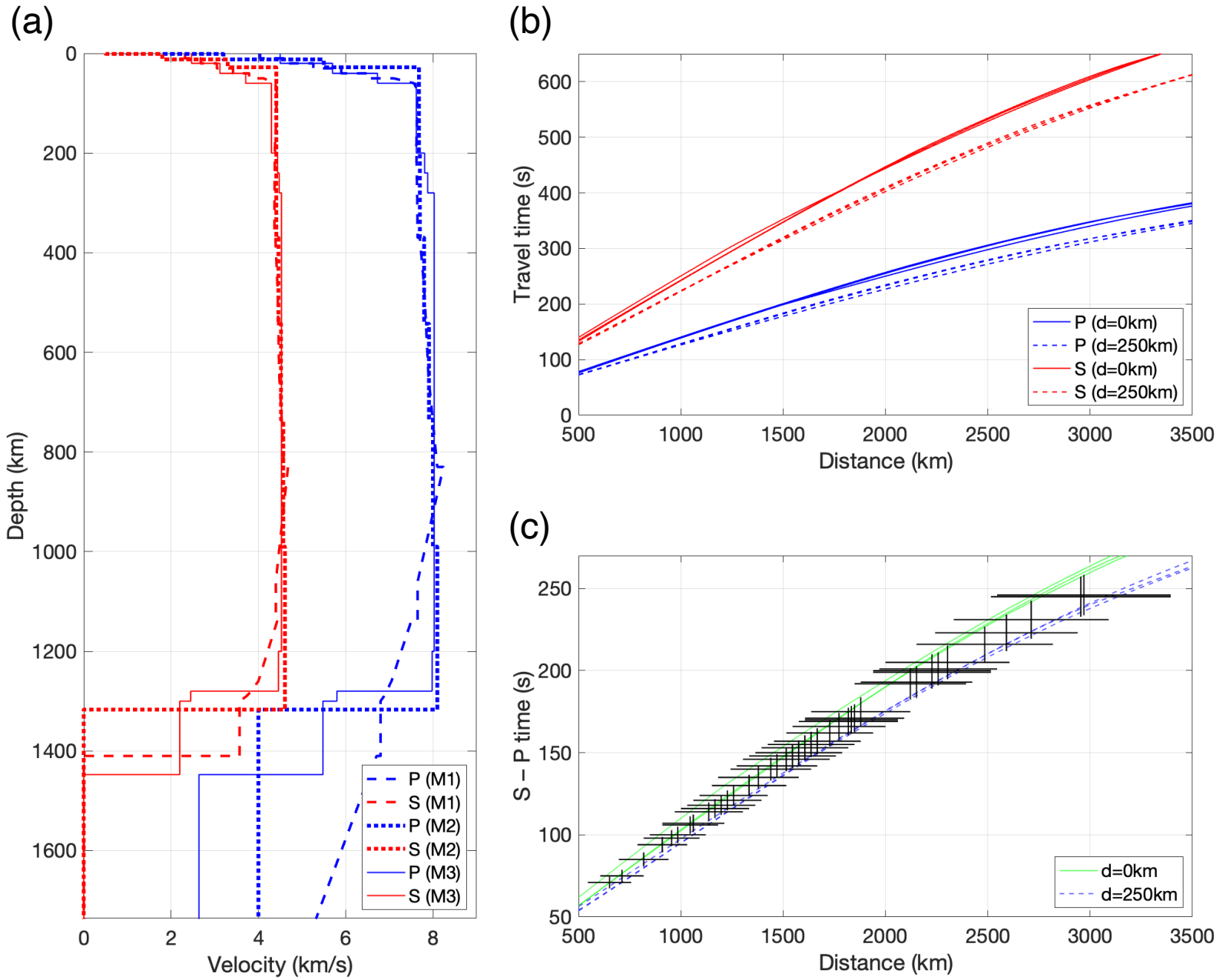
(a)
Depth (km)
Velocity (km/s)
P (M1)
S (M1)
P (M2)
S (M2)
P (M3)
S (M3)
(b)
Travel time (s)
Distance (km)
P (d=0km)
P (d=250km)
S (d=0km)
S (d=250km)
(c)
S – P time (s)
Distance (km)
d=0km
d=250km

Figure14.

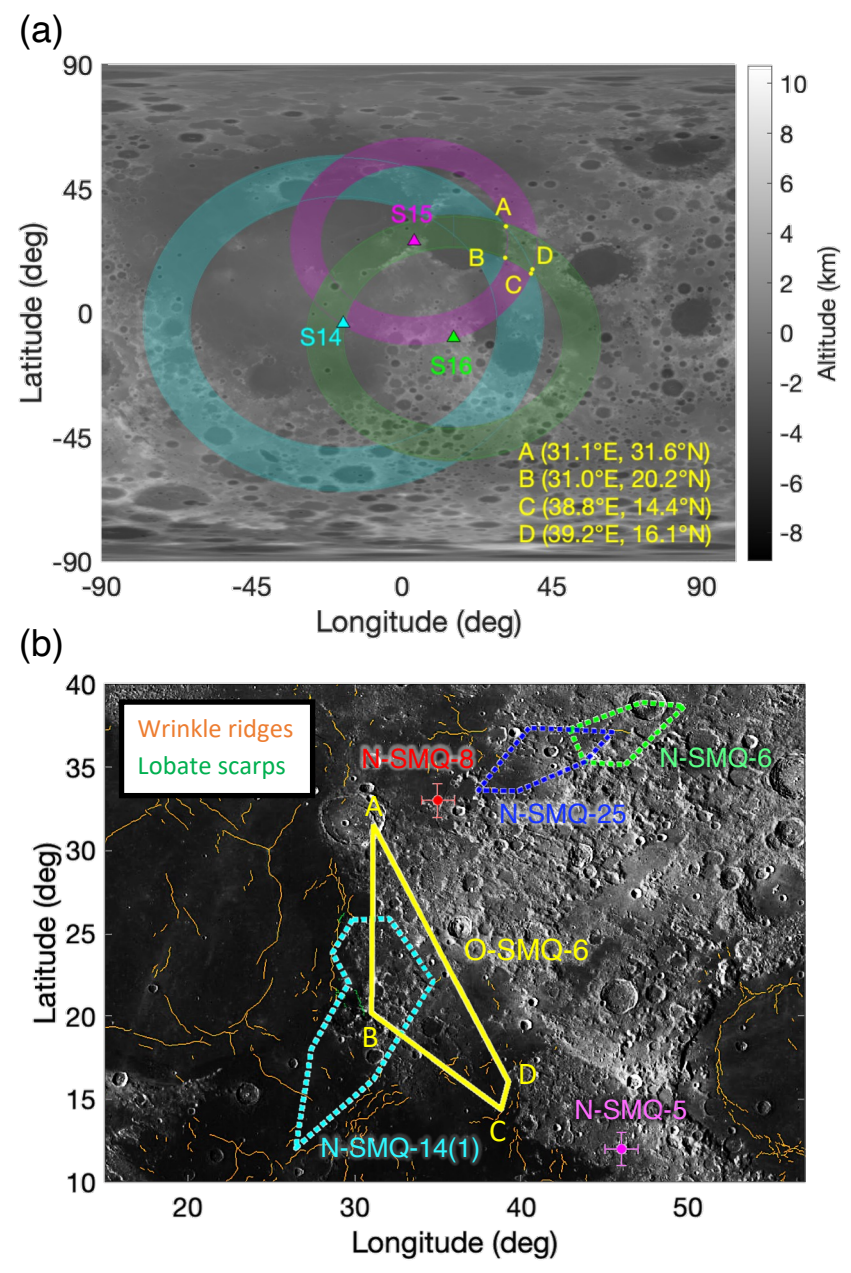
(a)
90
45
0
-45
-90
Latitude (deg)
-90
-45
0
45
90
Longitude (deg)
10
8
6
4
2
0
-2
-4
-6
-8
Altitude (km)
S15
S14
S16
A
B
C
D
A (31.1°E, 31.6°N)
B (31.0°E, 20.2°N)
C (38.8°E, 14.4°N)
D (39.2°E, 16.1°N)
(b)
Wrinkle ridges
Lobate scarps
N-SMQ-8
N-SMQ-6
N-SMQ-25
O-SMQ-6
N-SMQ-5
N-SMQ-14(1)
A
B
C
D
40
35
30
25
20
15
10
Latitude (deg)
20
30
40
50
Longitude (deg)

Figure15.

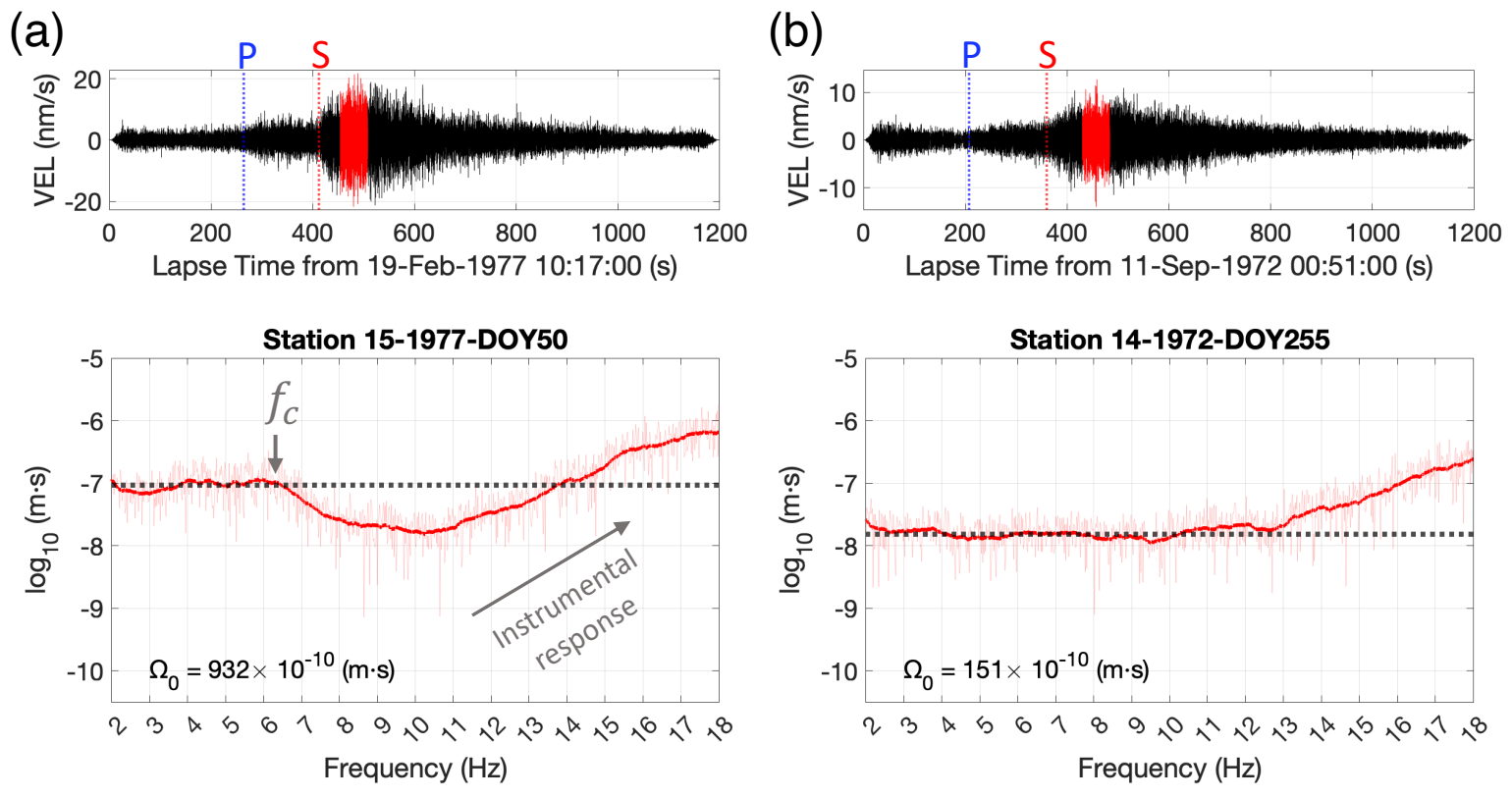
(a)
P
S
VEL (nm/s)
20
0
-20
0
200
400
600
800
1000
1200
Lapse Time from 19-Feb-1977 10:17:00 (s)
(b)
P
S
VEL (nm/s)
10
0
-10
0
200
400
600
800
1000
1200
Lapse Time from 11-Sep-1972 00:51:00 (s)
Station 15-1977-DOY50
f_c
$\log_{10}$ (m·s)
-5
-6
-7
-8
-9
-10
Ω_0 = 932× 10^{-10} (m·s)
Instrumental response
2
3
4
5
6
7
8
9
10
11
12
13
14
15
16
17
18
Frequency (Hz)
Station 14-1972-DOY255
$\log_{10}$ (m·s)
-5
-6
-7
-8
-9
-10
Ω_0 = 151× 10^{-10} (m·s)
2
3
4
5
6
7
8
9
10
11
12
13
14
15
16
17
18
Frequency (Hz)

Figure16.

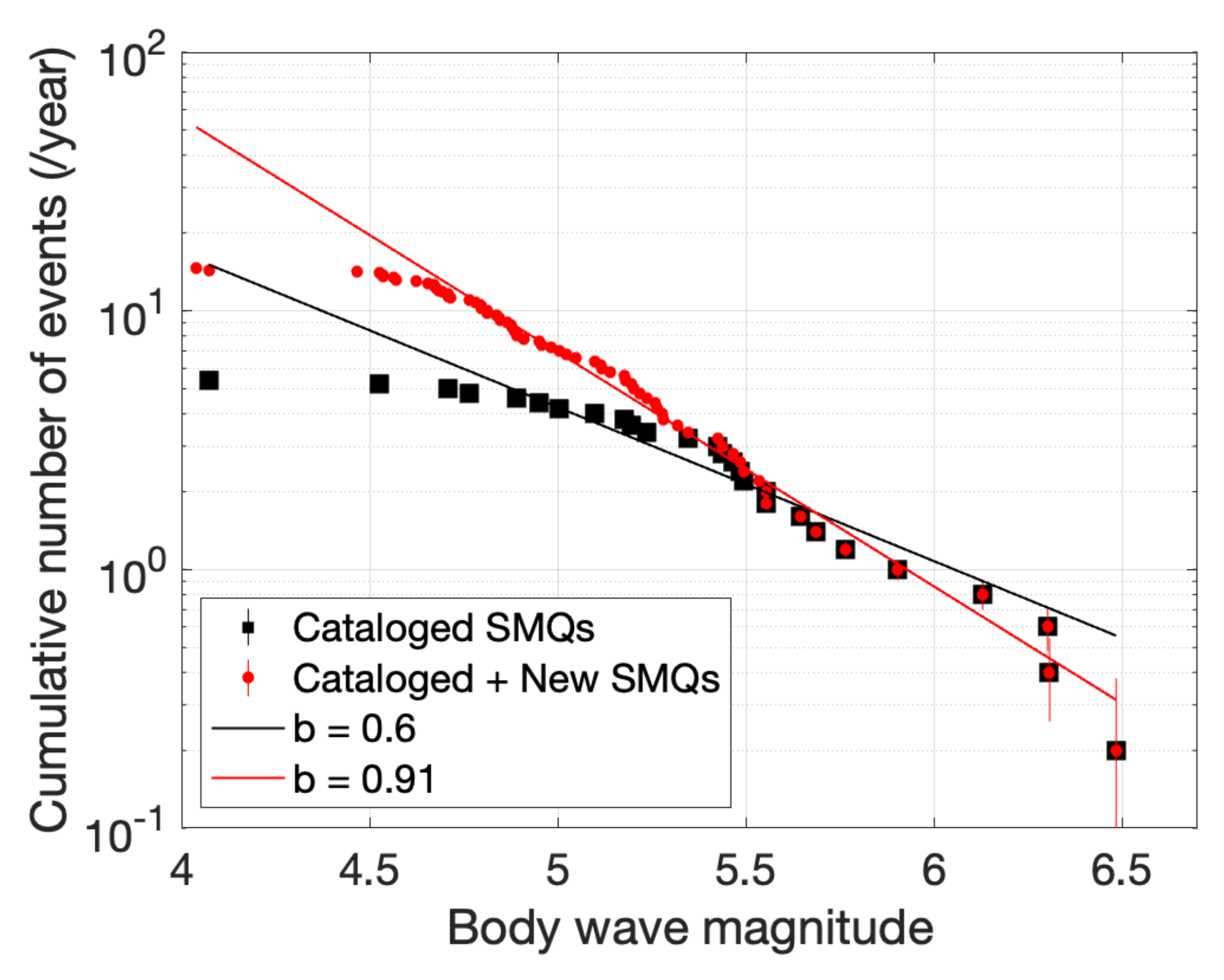
Cumulative number of events (/year)
10^2
10^1
10^0
10^{-1}
4
4.5
5
5.5
6
6.5
Body wave magnitude
Cataloged SMQs
Cataloged + New SMQs
b = 0.6
b = 0.91

Figure17.

(a)

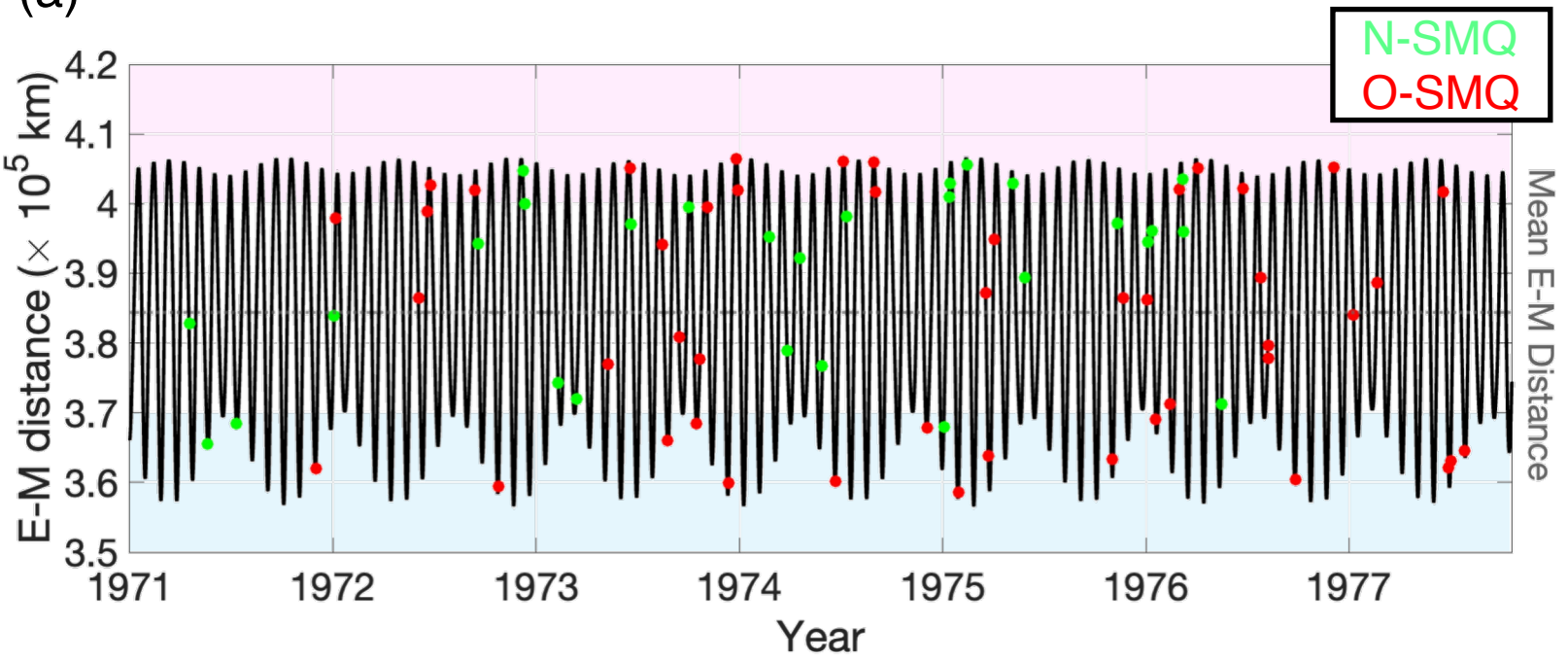

(b)

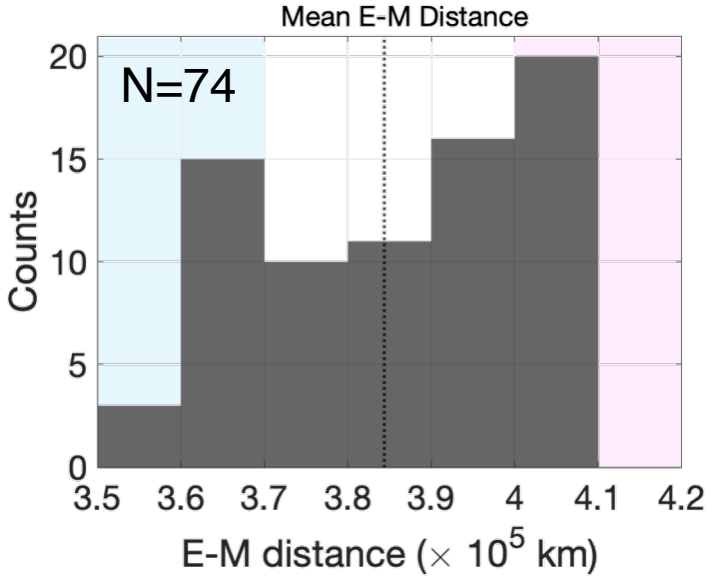

(c)

d_{EM}	$\geq 4.0\times10^5$	$\leq 3.7\times10^5$
P_{EMD}	24.9 %	22.0 %
P_{SMQ}	27.0 %	24.3 %
P_{occ}	6.7 %	5.4 %
P_{rnd}	6.2 ± 1.3 %	4.8 ± 1.1 %

Figure18.

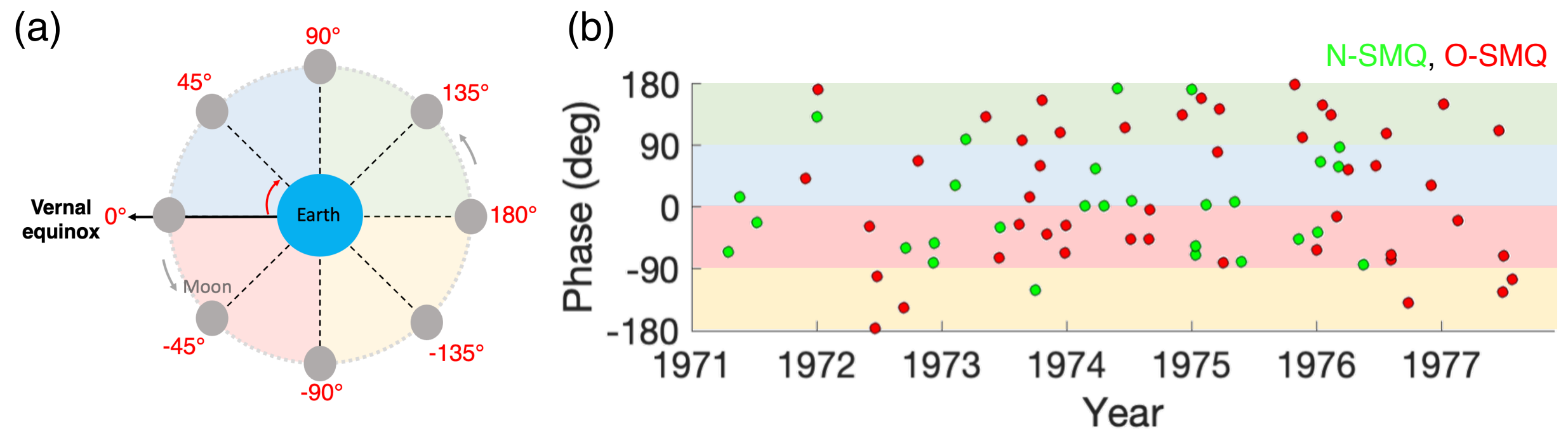
(a)
90°
45°
135°
Vernal
equinox
0°
Earth
180°
Moon
-45°
-135°
-90°
(b)
N-SMQ, O-SMQ
Phase (deg)
180
90
0
-90
-180
1971
1972
1973
1974
1975
1976
1977
Year

Figure19.

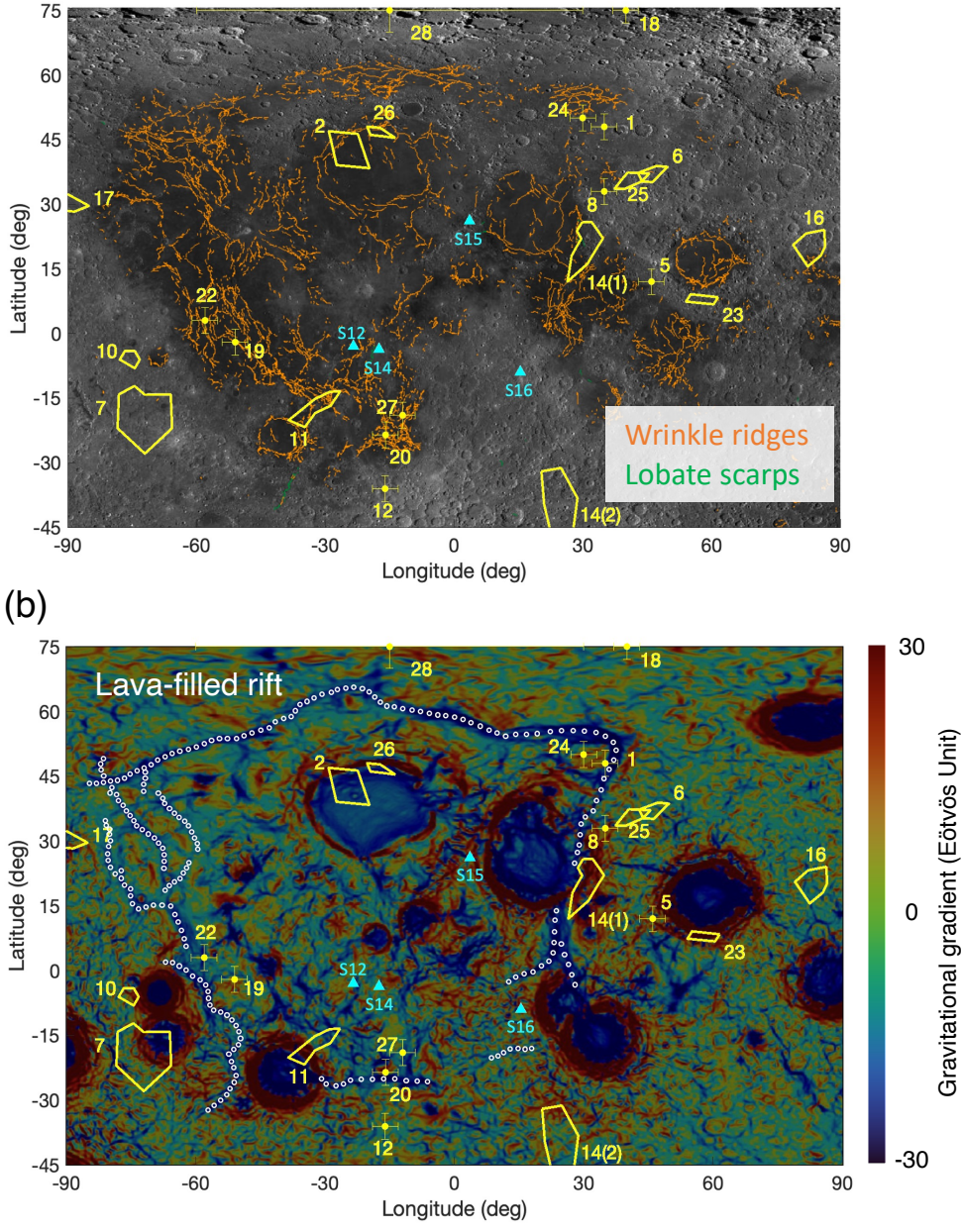
(a)
Wrinkle ridges
Lobate scarps
Lava-filled rift
(b)
Latitude (deg)
Longitude (deg)
Gravitational gradient (Eötvös Unit)
30
0
-30
75
60
45
30
15
0
-15
-30
-45
-90
-60
-30
0
30
60
90
1
2
5
6
7
8
10
11
12
16
17
18
19
20
22
23
24
25
26
27
28
14(1)
14(2)
S12
S14
S15
S16

Figure20.

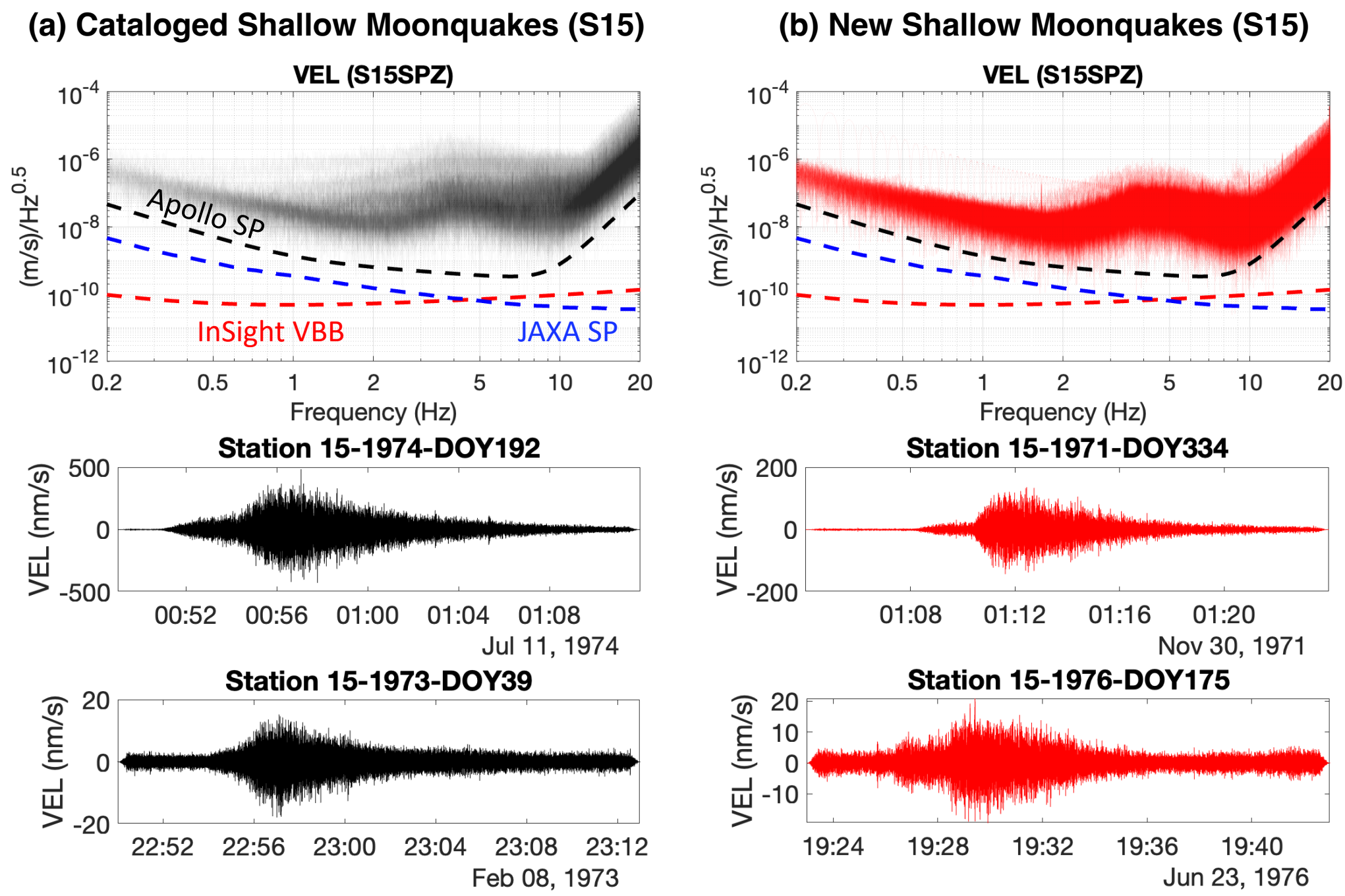
(a) Cataloged Shallow Moonquakes (S15)
(b) New Shallow Moonquakes (S15)
VEL (S15SPZ)
VEL (S15SPZ)
(m/s)/Hz^0.5
Apollo SP
InSight VBB
JAXA SP
Frequency (Hz)
Station 15-1974-DOY192
Station 15-1971-DOY334
VEL (nm/s)
Jul 11, 1974
Nov 30, 1971
Station 15-1973-DOY39
Station 15-1976-DOY175
Feb 08, 1973
Jun 23, 1976

Figure A1.

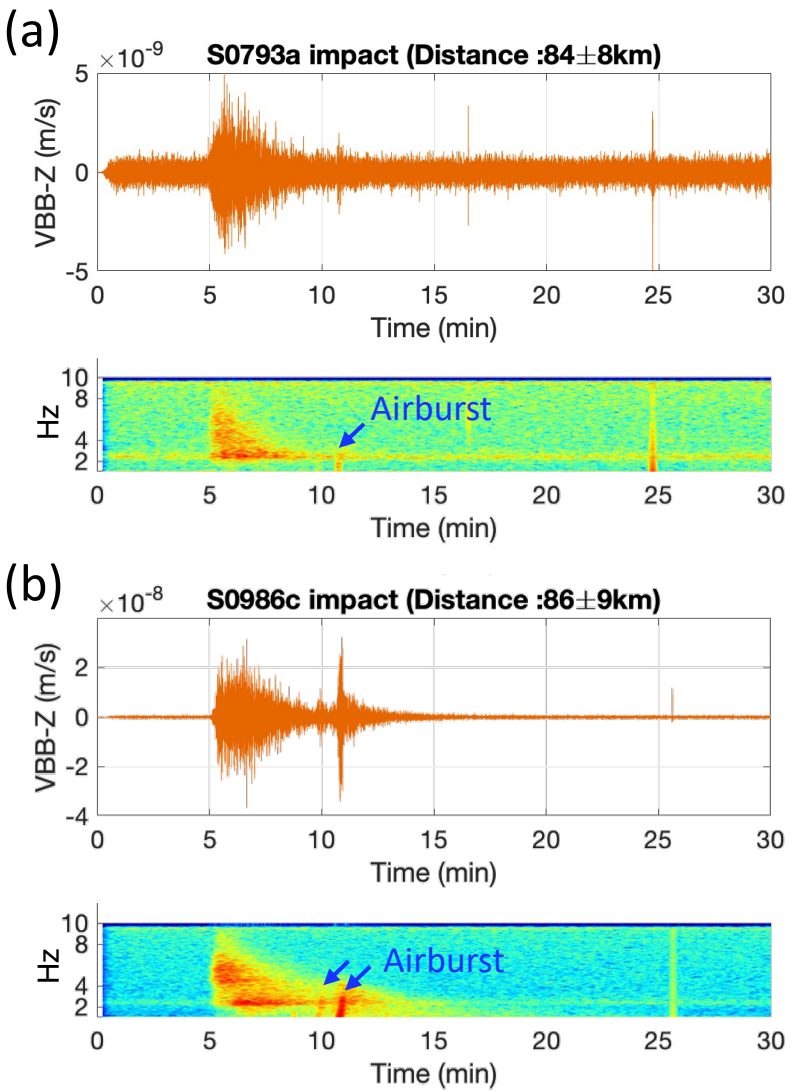
(a)
S0793a impact (Distance :84±8km)
×10^-9
VBB-Z (m/s)
Time (min)
Hz
Airburst
(b)
S0986c impact (Distance :86±9km)
×10^-8
VBB-Z (m/s)
Time (min)
Hz
Airburst

Figure A2.

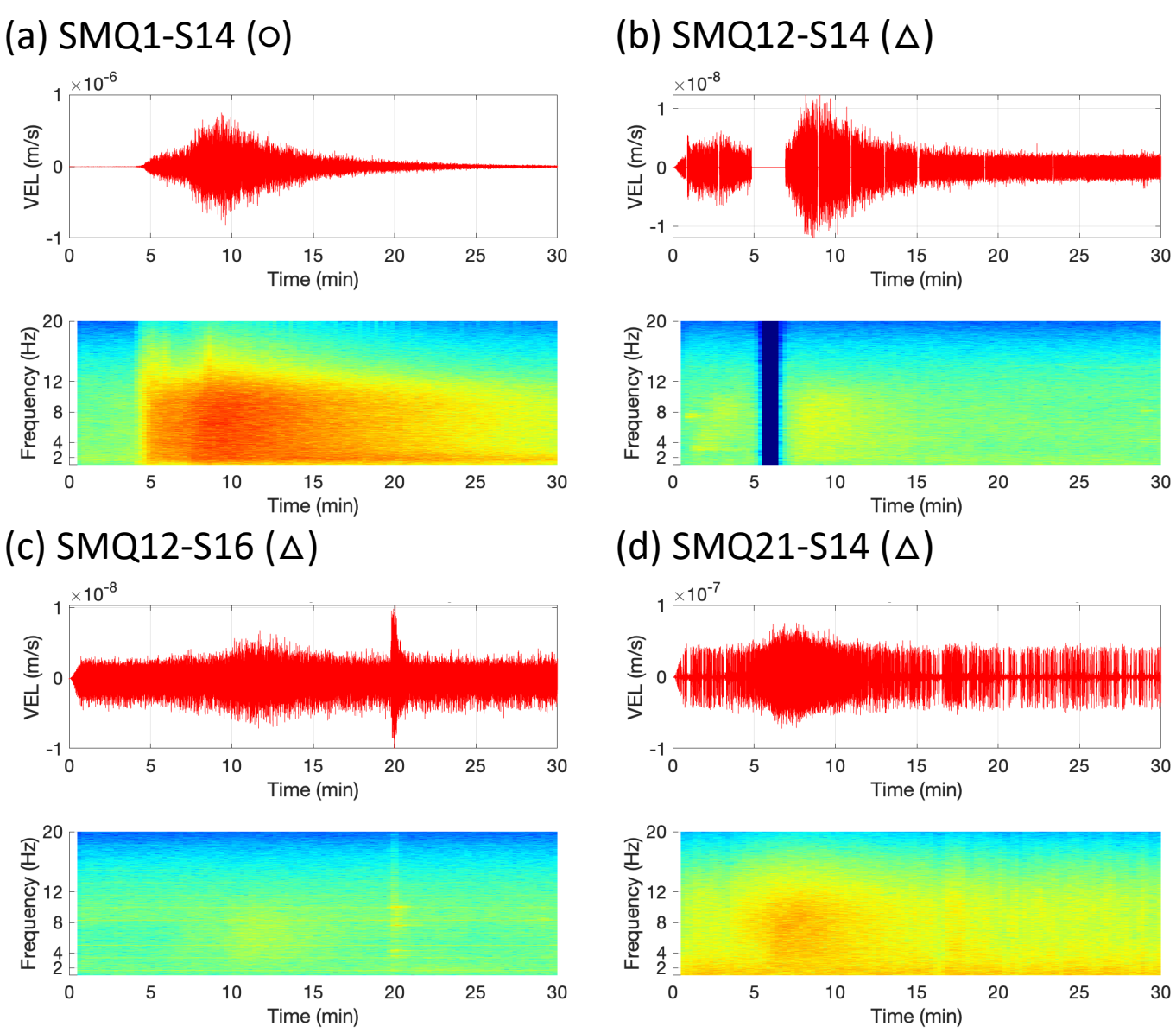
(a) SMQ1-S14 (○)
(b) SMQ12-S14 (△)
(c) SMQ12-S16 (△)
(d) SMQ21-S14 (△)
VEL (m/s)
Frequency (Hz)
Time (min)

Figure A3.

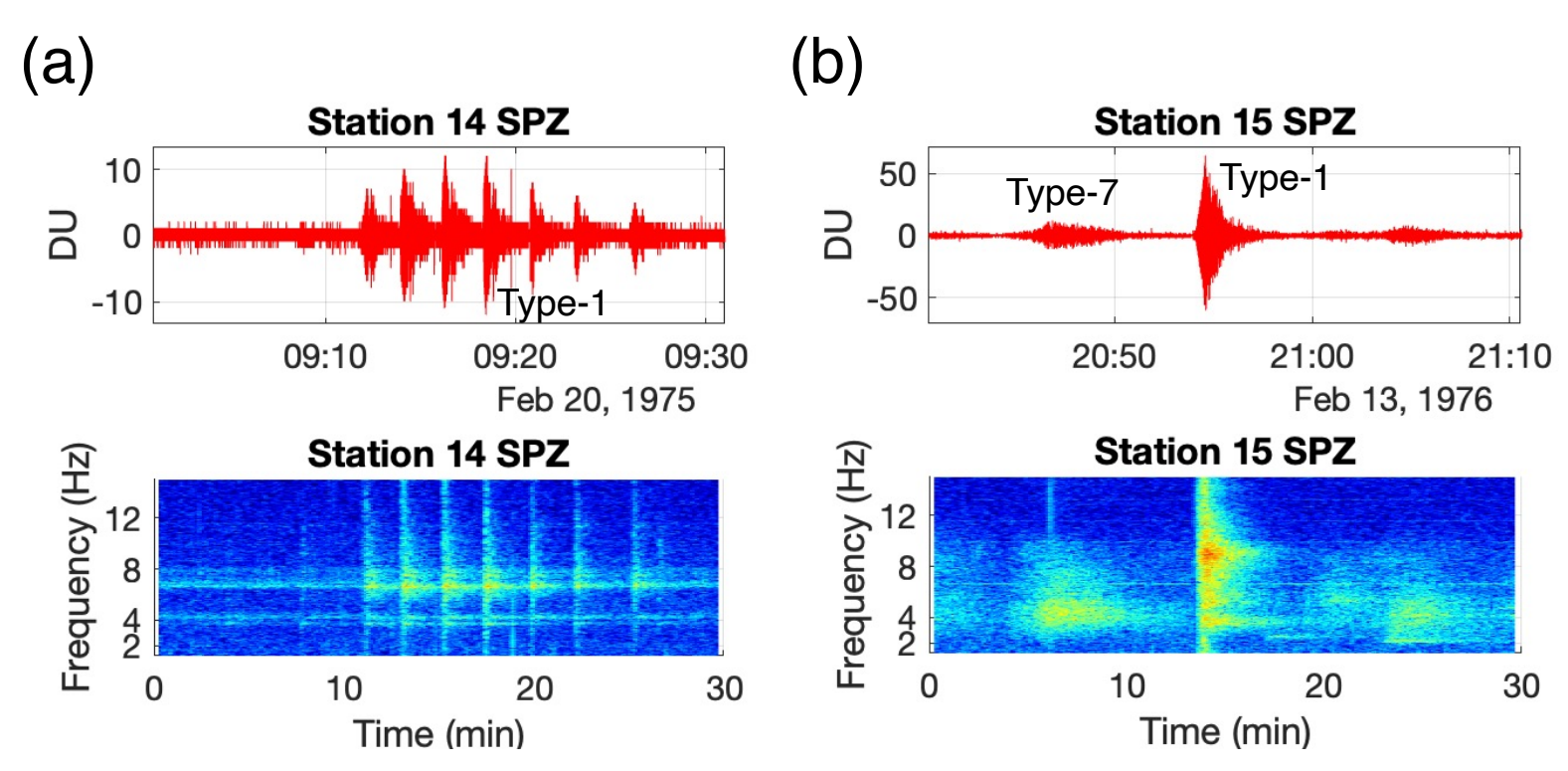
(a)
Station 14 SPZ
DU
10
0
-10
Type-1
09:10
09:20
09:30
Feb 20, 1975
Station 14 SPZ
Frequency (Hz)
12
8
4
2
0
10
20
30
Time (min)
(b)
Station 15 SPZ
DU
50
0
-50
Type-7
Type-1
20:50
21:00
21:10
Feb 13, 1976
Station 15 SPZ
Frequency (Hz)
12
8
4
2
0
10
20
30
Time (min)

Figure A4.

(a) O-SMQ-4

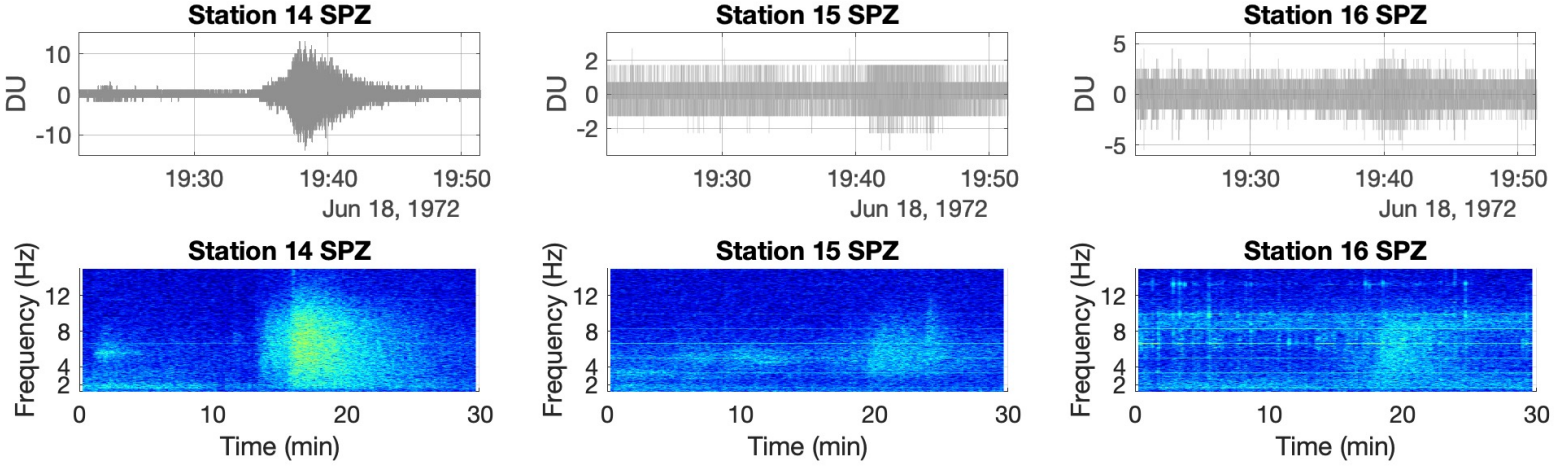

(b) O-SMQ-6

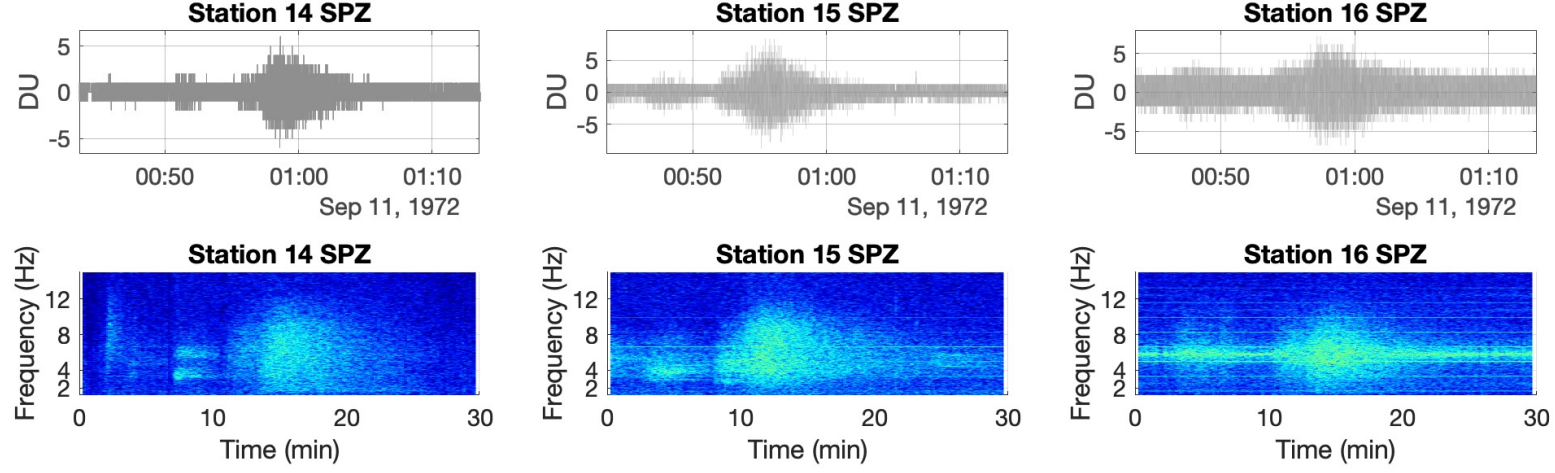

Figure B1.

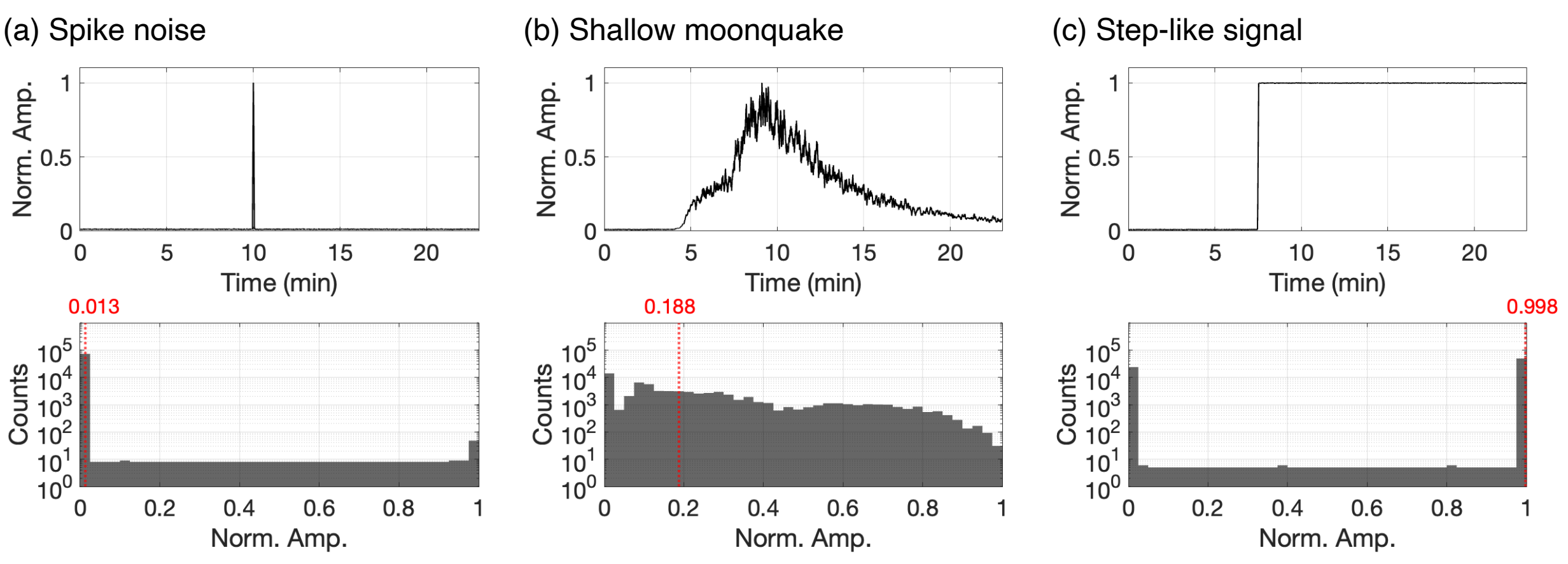
(a) Spike noise
(b) Shallow moonquake
(c) Step-like signal
Norm. Amp.
Time (min)
0.013
0.188
0.998
Counts
Norm. Amp.